The Influence of Tropical Cyclones on the Temporal Evolution of Flood Hazards in Puerto Rico

by Yihan Li

A dissertation submitted in partial fulfillment of the requirements for the degree of

Doctor of Philosophy

(Environment and Resources)

at the

UNIVERSITY OF WISCONSIN-MADISON

2022

Date of final oral defense: 05/06/2022

The dissertation is approved by the following member of the Final Oral Committee:
Advisor:
      Daniel B. Wright, Associate Professor, Civil and Environmental Engineering
Committee members:
      Christian Andresen, Assistant Professor, Geography
      Sheldon X. Du, Associate Professor, Agricultural and Applied Economics
      Nimish Pujara, Assistant Professor, Civil and Environmental Engineering
      Brian P. Bledsoe, Professor, College of Engineering, University of Georgia

Abstract

Tropical cyclones (TCs) frequently hit the Caribbean area, causing enormous economic and social impacts. In Puerto Rico and similar island environments, the interactions of the storms and geographic features can produce some of the largest per-unit area flood peaks in the world. During such floods, sediment is redistributed and river channels can experience substantial geomorphic changes, which can alter local flood hazard. However, these changes are not usually considered by conventional flood frequency analysis (FFA), which assumes that flood events are statistically independent and identically distributed. This dissertation aims to better understand "path dependency" in flood susceptibility in such environments, first by examining how channel geomorphology evolves in response to major hurricanes, then by considering a case study of floodplain change after Hurricane Maria. These analyses are put into the context of broader range of social and geographic responses to TCs in the Caribbean.

Daily streamflow records containing discharge, stage, velocity, and wetted width were obtained. Rating curves, the relationship between stage and discharge, were fitted to understand how conveyance capacity changes. At-a-station hydraulic geometry assumes the relationships between discharge and water depth, wetted width and velocity follow power laws. By fitting the records to these power laws, we studied the changes of channel hydraulic geometry. Terrain models from different periods can translate such geomorphic changes into more meaningful metrics such as floodplain depth and extent. Two high-quality digital elevation models (DEM), one before and one after Hurricane Maria, were used to evaluate how flood hazards may have changed after that storm.

River channel conveyance capacity and hydraulic geometry were found to experience significant changes after major floods, while geomorphic changes from Hurricane Maria were shown to result in substantial floodplain extent and depth changes. In addition to these short geophysical changes, TCs can also leave a trail through which understanding of and social responses to hurricanes evolve in Caribbean societies. This dissertation closes with a review of this evolution and discusses hurricanes' influence in a broader context.

Acknowledgements

My Ph.D. journey came to the point where I'm going to submit my Ph.D. dissertation at this moment. Looking back on my Ph.D. journey, I'm thrilled and at the same time surprised that I've come a long way to make it here. I know deeply in my heart that I cannot finish my Ph.D. without extensive support that I received from many people.

There's no doubt that Daniel Wright, my Ph.D. advisor, is the person who provided me with most support, guidance, and help. As an advisor, Dan is always creative about research ideas, knowledgeable, and excel at scientific writing, which clearly guided me through the Ph.D. studies. Dan is also a caring person which greatly reduced the pressure along the way. I can never be grateful enough to Dan, and it was a really lucky chapter in my life to finish my Ph.D. under his guidance.

My next round of thanks goes to my committee members, Professor Christian Andresen, Professor Brian Bledsoe, Professor Sheldon Du, and Professor Nimish Pujara. I can never complete this interdisciplinary study without background knowledges in different fields, which I learnt from my committee members during my Ph.D. In addition, I would also like to thank other professors from whose lectures I learnt a lot: Annemarie Schneider, Steve Loheide, and Raymond Deneckere.

I would thank all coordinators of Bio 152 from the Department of Integrative Biology: Jean Heitz, Carlos Peralta, Nazan Gillie, Julie Collins, Kerry Martin, and Jeremiah Yahn. It is the coordinators who provided me with the first funding source, TA for Bio 152, which made my Ph.D. journey possible at the first place. I would also thank Jim Miller, graduate advisor of my program, to provide comprehensive logistic support, especially for a student of special conditions like me.

I would thank all friends that I made along the journey. Members of both our small research HER group and the larger WRE group are the major source of mental support to me. I enjoyed our weekly seminar, all those small talks, games and parties which lightened my normal life. I

would especially thank Bowen Zhang, my roommate, for all efficient collaborations on the housework which greatly saved us both time on research.

Finally, thank you mom and dad. You never imposed any personal goals or thoughts on me, and provided all the emotional support that I need.

Table of Contents

Chapter 1   Introduction

1.1   Background and Motivation

Rainfall-induced flooding, often associated with the passage of tropical cyclones (TCs), is a frequent and devastating natural hazard in Puerto Rico and other similar environments. Interactions of moisture-laden storm systems with the island's steep mountainous terrain are capable of producing some of the largest flood peaks per unit watershed area in the United States (Smith et al., 2005) and can mobilize large amounts of sediment via landslides and debris flows (West et al., 2011a). Rainfall-driven floods in tropical regions can cause staggering economic losses and fatalities (Diakakis et al., 2015a; Ogden, 2016a; Palm & Hodgson, 1993a). The Caribbean region's history includes multiple examples of major changes in agricultural land use in response to TC damages, often in conjunction with other socioeconomic forces (Bulmer-Thomas, 2012; Schwartz, 2015). Devastating TC impacts continue to this day: Hurricane Maria, which made landfall in PR on 20 September 2017, resulted in unprecedented flooding and mudslides (Keellings & Hernández Ayala, 2019), greatly increased mortality rates (Kishore et al., 2018), and caused an estimated $90 billion in damages, making it the third costliest TC in U.S. history (National Weather Service, 2021). Economic constraints in the region often limit the ability to respond and rebuild (López-Marrero & Yarnal, 2010a). At the same time, the impacts of climatic and land use changes on future flood risks in tropical regions are poorly understood (Khan et al., 2015; Taniwaki et al., 2017).

An important step toward mitigating flood risk is quantitative estimation of the frequency and severity of flooding. This has long been the objective of flood frequency analysis (FFA; e.g. Stedinger et al., 1993), by which particular metrics such as the "100-year" streamflow magnitude and inundated area are derived. FFA generally assumes that flood events are statistically independent and identically distributed (i.i.d.) at the annual time scale (e.g. Obeysekera & Salas, 2016). Implicit in the i.i.d. assumption, and central to FFA, is the supposition that any particular flood event does not influence the likelihood or severity of subsequent floods.

This assumption can be violated by extreme floods, which are capable of moving sufficient sediment loads to "reconfigure" river channel-floodplain systems and thus influence a channel's conveyance capacity and geometry (Dai & Lu, 2010; Dingman, 2007; Harvey, 2007; Heritage et al., 2004; Konrad et al., 2011; Krapesch et al., 2011; Smith et al., 2000). Societal responses, such as building flood control structures and land cover/land use transitions can also affect the occurrence and magnitude of subsequent flood events, further challenging this i.i.d. assumption (Ramos-Scharrón et al., 2015). The frequent and intense flooding brought by TCs in Puerto Rico, together with the island's highly varied terrain and land use characteristics, make it an ideal study region to examine the ability of extreme floods to alter subsequent flood risks.

Understanding past and predicting future changes in flood flows and river channel characteristics also requires better understanding of the landscape features that control them. Remote sensing and GIS technologies facilitate analyses of land cover and land use characteristics including forested, developed and planted areas, and also enable researchers taking measurements of some river channel geometry like reach width and length remotely. At the same time, the region's long recorded history beginning in 1492 (and to some extent even its prehistory) provides

opportunities to examine the broader roles that TCs have played in shaping both physical and socioeconomic landscapes.

The ultimate goal of reducing flood risks from TCs will require more than understanding and managing physical dimensions and physical changes to flood hazard. The history of popular conceptions of hurricanes and how people and institutions have organized to cope in the wake of major hurricanes can provide perspectives on current and future flood risk in the Caribbean region. Integrating the knowledge of socioeconomic impacts left by historical TCs with flood hazard changes could help risk managers to identify "root cause" approaches to reduce flood risks associated with TCs.

1.2   Dissertation Goals and Overview

This dissertation explores effects of TCs in Puerto Rico on flood hazard and risk from multiple perspectives, including channel conveyance capacity, hydraulic geometry, floodplain extent, and socioeconomic response. The following research questions were studied:

1. Can TCs cause sediment redistribution, which result in sediment deposition and scour along the river system in PR? Can this redistribution change river channel conveyance capacity?

2. Are there long-term changes of high flows and river conveyance capacity, which can affect future flood hazards? How large and widespread are those changes in PR?

3. Does channel hydraulic geometry change in response to TCs in PR?

4. Are there watershed and river reach characteristics associated with hydraulic geometry parameters in PR? Could these characteristics be used to predict hydraulic geometry parameters for under or ungaged locations?

5. Can TC-associated geomorphic changes affect floodplain maps? How important are those changes compared to the changes of flood hazard mapping caused by adding new TC observations?

6. How have peoples' perceptions and coping strategies adjusted in response to TCs in the Caribbean region?

TCs noticeably produce frequent and severe floods in Puerto Rico. Chapter 2 (published; Li et al., 2020) found that floods of roughly 10-year recurrence interval and above can result in sediment redistribution through river systems, causing sediment deposition and scour along the river systems. Both high flow trends and river conveyance capacity trends are found to affect flood hazard trends. High flow trends have effects of greater magnitude, while conveyance capacity trends are more widespread in Puerto Rico. TCs are found to be related to instantaneous conveyance capacity changes, which are followed by short-term (i.e. multi-year) recovery periods.

Though Chapter 2 shows conveyance changes after major TCs, it doesn't explain how the changes manifest in terms of channel geometric characteristics and roughness. It also fails to identify which upstream watershed and river reach characteristics can influence such changes. Chapter 3 (under review) studies how channel geometry and roughness changes in response to TC-induced floods, using the proxy of at-a-station hydraulic geometry (AHG) parameters. It identifies the significant watershed and river reach characteristics, and builds regression models

with them to predict AHG parameters. These predictive models could be used to predicting channel geometry and roughness properties at ungaged sites.

With conveyance capacity and AHG changing in response to TCs, the question arises: how do floodplain extent and depth change before and after major hurricanes? This question is the main focus of Chapter 4 (under review). Chapter 4 builds hydraulic models on terrain models created shortly before and after Hurricane Maria, a major hurricane that hit Puerto Rico in September 2017, and finds that floodplain extent and depth changes caused by geomorphic changes are of similar magnitude to those caused by peak flow quantile estimate changes associated with including Maria's observation into the annual peak flow time series. The results show that Hurricane Maria caused areal flood hazard changes through geomorphic modifications.

Chapter 5 attempts to broaden the perspective of Chapters 2-4, while still focusing on path-dependent system response to TCs. It does so by examining the evolution of how people and institutions view and respond to major TCs. Chapter 5 takes a panoramic look at the socioeconomic history of hurricanes in the Caribbean area, summarizing a timeline of the conceptual, political, and social transitions that hurricanes have brought to the region. People's understandings of TCs determined how and how accurately they predict TC occurrences, and how they plan for future TCs. Social responses, including community and government responses, to TCs showed how different practices can help relief and rebuilding and the resilience of affected communities to this frequent and devastating nature hazard. These transitions, while shaped by historical TCs, also in turn influence future TCs' impacts. With this information, this dissertation provides a more comprehensive context for discussion of flood risks.

Chapter 6 summarizes the findings from the former chapters and concludes that TCs can influence flood hazards and risks from multiple aspects. It closes with discussion of limitations of this dissertation research and potential future study directions to further understand the influence of TCs on flood hazards and flood risks in the Caribbean area.

Chapter 2   The Influence of Tropical Cyclones on the Evolution of River Conveyance Capacity in Puerto Rico

Adapted from: Li, Yihan, Daniel B. Wright, and Patrick K. Byrne. "The Influence of Tropical Cyclones on the Evolution of River Conveyance Capacity in Puerto Rico." Water Resources Research 56.9 (2020): e2020WR027971.

2.1   Introduction

Rainfall-induced flooding, often associated with the passage of tropical cyclones (TCs), is a frequent and devastating natural hazard in Puerto Rico. Interactions of moisture-laden storm systems with the island's steep mountainous terrain are capable of producing some of the largest flood peaks per unit watershed area in the United States (Smith et al., 2005) and can mobilize large amounts of sediment via landslides and debris flows (West et al., 2011b). Rainfall-driven flood events in Puerto Rico and similar tropical regions can cause staggering economic losses and fatalities (Diakakis et al., 2015b; Ogden, 2016b; Palm & Hodgson, 1993b; Rodríguez, 1997), while economic constraints in such locations often limit the ability to respond and rebuild (López-Marrero & Yarnal, 2010b). At the same time, the impacts of climatic and land use change on future flood risk in tropical regions areas are poorly understood (Khan et al., 2015; Taniwaki et al., 2017).

An important step toward mitigating flood risk is quantitative estimation of the frequency and severity of flooding. This has long been the objective of flood frequency analysis (FFA; e.g. Stedinger et al., 1993), by which particular metrics such as the "100-year" streamflow magnitude

and inundated area are derived. FFA generally assumes that flood events are statistically independent and identically distributed at the annual time scale (e.g. Obeysekera & Salas, 2016).

This assumption can be violated by extreme floods, which are capable of moving sufficient sediment loads to "reconfigure" river channel-floodplain systems and thus influence a river's conveyance capacity and potential future flood hazards (Dai & Lu, 2010; Heritage et al., 2004; Krapesch et al., 2011; Smith et al., 2000). Specifically, major floods can increase conveyance capacity (i.e. a river channel's ability to transmit water downstream) in some locations via sediment scour and decrease capacity at other locations due to deposition (Guan et al., 2016a). Previous research into floods' ability to alter conveyance capacity has focused on long recurrence intervals: Krapesch et al. (2011) and Heritage et al. (2004), for example, examined morphologic response to flood events with recurrence intervals greater than 100 years in Austria and 200 years in South Africa, respectively, while Dai et al. (2010) evaluated channel reconfiguration due to the two largest Yangtze river floods of the last century. The combination of extreme and relatively frequent TC rainfall, steep terrain, and erosive soils, however, means that such events may be much more common in certain tropical regions including Puerto Rico (e.g. Nugent & Rios-Berrios, 2018).

The frequency of flooding can change over time due to changes in both peak streamflow magnitude and river channel conveyance capacity (Slater et al., 2015; Zischg et al., 2018). Conveyance capacity is represented by cross-sectional geometric characteristics and roughness, which determines the flow-carrying capacity (Ponce, 1989; Wu & He, 2009). Streamflow trends can occur due to changes in climate (Pall et al., 2011), land cover (López-Moreno et al., 2006), and river regulation including dams and reservoirs (e.g. Hatcher & Jones, 2013; Lorenzo-Lacruz

et al., 2012; Ye et al., 2003). These factors can also lead to trends in conveyance, as can flow diversions, channel straightening (e.g. Surian, 1999), changes in bed texture (e.g. Doyle & Shields, 2000), and loss of riverbank vegetation (e.g. Masterman & Thorne, 1992). Slater et al. (2015) showed that conveyance capacity changes are generally smaller in magnitude but more widespread than significant changes in streamflow in the continental U.S., while Slater et al. (2019) argued that river channels can adjust to climate relatively quickly.

Though the physical mechanisms involved in conveyance capacity change have been documented in Puerto Rico and elsewhere (see Section 2.2), their frequency and potential role in the evolution of long-term flood behavior has received relatively little attention. This study examines the frequency and magnitude of conveyance capacity changes in Puerto Rico, focusing on both abrupt and more gradual changes, which together comprise long-term conveyance capacity trends. Conveyance trends are also compared against trends in streamflow and rainfall. We also attempt to identify upstream watershed characteristics that may influence these changes.

The physical phenomena of conveyance capacity change, and relevant prior work in Puerto Rico and elsewhere, are briefly summarized in Section 2.2. Data and methodology are described in Sections 2.3 and 2.4, respectively. Results are presented in Section 2.5. We close with discussion in Section 2.6 and conclusions in Section 2.7.

2.2   Background

High intensity rainfall and resulting overland and channel flow velocities and shear stresses can mobilize large amounts of sediment (Neuhold et al., 2009; Staffler et al., 2008). The redistribution of this mobilized sediment can cause morphological changes that depend on both

local and upstream characteristics. For example, high discharges can scour headwater channels and move sediment downstream, where velocities typically decrease, leading to sediment deposition (Neuhold et al., 2009). This can in principle decrease subsequent flood hazard in upstream areas, since widened and deepened channels will have higher conveyance capacity; this comes at the cost, however, of potentially decreased conveyance and thus increased hazard downstream where rivers may be choked with sediment after a flood (Staffler et al., 2008; Zischg et al., 2018).

Major floods in Puerto Rico usually happen in late summer through early winter, corresponding with the North Atlantic TC season (Palm & Hodgson, 1993; Smith et al., 2005). TCs approach Puerto Rico from the south or east and proceed north or west over the island (Smith et al., 2005). The island's mountainous terrain, tropical climate, and human development including agricultural activities tend to promote sediment loss (Clark & Wilcock, 2000a), particularly in high-relief areas (Simon, 1990). Extreme rainfall and subsequent floods are often accompanied by substantial and varied sediment transport mechanisms including riverbank erosion, debris flows, rock falls and landslides (Arnone et al., 2016) which are amplified by steep hillslopes (Ahmad et al., 1993; Palm & Hodgson, 1993; Smith et al., 2005; Yuan et al., 2015). Colluvial and alluvial sediments that have been transported to the river system are then redistributed (Larsen & Román, 2001), causing varied geomorphic changes in headwaters and downstream channels (Clark & Wilcock, 2000a). Previous work has shown that the vast majority of annual suspended sediment load in Puerto Rican rivers occur during relatively few storm events, often associated with TCs (Gellis, 1993); notable examples include Hurricane Hugo, Hurricane Hortense, and Hurricane Georges (in 1989, 1996, and 1998, respectively; Yuan et al., 2015).

These prior studies highlight the potentially important role of conveyance capacity changes in flood hazard and risk in Puerto Rico. While climate-related streamflow changes are believed to happen on multidecadal time scales, conveyance capacity can respond very quickly to both natural and artificial changes (Phillips & Jerolmack, 2016). This implies that conventional hazard and risk analyses may substantially misstate conditions at any particular time, since short-term conveyance capacity may deviate substantially from longer-term behavior. While prior research on conveyance capacity changes in Puerto Rico has focused on long-term trends (Clark & Wilcock, 2000a), the frequency and magnitude of short-term channel changes are not well understood (Guan et al., 2016a; Phillips & Jerolmack, 2016).

2.3 Study Region and Data

Puerto Rico is an island in the northeastern Caribbean. Elevations in the mountainous interior range from 500 to more than 1300 m above sea level, while the coastal lowlands average 260 m. Annual precipitation in the interior is on the order of 500 cm, dropping to 100-400 cm in coastal areas. A wet season runs from May to October, mostly coinciding with the June-November North Atlantic TC season.

The US Geological Survey (USGS) maintains both historical continuous streamflow records and field measurements for several hundred stream gage stations in Puerto Rico, which are publicly available on the National Water Information System (NWIS). Records of both daily discharges and instantaneous annual peak flows were used in this study. We also examined historical daily precipitation records from four stations of the Global Historical Climatology Network (GHCN; Menne et al., 2012).

The USGS uses stage-discharge relationships, known as rating curves, to convert automatically-collected water height measurements to indirect estimates of river discharge. To maintain the accuracy of estimates generated using this approach, direct (i.e. manually performed) field measurements of streamflow and channel morphology must be made periodically and, if necessary, stage-discharge relationships are updated. The following field measurements are available through NWIS: discharge, water height, channel width, flow cross-sectional area, and flow velocity, as well as time of the measurements and other ancillary information. We used daily discharge records and peak flows to examine streamflow trends and to identify major flood events, and field measurements to build long-term stage-discharge relationships for each stream gage site. We used these data jointly to better understand the time evolution of river channel conveyance.

We only considered USGS stream gage stations which have roughly complete overlapping records of daily discharge and field measurements from 1990 or earlier until February 2019; most measurement records we used began around 1990, while some extend back to the early 1980s. Stations reported by the USGS as influenced by dams were excluded from the analysis, as were those co-located with man-made structures such as weirs since these would preclude channel morphological changes (Reisenbüchler et al., 2019a). If a station was reported by the USGS to have undergone a measurement datum change, then all field measurements prior to the most recent change were discarded. Stations were removed from the analysis if the most recent datum change resulted in incomplete records between 1990 and 2019. We also adopted the criteria of Slater et al. (2015) of only considering field measurements in which the discharge is within one percent of the product of channel velocity and cross-sectional channel area, as

reported by the USGS. Only field measurements made within 300 ft (roughly 90 m) of the gaging station were included; very few measurements were made directly at gage locations. The 39 sites satisfying these criteria are shown in Fig. 2.1, as are the four rainfall stations. The small number of sites in the northwest is linked to the much lower drainage density in that part of the island. Further details on the 39 sites are provided in Table S1.
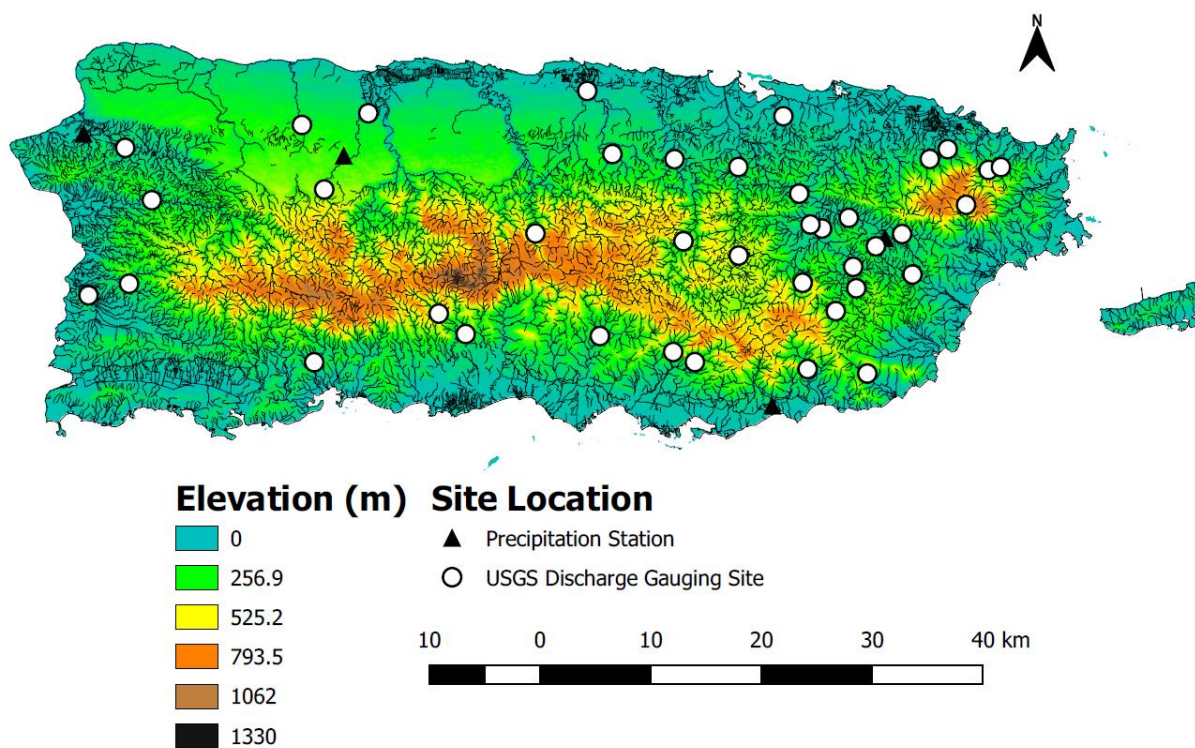
Fig. 2.1: Map of Puerto Rico, showing the USGS stream gages and GHCN precipitation stations considered in this study. The river network and land surface elevation above mean sea level are also shown.

Upstream watershed characteristics including elevation, slope, and land cover characteristics were used to assess potential drivers of flood hazard changes. Average elevation and slope were calculated for each gage based on a digital elevation model published by the NOAA National Centers for Environmental Information. Watershed boundaries corresponding to each stream

gage were downloaded from NWIS. Percentages of both developed and forested area were taken from the USGS GAGES-II dataset (Falcone et al., 2010). These are static values representing land cover composition at the time of measurement.

A list of TCs that affected Puerto Rico during the study period was obtained from NOAA's HURDAT-2 hurricane database (Landsea & Franklin, 2013). The names, dates, and durations of TCs considered in this study are provided in Table 2.1. If a high streamflow event happened within the duration of a TC, then we assumed that it was caused by that TC. Not all of the largest daily discharges were associated with TCs; other types of major rain producing systems can occur in the region (Smith et al., 2005).

Table 2.1. TCs considered in this study.

Tropical Cyclone	Start Date	End Date
Hurricane Debby	9/13/1982	9/20/1982
Hurricane Hugo	9/10/1989	9/25/1989
Hurricane Luis	8/28/1995	9/12/1995
Hurricane Hortense	9/3/1996	9/16/1996
Hurricane Georges	9/15/1998	10/1/1998
Hurricane Jeanne	9/13/2004	9/29/2004
Hurricane Noel	10/28/2007	11/7/2007
Tropical Storm Olga	12/11/2007	12/17/2007
Hurricane Otto	10/6/2010	10/18/2010
Hurricane Irene	8/21/2011	8/30/2011
Hurricane Irma	8/30/2017	9/13/2017

Hurricane Maria	9/16/2017	10/2/2017

2.4   Methodology

2.4.1 Rainfall and Streamflow Trend Analysis

Trend analyses were conducted on annual (water year, 1 October to 30 September) maximum three-day precipitation, annual total precipitation, annual total streamflow, and annual peak streamflow. Trends were assessed using both the non-parametric Mann-Kendall (M-K) test for monotonic trends (Mann, 1945) and Theil-Sen (T-S) nonparametric linear regression (Sen, 1968). Further discussion of these trend assessment methods is provided in Section 2.6.1.

Rainfall records, though few in number across Puerto Rico, tend to cover a longer time period than the discharge and field measurement records. To roughly match the time window of discharge and field measurement records, we chose to conducted rainfall trend analyses for the period 1980-2019. The 1980 start date was chosen to roughly coincide with the earliest available direct discharge measurements.

2.4.2 Conveyance Capacity Trend Analyses

2.4.2.1 Fitting Stage-Discharge Relationships

Long-term stage-discharge relationships (i.e. rating curves) were used to model the average state of conveyance capacity for each stream gage site; as described in Section 2.4.2.2, deviations from these relationships were then used to indicate temporal changes in conveyance. All streamflow field measurements for a site that meet the criteria described in Section 2.3 were used to fit a curve that describes the long-term stage-discharge relation. We chose to use shape

constrained additive models (SCAM; Pya & Wood, 2015) for this curve fitting. SCAM offer two benefits: 1.) akin to better-known smoothing methods such as locally-weighted scatterplot smoothing (LOESS), SCAM do not require a predefined model structure; 2.) unlike LOESS, a SCAM can be constrained to be monotonically increasing, which is conceptually consistent with stage-discharge relations and preserves reasonable curve behavior in the face of major conveyance capacity shifts. For SCAM fitting, we used tenth-order spline smoothing based on visual inspection of resulting fits.

2.4.2.2 Conveyance Capacity Trends

We illustrate our approach to estimate conveyance capacity trends using the USGS stream gage on Rio Grande Loiza at Caguas. The basic relationship between sediment movement and conveyance capacity is depicted in Fig. 2.2a: when sediment is deposited, channel cross-sectional area and thus conveyance capacity decreases. This translates to a decreased discharge, relative to pre-deposition conditions, for a given stage value, or conversely, an increased stage for a given discharge value. On the other hand, conveyance capacity increases when a channel is scoured, which will result in a higher discharge for a given stage, or a reduced stage value for a given discharge. (This assumes that there are no changes of velocity, which could be affected by changes in channel roughness due to vegetation growth or change in bed material—see Section 2.6.5.)

The gage's daily discharge record shows a number of high-magnitude flood events, including the largest, which resulted from Hurricane Hortense in 1996 (Fig. 2.2b and Table 2.1). Extreme discharge events that are used to separate the field measurements into different periods are

identified by picking the dates with high daily discharge, as explained below. In this example, the highest date of daily discharge occurred during Hurricane Hortense.

As explained in Section 4.2.1, the fitted stage-discharge relation is an indicator of long-term average channel conveyance capacity (Fig. 2.2c). We refer to differences between this fitted relation and observations as conveyance residuals. Systematic deviation of conveyance residuals from the curve for a particular time period indicates that a different stage-discharge relationship existed for that location over that period, which in turn indicates that the channel's conveyance capacity differed from the long-term average for that time period. While a single measurement's deviation from this long-term average could be attributable either to error in that measurement or in the fitted curve, a sudden and sustained systematic deviation in these residuals indicates a rapid change in channel conveyance in response to sediment scour or deposition at that location. This can be seen in Fig. 2.2c-d: residuals tended to be below the long-term curve prior to Hurricane Hortense, and above it afterward. Negative residuals suggest a loss of conveyance capacity due to deposition; positive residuals suggest higher conveyance capacity from scouring (Fig. 2.2c), assuming no changes in velocity. Thus, for this site, flooding associated with Hurricane Hortense caused substantial scour, which led to an abrupt increase in channel conveyance capacity.

We estimated long-term trends in conveyance residuals by fitting a T-S regression to the entire time series of conveyance residuals (Fig. 2.2d, gray line). For Rio Grande de Loiza at Caguas, this long-term trend was upward, suggesting an increase in capacity over time. This long-term trend, however, overlooks the role of the abrupt scour brought by Hurricane Hortense, as well as potential gradual changes before or after that flood. These effects are shown in Fig. 2.2d, with

separate T-S regressions for the time periods before and after Hortense. These regressions highlight that the actual behavior of conveyance capacity before and after Hortense differ substantially from the long-term trend. Specifically, these show a "gradual" loss of conveyance capacity over time before Hurricane Hortense and roughly constant behavior afterward, punctuated by intense scour during the storm.

To examine these issues in all 39 stream gage sites, we separated each conveyance residual time series by the n dates of highest daily streamflow. This produced $n + 1$ subperiods. The chosen value of n is discussed in Sections 2.4.2.3 and 2.6.3. As shown in Fig. 2.2d, T-S regressions were fit to the residuals within each subperiod. A regression slope represents the rate of conveyance capacity change within a subperiod; total change over the subperiod is calculated by multiplying that slope by the length of the subperiod. Instantaneous changes between consecutive subperiods were calculated by subtracting the T-S value corresponding to the end date of the first subperiod from the T-S value of the starting date of the next subperiod (e.g. the difference between points 2 and 3 in Fig. 2.2d).
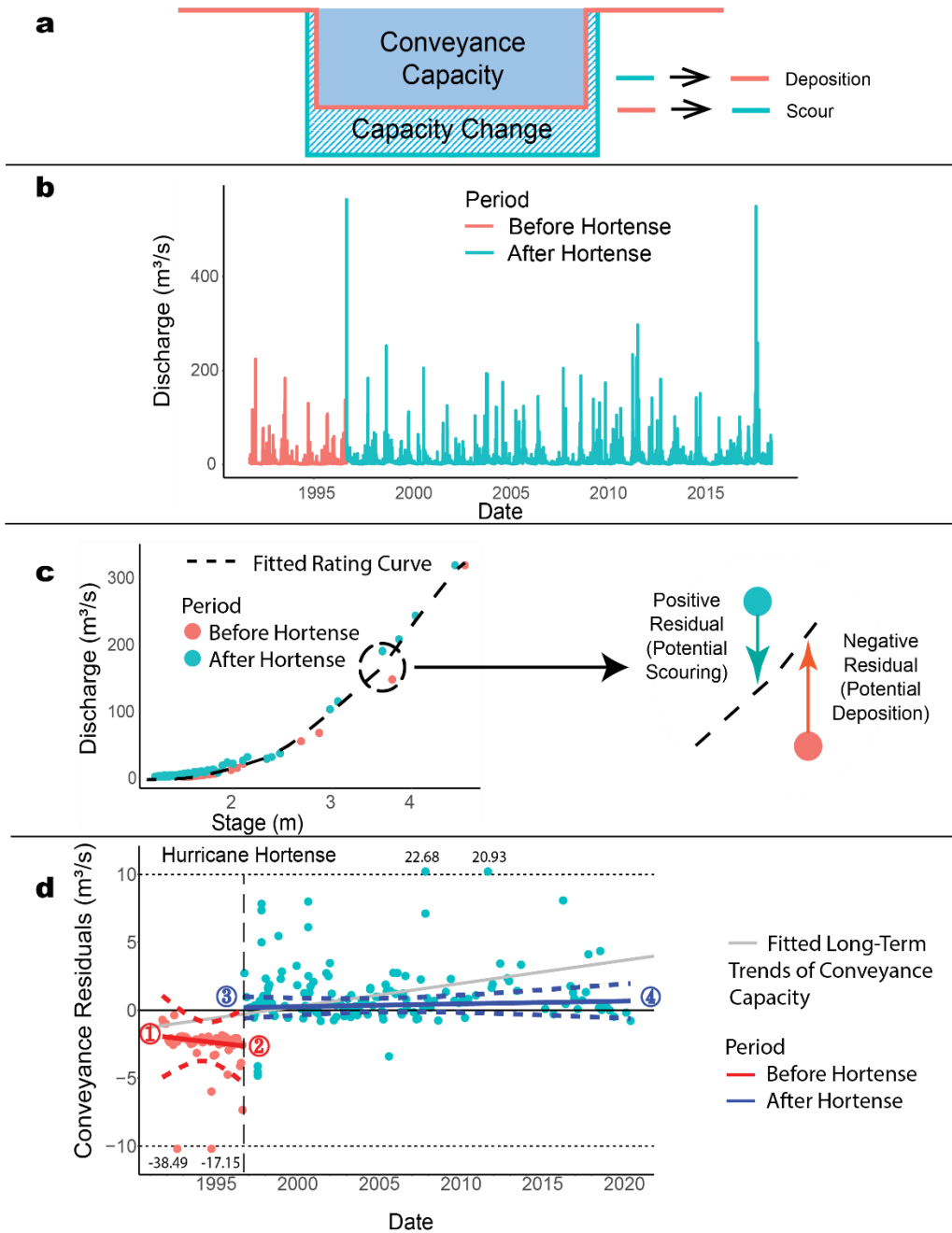
Fig. 2.2: Illustration of the conveyance analysis for the USGS stream gage Rio Grande de Loiza at Caguas (USGS station 50055000). a) Conceptual model of river channel conveyance capacity change. b) Time series of daily discharge at the site including Hurricane Hortense in September 1996. c) Stage-discharge relation (i.e. rating curve) fitted to field measurements, and residuals to the rating curve. d) Time series of conveyance residuals, fitted long time conveyance capacity change, instantaneous conveyance capacity change due to Hurricane Hortense (the difference between points 2

and 3), and gradual conveyance capacity change before Hortense (the difference between points 1 and 2) and after Hortense (the difference between points 3 and 4). 95% confidence intervals for the Theil-Sen fits to the gradual changes are shown by dashed lines. Individual conveyance residuals in Fig. 2.2d that are beyond the range of the y-axis are annotated.

2.4.2.3 Definition of Flood and TC-Related Flood Events

As described in Section 2.4.2.2, *n* flood events were picked from the daily discharge records for each site. The chosen value of *n* was equal to the number of years of available overlapping daily discharge and direct discharge records divided by ten and rounded down. This is equivalent to selecting flood events that have approximate recurrence intervals of at least ten years. We also re-ran analyses by selecting flood events that have approximate return periods of at least 5 years and at least 20 years, for comparison. We discuss this choice in Section 2.6.3. In the rare instance that two qualifying high-discharge events happened within a 14-day period, we omitted the smaller event from subsequent analysis, since few if any direct discharge measurements were available between the two floods. In addition, the 39 stations analyzed in this study had at least two direct discharge measurements within each subperiod; typically the number of measurements was substantially more—subperiods had on average 65.5 measurements.

2.4.2.4 Volatility of Conveyance Capacity

As illustrated in the previous section and Fig. 2.2, long-term trends in conveyance capacity are the result of a both gradual and instantaneous change components. We quantified this in terms of conveyance capacity "volatility" (i.e. the instability or unpredictability of conveyance relative to its long-term behavior), to describe the magnitude of these components relative to the overall long-term change. This volatility indicates how much the short-term conveyance capacity behavior at a site deviates from the long-term behavior. Thus, a site could have high conveyance

capacity volatility either by exhibiting substantial instantaneous changes during floods, substantial but more gradual changes during interflood periods, minimal long-term change, or some combination of these. We defined "total volatility" (TV) for a particular site as

$$TV = \frac{\sum_i |Gradual\ Change\ in\ ith\ Subperiod| + \sum_j |Instantaneous\ Change\ Caused\ by\ jth\ Flood\ Event|}{Long-Term\ Change}$$ Eqn. 2.1

We also defined "gradual volatility" (GV) and "instantaneous volatility" (IV) as

$$GV = \frac{\sum_i |Gradual\ Change\ in\ ith\ Subperiod|}{Long-Term\ Change}$$ Eqn. 2.2

$$IV = \frac{\sum_j |Instantaneous\ Change\ Caused\ by\ jth\ Flood\ Event|}{Long-Term\ Change}$$ Eqn. 2.3

TV, GV and IV satisfies that

$$TV = GV + IV$$ Eqn. 2.4

Both numerators and denominators of Eqns. 2.1-2.4 have the same units, rendering volatilities unitless. These volatilities are used to evaluate the manner in which conveyance changes over time (i.e. gradually or abruptly).

2.4.2.5 Watershed Drivers of Long-Term Trends

In an attempt to identify factors that contributed significantly to both streamflow and conveyance capacity trends, we conducted correlation analyses using linear (i.e. Pearson) and nonparametric rank (Kendall's tau; Kendall, 1938) correlation coefficients. Factors used in this analysis were elevation, slope, fraction of developed (i.e. settled) area, fraction of forested area, and the two-

year flood normalized by the watershed area. The latter was used as an indicator of watershed "flashiness."

2.5 Results

2.5.1 Precipitation and Streamflow Trends

A majority of stream gage sites show increasing trends in total annual discharge, while a majority of precipitation gages show increasing trends in total annual precipitation. T-S and M-K tests results both found that 35 (4) stream gage sites showed increasing (decreasing) trends in total annual discharge (see Fig. 2.3a for T-S results; see Fig. S1a for M-K results). The two methods disagreed, however, on the significance of these trends: T-S yielded 22 locations with significant trends (21 increasing and 1 decreasing; Fig. 2.3a), while M-K showed significant trends (all of which were increasing; at the 5% level) at only seven stream gage locations (Fig. S1a). No obvious spatial patterns to these trends are evident. Using T-S, all four rain gages showed increasing trends, three of which were significant at the 5% level. In contrast, no rain gages showed significant trends in annual precipitation using M-K: three (one) out of four showed insignificant increasing (decreasing) trends using M-K. While these results suggest increases in annual rainfall and streamflows in Puerto Rico, they also highlight a strong dependency on the particular method selected for trend analysis. This dependency is discussed further in Section 2.6.1.

Though the total annual discharge is generally increasing, a majority of stream gage sites showed decreasing trends in instantaneous annual peak discharge. T-S resulted in 27 stream gage sites showing decreasing peak discharge trends, while 12 showed increases (Fig. 2.3b). Twenty of

these showed significant trends in peak discharge (2 increasing; 18 decreasing). M-K resulted in 29 (10) stream gage sites with decreasing (increasing) peak discharge trends (Fig. S1b), only 6 of which (5 decreasing; 1 increasing) were significant at the 5% level. As with the trends in annual totals, there is no obvious spatial pattern to the extreme streamflow and rainfall trends. Three rain gages showed decreasing trends in annual maximum three-day rainfall (one of which was significant at the 5% level) and one showed an insignificant increasing trend according to T-S. Using M-K, two rain gages showed increasing trends and two showed decreasing trends, none of which were significant.
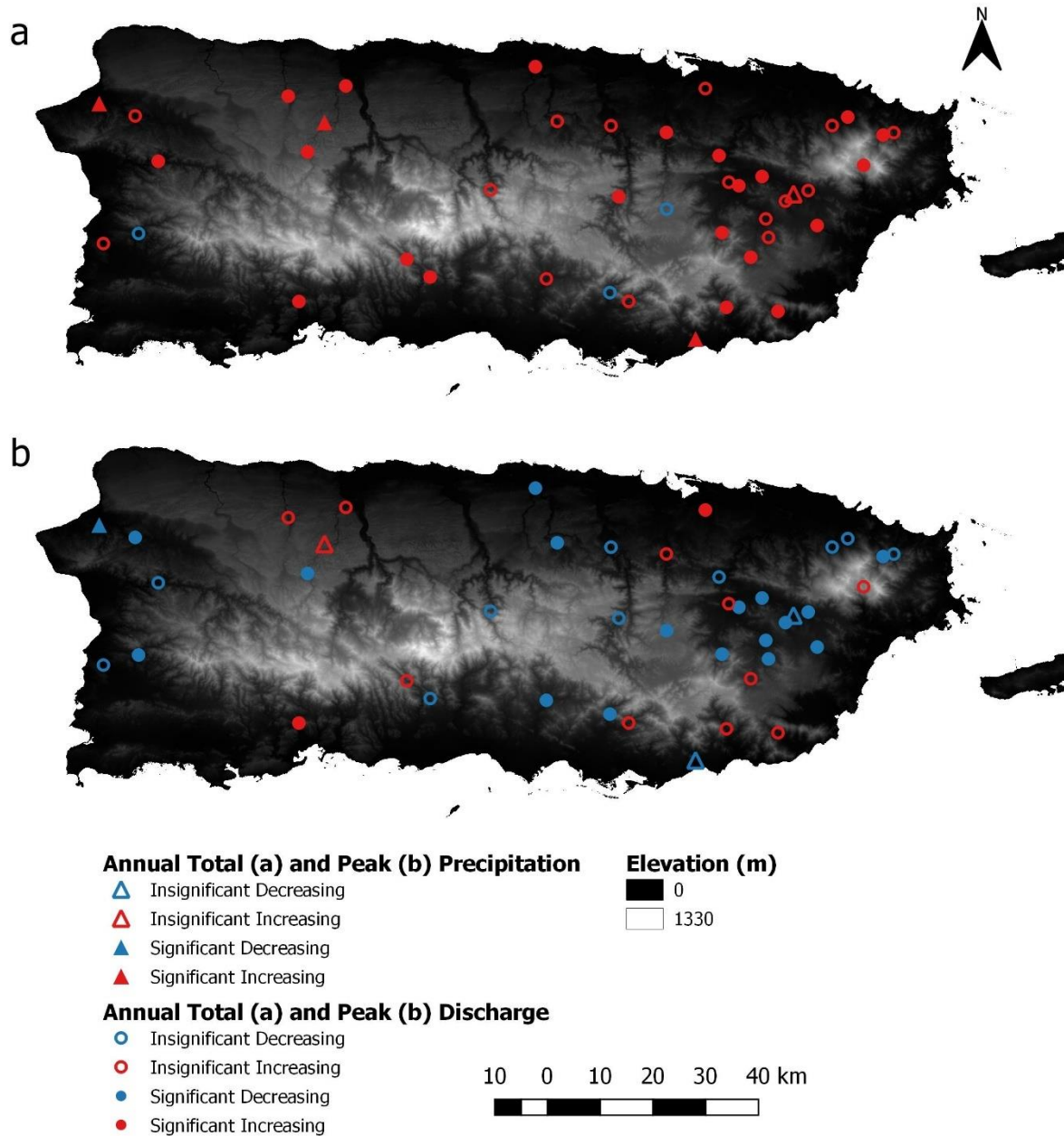
Fig 2.3: (a) Annual precipitation and discharge trend analysis using the T-S regression. Statistical significance is determined at the 5% level. (b) Annual maximum of three-day average precipitation and annual peak discharge trend analyses using T-S regression. Statistical significance is determined at the 5% level.

For the 36 stream gages that are part of the GAGES II dataset and thus for which land use and

other related information were available, we calculated both linear (Pearson) and rank (Kendall's

tau) correlation between T-S regression slopes and land cover, as well as other characteristics (Table S2). To remove the effect of watershed area, T-S slopes were normalized by upstream drainage area. We found a significant negative Pearson correlation (of -0.52; p=0.001) between T-S slope and area-normalized two-year flood, but this significance did not appear when rank correlation was used (-0.14; p=0.24). No other relationships between T-S slope and other factors were found to be significant at the 5% level.

2.5.2 Long-Term Conveyance Capacity Change

15 sites showed decreasing trends in long-term channel conveyance capacity using T-S, while the others showed increasing trends (Fig. 2.4). 34 of the 39 trends were significant at the 5% level, though no obvious spatial pattern is seen. Thus, similar to Slater et al. (2015)'s analysis in the continental U.S., long term conveyance capacity change in Puerto Rico is more widespread than streamflow change in that more sites show significant trends in conveyance capacity than in peak streamflow. No environmental factors were found to be significantly correlated (at the 5% level) with conveyance capacity T-S slopes (Table S3).

Long-Term Conveyance Capacity Change
○ Insignificant Decreasing
○ Insignificant Increasing
● Significant Decreasing
● Significant Increasing

Elevation (m)
■ 0
□ 1330

10 0 10 20 30 40 km
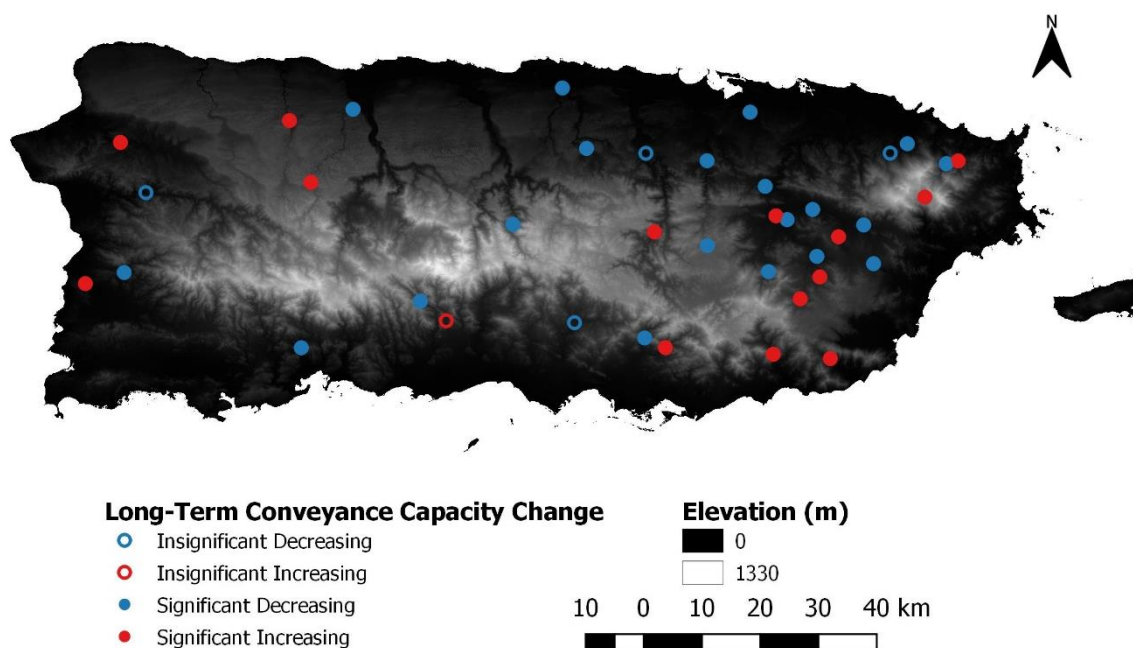
Fig. 2.4: Long-term conveyance capacity changes. Statistical significance is determined at the 5% level.

2.5.3 Instantaneous and Gradual Conveyance Capacity Changes and Volatility

Using the methods described in Section 2.4.2, we calculated instantaneous conveyance capacity change associated with each flood event, as well as gradual conveyance capacity changes for each subperiod between floods for all sites. We normalized these changes by upstream drainage area to remove the impact of watershed size. As described in Section 2.4.2.3, we focused on changes in response to floods with approximately recurrence intervals of 10 years and above. This yielded two or three flood events and corresponding instantaneous conveyance changes, and thus three or four inter-flood gradual changes, per site depending on the length of the site's direct discharge record. Correlation analyses were done by pooling together the data points from all sites. We found a significant negative linear correlation (-0.23; p=0.03) between normalized instantaneous conveyance capacity change and the normalized discharge of the flood event

(Table S4). This result was insignificant, however, when rank correlation was used, and no relationships between T-S slope and any other factor were found to be significant at the 5% level using either type of correlation. Long-term conveyance capacity trends depict linear change over multidecadal periods. As argued in Section 2.4.2 and illustrated in Fig. 2.2, however, long-term trends result from roughly instantaneous step changes associated with floods, separated by more gradual changes between flood events. As mentioned in Section 2.4.2.4, we are particularly interested in conveyance volatility, i.e. the instability of conveyance capacity relative to its long-term behavior. Here, we show several additional examples before presenting analysis of island-wide volatility.

In locations with little evidence of instantaneous conveyance capacity change, the sum of short-term (i.e. gradual) changes between floods will roughly coincide with the long-term change, TV and GV will be close to 1.0, and IV will be close to zero (Fig. 2.5; see Eqns. 1-4). On the other hand, when long-term change is minimal, there can still be substantial temporal variability—both rapid changes associated with the passage of a flood and gradual change between floods, the latter often showing a gradual "recovery" of preflood conveyance conditions (Fig. 2.6, 2.7 and 2.8), which is consistent with quasi-equilibrium theory (e.g. Ritter et al., 2002; see Section 2.6.2 for discussion). This can produce very large volatility values when the small denominator in Eqns. 2.1-2.3 is small. This phenomenon is supported by statistically significant negative correlation between the magnitudes of instantaneous changes and subsequent gradual changes (linear correlation of -0.37 with $p < 10^{-3}$; rank correlation of -0.36, $p < 10^{-6}$).
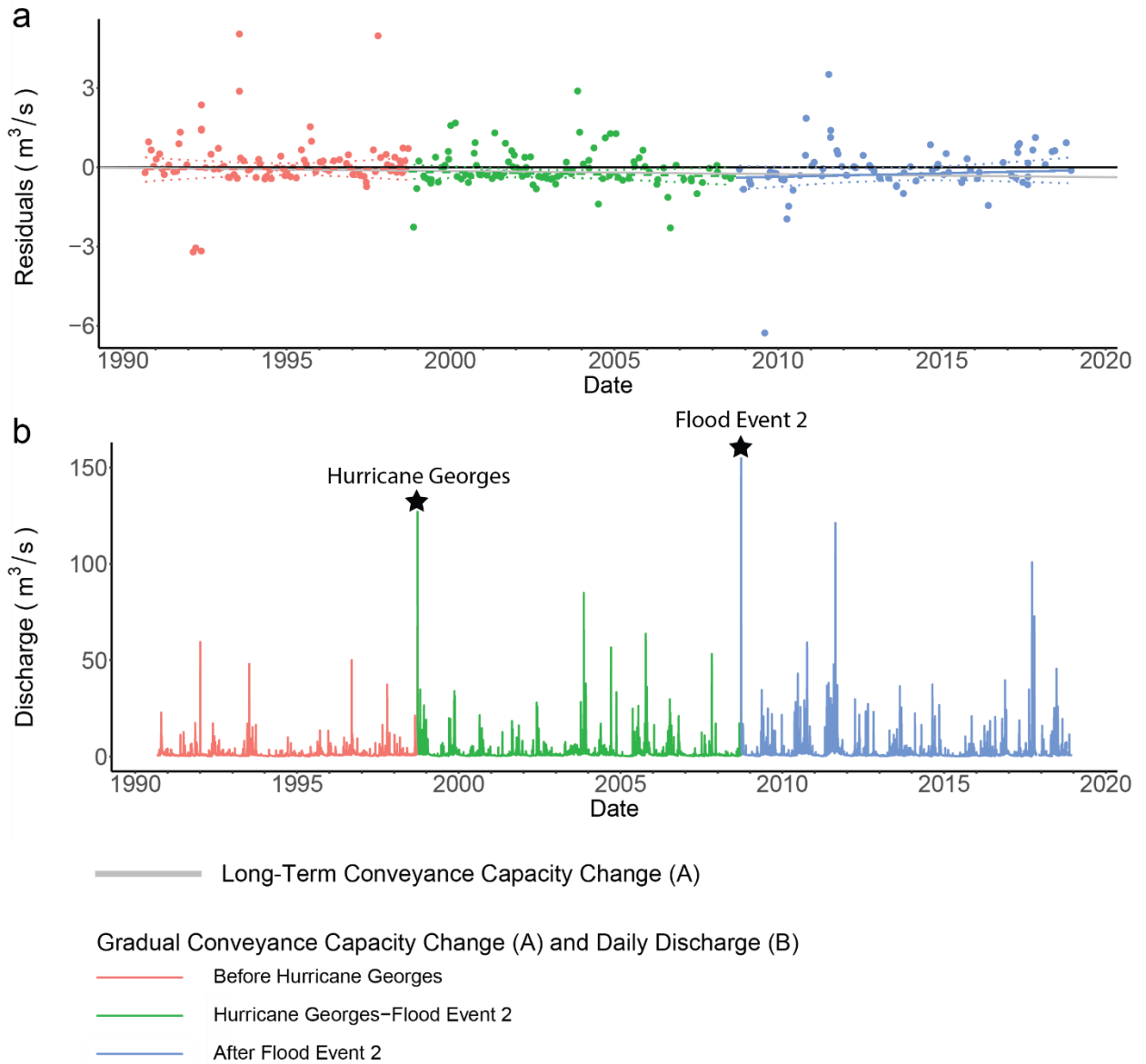
Fig. 2.5: (a) Conveyance capacity residual and (b) daily discharge time series at Rio Grande de Patillas near Patillas (USGS station 50092000). Total volatility is -2.17. The long-term trend of conveyance capacity residuals is represented by the gray solid line, which is significant at 5% level.
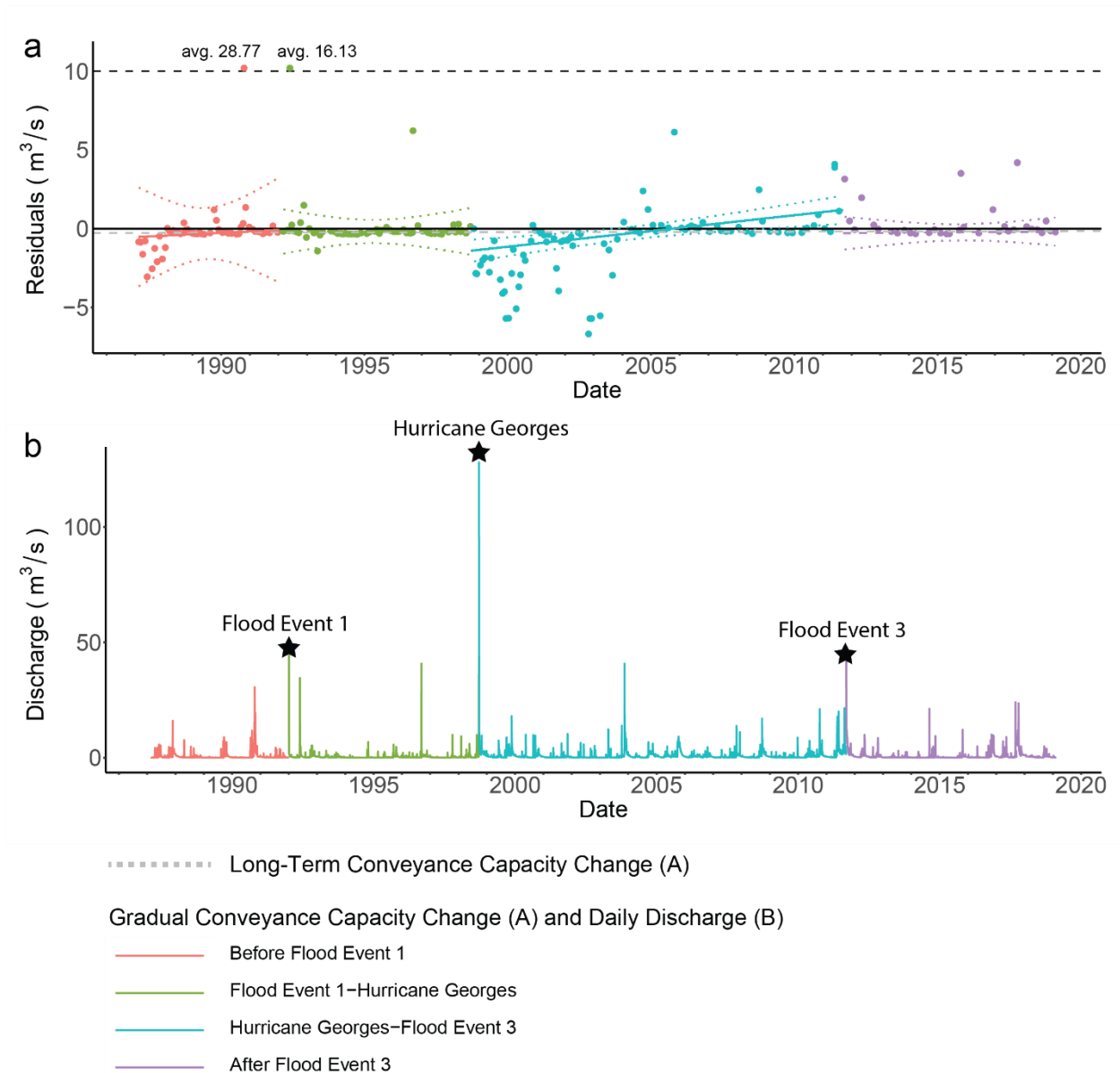
Fig. 2.6: (a) Conveyance capacity residual and (b) daily discharge time series at Rio Coamo at Highway 14 at Coamo (USGS station 50106100). Total volatility is 63.28, due to the very low denominator in Eqn. 2.1. The long-term trend of conveyance capacity residuals is represented by the gray dashed line, which aligns approximately with the x-axis and is insignificant at 5% level. Conveyance residual values beyond the range of the y-axis (dashed lines) are provided.
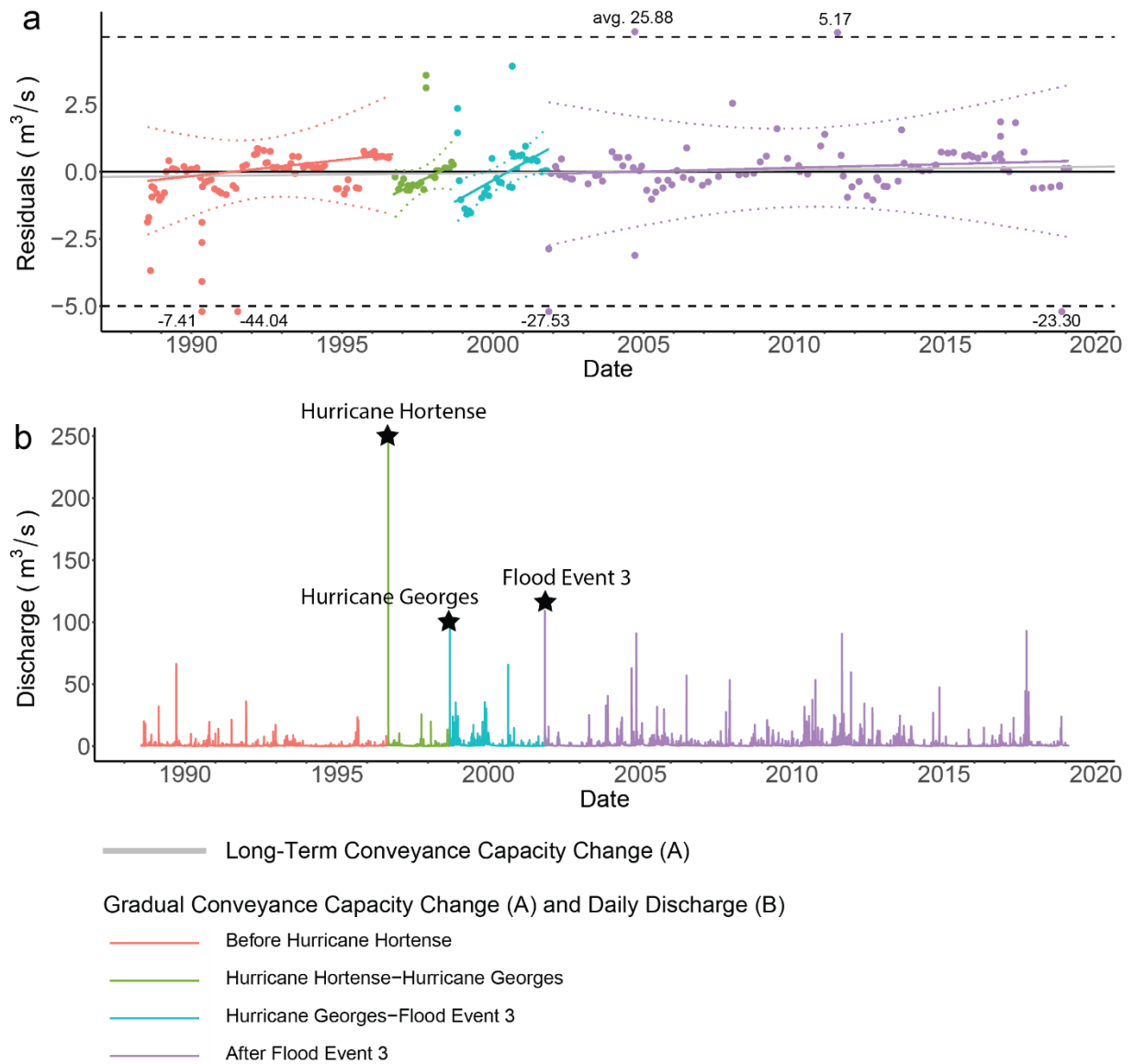
Fig. 2.7: (a) Conveyance capacity residual and (b) daily discharge time series at Rio de Bayamon near Bayamon (USGS station 50047850). Total volatility is 23.69. The long-term trend of conveyance capacity residuals is represented by the gray solid line, which is significant at 5% level. Conveyance residual values beyond the range of the y-axis (dashed lines) are provided. The three instantaneous conveyance capacity changes are negative (indicative of deposition), while the four gradual conveyance capacity changes are positive (indicative of scour).
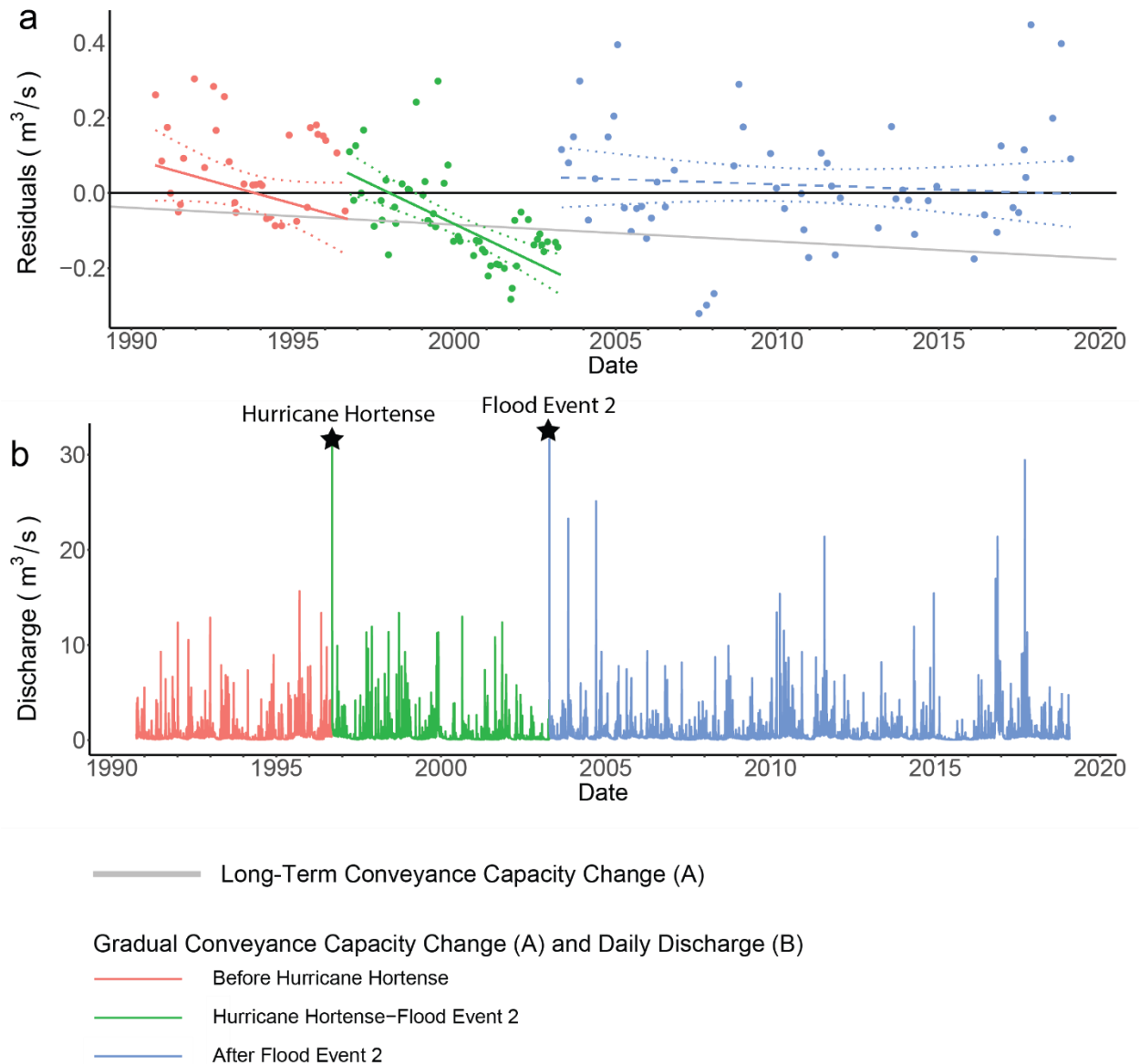
Fig. 2.8: (a) Conveyance capacity residual and (b) daily discharge time series at Rio Sabana at Sabana (USGS station 50067000). Total volatility is -6.58. The long-term trend of conveyance capacity residuals is represented by the gray solid line, which is significant at 5% level. Both instantaneous conveyance capacity changes are positive (indicative of scour), while the three gradual conveyance capacity changes are negative, indicating deposition.

TV ranges from -35 to more than 300, and 38 out of 39 sites have an absolute value of TV greater than 1.0. The median absolute value of TV is 6.8, highlighting the prevalence of both

instantaneous and inter-flood changes in channel conveyance throughout Puerto Rico. Results for

the three volatility metrics (Eqns. 2.1-2.3) are shown both spatially and in boxplots in Fig. 2.9.
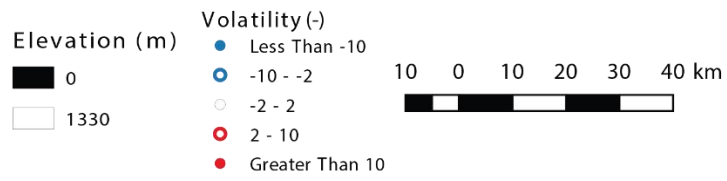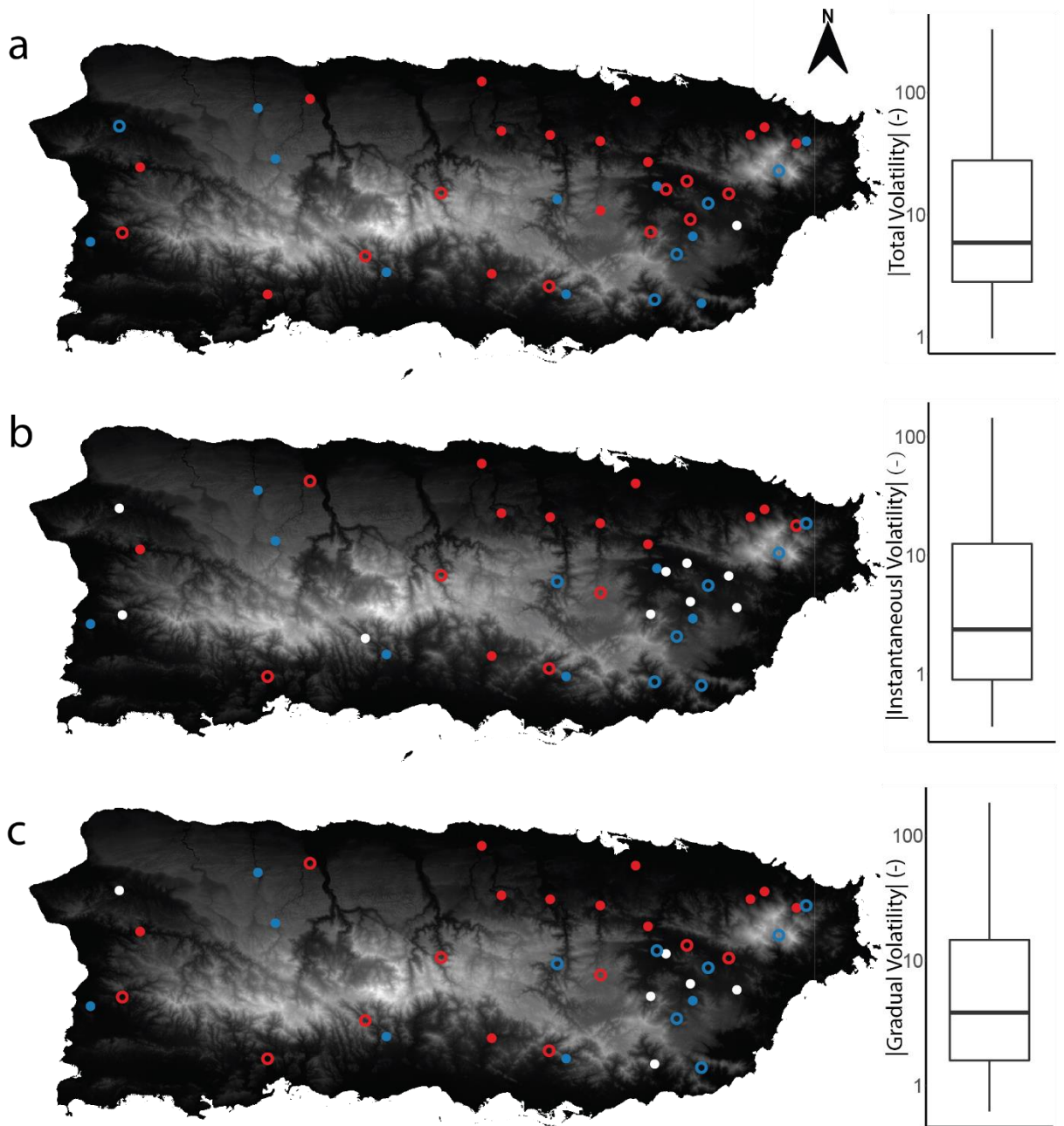
Fig. 2.9. Left column: spatial distribution of conveyance volatilities in Puerto Rico. Right column: boxplots of absolute values of volatilities. (a) Total Volatility (TV), (b) Instantaneous Volatility (IV), (c) Gradual Volatility (GV).

We conducted correlation analyses of TV, GV, and IV against watershed characteristics (slope, forested fraction, etc.). Results were similar for all the three metrics, and no significant correlations were found with any watershed characteristic (Tables S5, S6, and S7).

We also calculated the relative prevalence of instantaneous changes due to scour and deposition. Recall that we considered two or three flood events per site. We thus grouped sites into three classes based on the relative frequency of floods that caused scour and deposition: 1.) more depositional events than scour events; 2.) more scour events than depositional events; 3.) equal number of depositional and scour events. There does not appear to be a tendency toward scour or deposition at the island scale (Fig. 2.10), though scour-prone sites are concentrated in the eastern portion of the island. We also conducted rank correlation analyses and multiclass ANOVA between the relative frequencies of scouring and deposition and watershed characteristics; no result was found to be significant at the 5% level (results not shown).
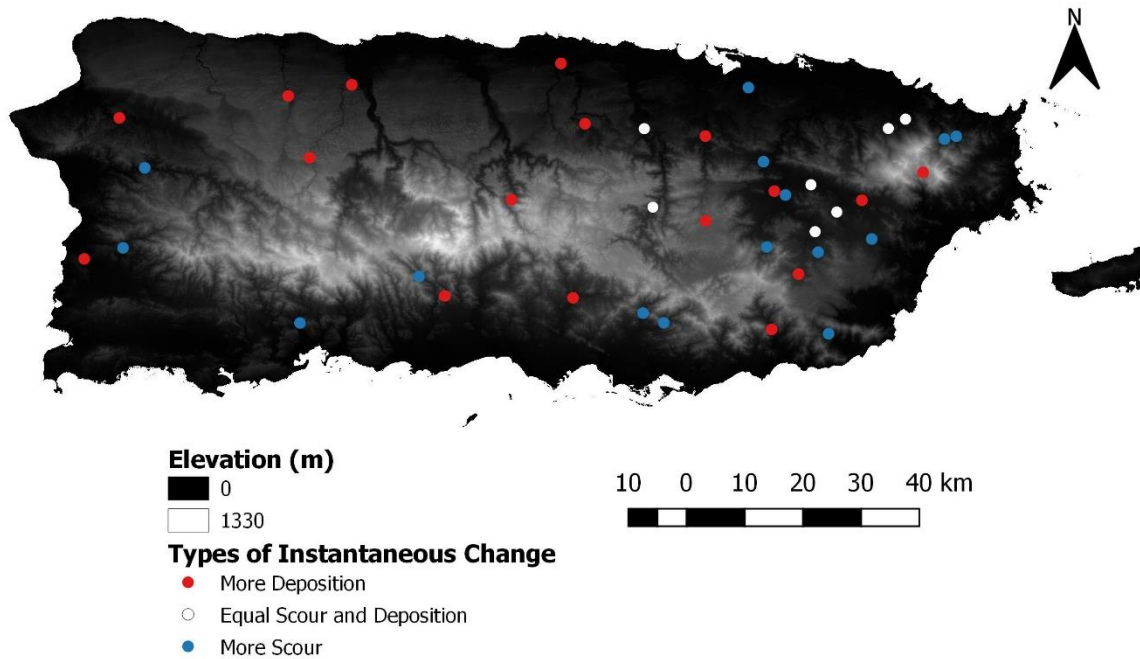
Fig. 2.10. Relative prevalence of instantaneous changes due to scour and deposition.

2.5.4 Comparison of Peak and Conveyance Capacity Trends

All 39 sites had greater peak discharge changes than conveyance capacity changes. On average, annual peak discharge trend slopes are about 25 times of annual conveyance capacity trend slopes (in unit of $m^3 s^{-1} y^{-1}$). A majority (27 of 39 sites) had peak discharge and long-term conveyance capacity changes which are complementary of each other, i.e. both leading to increased or decreased flood hazard.

Though long-term conveyance capacity changes are smaller in magnitude than peak discharge changes, both instantaneous and gradual changes are in some cases comparable to peak discharge change. Specifically, at sites 50028400 and 50138000, the absolute sums of instantaneous capacity changes exceed the peak discharge changes. At site 50138000, the absolute sum of the gradual conveyance capacity changes also exceeds the peak discharge changes. These results

emphasize that the conveyance capacity changes during and between floods can cause potentially substantial fluctuations of flood hazard at time scales up to roughly a decade, even if conveyance capacity on longer time scales changes very little (e.g. Fig. 2.6).

It should be noted that these comparisons of trends in peak discharge and conveyance residuals is not without limitations. These are discussed further in Section 2.6.5.

2.6   Discussion

2.6.1 Trend Test Selection and Change Point Test

It is common in the hydrologic trend literature to report both M-K statistical significance and the T-S slope magnitude (e.g. Hannaford & Buys, 2012; Yeh et al., 2015). Combining the two tests is straightforward when hydrologic records have regularly-spaced data, such as the annual total or maximum precipitation or streamflows (i.e. Section 2.4.1). Many hydrologic measurements, including USGS direct-discharge measurements (Section 2.4.2), however, are irregular in time, with large gaps interspersed with periods of more intense sampling. Trend analysis on irregularly-spaced time series is an understudied area (Eckner, 2012). While it is possible to convert unevenly spaced data to regular intervals through interpolation (e.g. Goudarzi et al., 2013), doing so neglects the stochasticity around the conditional mean, potentially changes causal relationships, and introduces data loss (Eckner, 2012). It has been argued that T-S is better suited for analyzing irregularly-spaced time series since it explicitly considers the time difference between each pair of data points (Sen, 1968; Sievers, 1978). Nonetheless, comparison of T-S and M-K trend results in Section 5.1 suggest that these two methods can produce quite different results. In our experience, T-S tended to give more significant results than M-K tests (e.g. Figs.

2.3 and S1). Potential differences in results and conclusions arising from different trend analysis techniques have led others to argue that it is necessary to use the same technique when comparing different datasets (as we do here), since application of distinct methods to different datasets introduces biases that limit intercomparison (Clarke, 2013). Given the temporal irregularity of direct discharge measurements, we chose to use T-S alone to analyze conveyance capacity trends.

Those issues notwithstanding, it should be noted that T-S and M-K did paint a similar overall picture of annual and peak discharge changes in Puerto Rico: annual discharge appears to be increasing while the peak discharge appears to be decreasing (Section 2.5.1; Figs. 2.3 and S1). Annual precipitation also appears to be increasing, while peak precipitation trends are unclear. Precipitation analyses, however, were limited by the small number of sites.

Despite the abrupt nature of instantaneous changes in conveyance capacity, we elected not to employ change-point detection such as the Pettitt test (Pettitt, 1979). This is a rank-based non-parametric change point test widely used in hydrologic trend studies. To our knowledge, however, its applicability to unevenly spaced time series has not been assessed, and prominent examples in the literature apply it to regularly-spaced data (e.g. Chen & Chu, 2014; Mallakpour & Villarini, 2016; Moknatian & Piasecki, 2019; Zhang et al., 2009). Likewise, due to the unevenly spaced time series, we were not able to examine autocorrelation or conduct "pre-whitening" techniques (e.g. Bayazit & Önöz, 2007) before applying T-S.

2.6.2 Relationship between Instantaneous and Gradual Conveyance Changes

Many sites (e.g. Figs. 2.6, 2.7 and 2.8) displayed instantaneous conveyance capacity change due to a flood event followed by a gradual conveyance capacity "recovery" in the opposite direction. This behavior is in agreement with river quasi-equilibrium theory, which states that rivers attempt to establish an equilibrium relationship between the dominant discharge and sediment load by adjusting its hydraulic variables (Ritter et al., 2006). It is believed that temporal changes in hydraulic geometry are the direct result of channel adjustments to natural or anthropogenic disturbances (Shugar et al., 2017; Mulahasan et al., 2017; Slater et al., 2019). The fact that long-term conveyance trends represented by T-S regressions to a site's entire records of conveyance residuals are often different from zero in our analysis suggests, however, that at least some river channels in Puerto Rico do not have a long-term quasi-equilibrium state, at least in the face of long-term changes in climate, land use, or other characteristics. Our lack of success in identifying watershed drivers of these trends (e.g. Tables S3, S4), however, suggests that the driving forces will take more effort to isolate. It is also not clear how long is "long enough" for quasi-equilibrium to be observed.

2.6.3 Drivers of Channel Capacity Change

We were largely unsuccessful in identifying watershed drivers of channel capacity change (e.g. Tables S3, S4). Yuan et al. (2015) reported similar difficulty in identifying drivers of sediment transport in Puerto Rico, though some other studies have shed some light on the issue. Clark and Wilcock (2000) reported a trend toward more frequent landslides due to agricultural expansion in the northeastern portion of the island, while Gellis (1993), focusing on a single watershed in the northeast, studied how vegetation damming complicates and potentially reduces sediment transport.

As described in Section 2.4.2, we examined instantaneous changes resulting from floods with recurrence intervals of roughly 10 years or greater. This threshold provided an automated way of identifying instantaneous conveyance capacity changes. It was necessary to use a flood threshold high enough to "capture" large instantaneous changes in the conveyance residual time series, and low enough so that these obvious changes were not overlooked. Visual inspection confirmed that this threshold nearly always produced reasonable identification of instantaneous changes. Nonetheless, we repeated selected analyses using floods of approximately 5-year and 20-year (or greater) recurrence intervals (Tables S4, S5, S6, S7). Due to the relatively short direct discharge records, using the 20-year recurrence interval and above led to many sites having either zero or one such flood events, despite having multiple visually-obvious conveyance capacity changes. When using the 5-year or greater recurrence interval, visual inspection revealed that a number of events (generally those close to the 5-year "cutoff") did not correlate with obvious changes. Taken together, these findings not only support our choice of using 10-year and above flood events to identify instantaneous conveyance capacity changes, but also suggests that the 10-year flood is the approximate threshold in Puerto Rico for producing major instantaneous channel reconfiguration and subsequent gradual response to re-establish quasi-equilibrium. This threshold is much lower than those examined in previous studies in different hydrologic, geologic, and climatic settings (Dai & Lu, 2010; Heritage et al., 2004; Krapesch et al., 2011; Smith et al., 2000).

2.6.4 Role of Tropical Cyclones

The highest daily discharges at 36 out of 39 sites can be matched to just three TCs: Hurricane Hortense, Hurricane Georges and Hurricane Maria. Across all sites, a total of 91 daily discharges

of at least ten-year return interval were identified; 81 of these 91 (89%) can be attributed to a TC. This shows the importance of hurricanes on both large floods and conveyance capacity changes in Puerto Rico. If instead the five-year recurrence interval threshold is used for identifying instantaneous capacity changes, 207 daily discharges are found, 125 (60%) of which are attributable to TCs. The reduction in the percentage of TCs for the lower recurrence interval threshold means that high recurrence interval flows are very often associated with TCs, while more frequent events are often not. This, combined with the argument that the 10-year recurrence interval appears to be the approximate threshold for major conveyance changes, suggests that TCs are the principal driver of conveyance capacity change in Puerto Rico.

The importance of TC-related extreme rainfall and freshwater flooding in Puerto Rico suggests that future changes in flood hazard there and in other similar settings will be driven to a large extent by changes in TC frequency, rainfall production, and other storm properties. Climate modeling suggests that North Atlantic TC rainfall rates will increase by 5-20% due the effects of global warming (Knutson et al., 2010; Walsh et al., 2016; Wuebbles et al., 2017). Furthermore, the mean translational speed of North Atlantic TCs over land has decreased by 20% since the mid-20th century (Kossin, 2018). Effects of these projected changes may be tempered by a projected decrease in TC frequency (Knutson et al., 2020). Nonetheless, these changes have important implications since more intense, slower-moving storms are more likely to generate large rainfall amounts and consequent flooding, which, based on our findings, can alter channel conveyance capacity and thus, exert influence over flood hazard and risk even after the immediate danger of the TC has passed. This in turn violates the assumption of statistical independence between flood events that is typically made in flood frequency analysis.

2.6.5 Additional Methodological Discussion

Our approach resembles that used in Slater et al. (2015)'s analysis of conveyance change in the continental United States: we quantified conveyance capacity change using residuals of fitted stage-discharge relationships. Our specific methodology differs somewhat from Slater et al. (2015), largely because we were more constrained by data limitations: USGS direct discharge measurements, particularly of high streamflows, are generally fewer and cover shorter time periods in Puerto Rico than in the continental United States.

Slater et al. (2015) compared trends in the frequency of streamflows and conveyance capacity exceeding approximately bankfull conditions. Their approach ensures that both streamflow and conveyance capacity trends are studied at the same flood stage, which facilitates comparison of streamflow and conveyance capacity changes. We were unable to replicate this approach, however, due to the sparsity of direct discharge measurements at and beyond bankfull conditions. In Section 2.5.4, we instead compare streamflow and conveyance residual trends in terms of their values (in $m^3s^{-1}yr^{-1}$) rather than their frequencies. This comparison is imperfect, however, in part because the conveyance residuals are generally associated with lower streamflow conditions than the annual flood peaks. While we cannot state this conclusively, we believe that this likely translates to an understatement of the actual magnitude of the conveyance changes for high flow regimes (i.e. bankfull and beyond), as one may expect the magnitude of conveyance residuals to increase with streamflow magnitude. However imperfect this comparison, we nonetheless still found that short-term conveyance capacity changes can exceed peak discharge changes at some sites. That our method may understate the importance of short-term conveyance capacity change

for high streamflow conditions further highlights the need for further research, including data collection and methodological development.

There are several more minor differences between the methods of Slater et al. (2015) and our study. They calculated residuals from LOESS-based stage-discharge relations; our particular research objective and stage-discharge concept both imply a need for monotonicity in these relations, which we ensured using SCAM-based fitting (e.g. Fig. 2.2).

As explained in Section 2.3, while few field measurements were made exactly at the location of the gage, we only considered measurements made within 300 feet (roughly 90 m) of the gage location, as reported in the field measurements. Differences in measurement location have the potential to introduce error to our analysis. Specifically, systematic variation in measurement location over time would seriously threaten the validity of our methodology, while random variation in measurement location would add noise but not otherwise compromise validity. We examined time series of the distances of field measurements to the gauging stations and found little evidence of systematic variation. We nonetheless advocate consistency in the locations of future measurements to improve accuracy of rating curves and to strengthen the validity of studies such as ours.

In this research, we assumed that the conveyance capacity changes are caused by sediment transport like deposition and scour. These are not the only processes that can cause conveyance capacity to change, however. Channel roughness, which can be influenced by in-channel vegetation (Wu & He, 2009) and sediment type (Robert et al., 1992), can affect channel velocity, which in turn can affect conveyance capacity. Our data did not allow us to examine these

roughness impacts, and we believe this is a necessary future step to fully understand these phenomena.

2.7   Summary and Conclusions

Although river channels can adjust to climate (Shugar et al., 2017) and land cover change (Mulahasan et al., 2017) on interannual to multidecadal scales (Slater et al., 2019), the role of both instantaneous and short-term (i.e. up to several years) changes in this process of adjustment has received relatively little attention. Nearly instantaneous changes can result from the mobilization of sediment during major floods; this sediment can then be redistributed under the less-extreme hydrologic and hydraulic conditions that follow. Prior work has suggested that in most climatic and geologic settings, floods capable of significantly reconfiguring river channels are relatively rare, perhaps beyond the 100-year recurrence interval (Dai & Lu, 2010; Heritage et al., 2004; Krapesch et al., 2011; Smith et al., 2000).

The extreme rainfall typically associated with tropical cyclones (TCs), combined with steep slopes and erosive soils in Puerto Rico and other tropical environments, however, suggests that flood events capable of channel and floodplain alterations may be much more common in such settings. Meanwhile, such reconfiguration is generally ignored in analyses of flood trends, flood frequency, and flood risk. Flood frequency analysis in particular assumes—for mathematical convenience—that successive flood events are statistically independent.

These issues, combined with the fact that Puerto Rico and other similar environments regularly suffer severe social and economic impacts from TC-related freshwater floods, suggests that better understanding of the temporal evolution of river channel conveyance capacity in such environments is needed. Our study attempts to deepen this understanding. Key findings and conclusions are summarized here:

1. Both annual total and peak streamflows, as well as channel conveyance capacity, are changing in Puerto Rico, though the drivers of these changes are not obvious. Long-term changes in annual flood peaks are often larger in magnitude than long-term changes in channel conveyance capacity, though the latter are more widespread in terms of statistically significant change, consistent with recent findings in more temperate climates (Slater et al., 2015).

2. Observed long-term channel conveyance capacity trends are composed of one or more relatively instantaneous changes resulting from sediment deposition or scour during major flood events (the most widespread of which was Hurricane Hortense in 1996), followed by short-term (typically several years in length) "gradual" changes between floods. For a given location, instantaneous and gradual changes typically have opposite signs, indicating quasi-equilibrium channel adjustment in response to major floods.

3. Multi-decadal records of direct discharge measurements can help to understand the temporal evolution of channel capacity changes. The limitations of these data are apparent, however, when it comes to understanding the climatic, landscape, and hydraulic controls on this evolution. Additional field work is likely required to remedy this.

4. It appears that substantial changes in channel conveyance capacity in Puerto Rico can result from floods of roughly ten-year recurrence interval and above. Such changes thus appear to be much more common in Puerto Rico than in the more temperate environments examined in previous studies. Furthermore, TC rainfall and the floods they produce are the dominant drivers of these changes. Thus, future changes in the frequency, rainfall production, and other properties of TCs will likely influence flood hazard in Puerto Rico and similar settings not only via direct impacts on streamflow but also through the alteration of channel conveyance in ways that can magnify or reduce subsequent susceptibility to flooding.

5. Instantaneous conveyance capacity changes can be several orders of magnitude larger than long-term conveyance capacity trends and can also be larger than extreme streamflow trends. This emphasizes the importance of channel evolution on flood hazard over short time scales and calls into question the statistical independence assumption that underpins conventional flood frequency and flood risk analysis.

In summary, our study shows that short-term conveyance capacity change in Puerto Rico is widespread and can be comparable in magnitude to those of long-term peak streamflow change. TCs, which are predicted to intensify in a warming climate, not only cause the largest floods in Puerto Rico but are also critical drivers of conveyance capacity changes, which can in part determine the severity of future floods. More work is needed to understand the time evolution of flood hazard, flood risk, and mitigation options in Puerto Rico and in other similar environments in response to the multiple influences exerted by TCs in a warming climate.

Chapter 3   Drivers of At-a-station Hydraulic Geometry (AHG) of Stream Reaches in Puerto Rico

Adapted from: Li, Yihan, Daniel B. Wright, and Brian P. Bledsoe. "Watershed Controls and Tropical Cyclone-Induced Changes in River Hydraulic Geometry in Puerto Rico", manuscript submitted to Journal of Hydrology: Regional Studies

3.1   Introduction

River cross sectional geometry is both a determinant and result of fluvial processes, including flood conveyance (Guan et al., 2016b; Kale & Hire, 2004), sediment transport (Bennet & Bridge, 1995; Bridge, 1993), riparian vegetation growth (Malkinson & Wittenberg, 2007) and channel erosion (Millar & Quick, 1993; Wiman & Almstedt, 1997). At-a-station hydraulic geometry (AHG) describes the relationships between discharge vs. water-surface width, mean depth, and mean velocity at individual river cross sections. Power law formulations have long been used to model AHG, and these formulations have been widely applied to understand river geomorphology (e.g. Andreadis et al., 2013; Barefoot et al., 2019; Knighton & Wharton, 2014; Leopold et al., 1964; Reid et al., 2010; Stewardson, 2005). The standard AHG formulation, which first appeared in Leopold & Maddock (1953), is

$$w = aQ^b \qquad \text{Eqn. 3.1}$$

$$d = cQ^f \qquad \text{Eqn. 3.2}$$

$$v = kQ^m \qquad \text{Eqn. 3.3}$$

where w is channel width (typically the wetted width), d is the hydraulic depth (i.e. cross-sectional area divided by w), v is mean stream velocity, and Q is the instantaneous discharge. The requirement of continuity,

$$Q = wdv = ackQ^{b+f+m} \qquad \text{Eqn. 3.4}$$

implies the constraints $ack = 1$ and $b + f + m = 1$.

The coefficients (a, c, and k) describe the relative magnitude of channel width, channel depth and velocity (or roughness), while the exponents (b, f, and m) provide insight into how channel width, channel depth and velocity change with discharge. Notwithstanding these constraints, the coefficients and exponents from Eqns. 3.1-3.4 can vary substantially from place to place (Morel et al., 2020b; Park, 1977), and researchers have yet to fully reveal the physical principles that underly AHG behavior (Jia et al., 2017; Morel et al., 2019), not for lack of trying (e.g. Dingman, 2007; Ferguson, 1986). Watershed and river reach characteristics that have been shown to explain some observed AHG variability include drainage area (Qin et al., 2020), watershed orientation and channel substrate (Turowski et al., 2008), suspended sediment load (Wang et al., 2006), and reach slope (David et al., 2010). While recent work has built predictive models for AHG exponents (b, f, and m; Morel et al., 2019, 2020a), the coefficients a, c, and k have received less attention (Morel et al., 2020a; Qin et al., 2020; Ran et al., 2012; Turowski et al., 2008). Relationships have also been shown between AHG parameters from various cross sections within individual river systems. Dingman (2007) found that there are theoretical interdependencies among AHG coefficients and exponents; Turowski et al. (2008) found that the relationship between the ratio $\frac{f}{b}$ and the exponent b follows a power law for data from Taiwan.

Gleason & Smith (2014) found that local AHG coefficient and exponent pairs (a and b, c and f, k and m) from different locations along the same river follow a log-linear relationship; they termed this at-many-station hydraulic geometry (AMHG). Barber & Gleason (2018) then verified that most rivers in continental U.S. follow AMHG. The empirical AMHG was reconciled theoretically with AHG by Brinkerhoff et al. (2019).

Channel morphology has also been shown to change over time due to natural processes like changes in suspended sediment load (Wang et al., 2006), changing high latitude river ice regimes (Best et al., 2005), floods (e.g. Hajdukiewicz et al., 2016; Magilligan et al., 2015; Pike et al., 2010; Sholtes et al., 2018; Yochum et al., 2017), and due to human activities including urbanization (e.g. Booth, 1990; Hawley et al., 2013), land cover changes (Clark & Wilcock, 2000b; Fitzpatrick & Knox, 2000), reservoir operations (Ran et al., 2012; Su et al., 2015), and sand excavation (Zhang et al., 2015). Nonetheless, analyses of temporal changes in AHG and its causes remain relatively rare (Qin et al., 2020), and most existing studies are confined to the mid-latitudes, while data limitations mean that AHG in more tropical zones—with their unique hydroclimatic and geologic conditions—have been less studied (see Lewis, 1969, Phillips & Scatena, 2013, and Turowski et al., 2008 for exceptions).

Tropical cyclones (TCs) hit Puerto Rico (PR) frequently and are often associated with heavy and intense rainfall. This rainfall, combined with the steep mountainous terrain in PR and similar environments, can produce some of the largest flood peaks per unit watershed area in the world (Ogden, 2016a; J. A. Smith et al., 2005a). These floods can cause landslides, debris flows, mass wasting, and fluvial erosion, which redistribute large amounts of sediment along the river (West et al., 2011a) and are capable of causing systematic lateral and vertical channel adjustments (e.g.

Yousefi et al., 2018). Li et al. (2020) found that channel conveyance capacity can change substantially as a result of TC flooding. That study did not, however, examine how these changes manifest in terms of channel geometric properties, and failed to isolate upstream watershed characteristics or local river reach influence (e.g., slope, land cover) that could explain the observed conveyance capacity evolution.

This study attempts to connect the findings of Li et al. (2020) with the AHG framework by examining the watershed and river reach determinants of AHG—including whether or not it is feasible to estimate AHG at ungaged sites—and also by evaluating the potential for AHG response to major flood events, which are almost always caused by TCs in Puerto Rico. Such findings could be valuable for applications such as simplified discharge estimation (Huang et al., 2018; Wang et al., 2019): with a suitable AHG relationship between width and discharge, one can obtain reasonably accurate estimates of discharge based on channel widths measured from *in-situ* or remotely-sensed imagery. Identification of relevant watershed and river reach characteristics and subsequent transferal to ungaged sites, meanwhile, could be used to inform flood risk management, river restoration, and related actions. Here we hypothesize that upstream watershed and river reach characteristics can predict AHG parameters at our study sites, and AHG parameters will change after extreme flood events.

This study examined AHG parameters for 24 sites in PR. Correlation analyses were used to identify the watershed and river reach characteristics that are potentially predictive of AHG parameter estimates. These characteristics were used to build multiple linear regression models for each parameter, with cross validation used to evaluate their applicability to ungaged sites. Channel geometry responses to TC floods were examined by calculating changes in AHG

parameters after major storms and comparing changes to watershed and river reach characteristics. The study region and data used in this study are described in Section 3.2. The methodology is described in Section 3.3. Results follow in Section 3.4, while discussion and conclusions are provided in Sections 3.5 and 3.6, respectively.

3.2 Study Region and Data
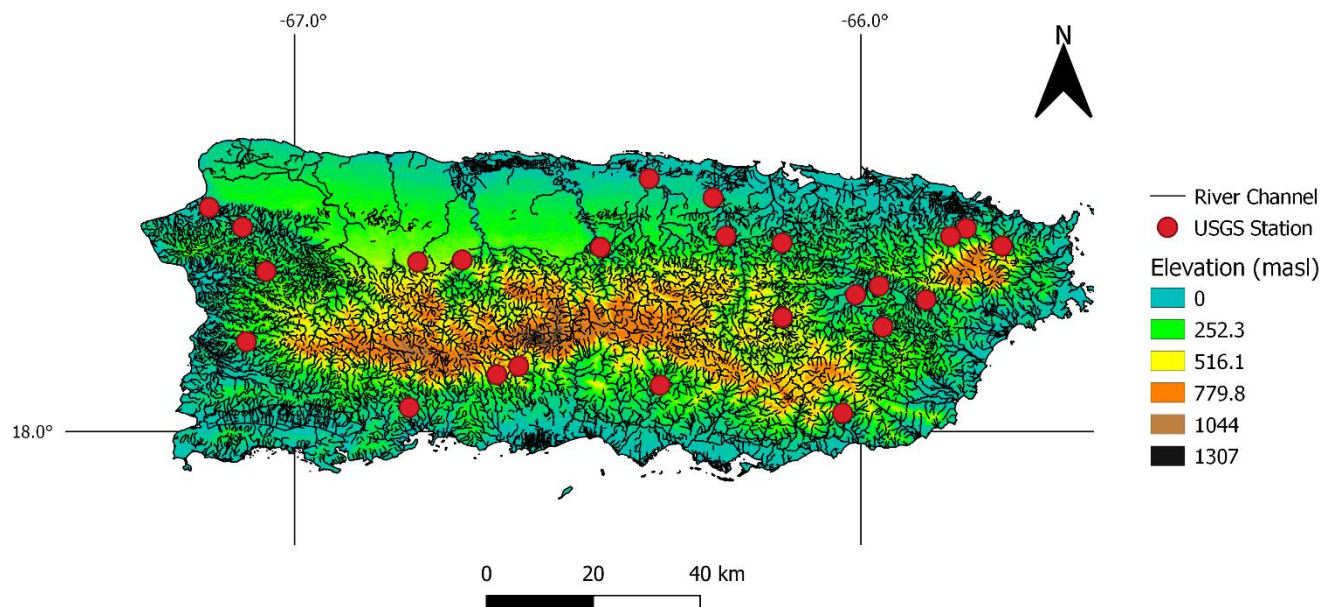
Fig. 3.1: Map of Puerto Rico, showing the USGS stream gages considered in this study and elevation in meters above sea level (masl; from OCM Partners, 2019). River networks (U.S. Geological Survey, 2006) are shown in thin black lines.

Puerto Rico (PR) is a mountainous island located in the northeast Caribbean. The average elevation of the mountainous middle part exceeds 1300 m above sea level (masl), while the average elevation of the less steep margin is about 500 masl. Annual precipitation ranges from

around 500 cm for the mountainous center to 100-400 cm in the coastal lowlands (Daly et al., 2003). A monsoon season begins in May and usually lasts until October, overlapping with the June-November North Atlantic TC season. Limited by the island's aspect and east-west mountain range, its rivers generally range from <10 kilometers to about 50 kilometers in length, with the longest—Rio de la Plata—measuring 74 kilometers, and from <10 meters to more than 60 meters in width.

Our AHG estimation relied on field measurements of channel geometry and velocity, which the US Geological Survey (USGS) performs at stream gage sites on a fairly regular basis (roughly monthly) to maintain accurate rating curves, which are then used for continuous discharge estimation (U.S. Geological Survey, 2021b). These field measurements were obtained from the National Water Information System (NWIS) maintained by the USGS. Annual instantaneous peak discharges (U.S. Geological Survey, 2021a) were used to identify the date with the largest flood in each site's record.

We applied rigorous screening to identify suitable USGS stream gage stations. Sites with recorded flags indicating influence by nearby dams, as well as those located in the vicinity of man-made structures such as weirs were excluded due to their influence on AHG (Reisenbüchler et al., 2019b). Field measurement records in PR available through NWIS usually start around 1990, though several sites' records date back to the early 1980s. If a station is reported to have experienced datum changes, we avoided all observations before the most recent datum change. The site was excluded from the analysis if the most recent datum change occurred later than 1990. We applied the data accuracy criteria of Slater et al. (2015), who only considered field measurements in which the discharge is within one percent of the product of channel velocity

and cross-sectional channel area, as reported by the USGS, and those made in close proximity to the gage station (within 300 feet [91 m]; hardly any field measurements were made directly at the gaged cross section). Only sites that have continuous daily discharge records in the same period of the field measurements were included. 24 sites satisfied these criteria (Fig. 3.1; Table S8). The limited number of sites in the northwestern portion of the island is linked to the lower drainage density there.

Upstream watershed and river reach characteristics were obtained or estimated from public GIS and remote sensing resources and used to calculate correlations with and to predict AHG parameters. Watershed boundaries, along with the upstream drainage area, corresponding to each stream gage were downloaded from NWIS. Watershed-averaged elevation and slope were calculated for each gage based on a digital elevation model from the National Oceanic and Atmospheric Administration (NOAA) National Centers for Environmental Information. We matched the reach segment from the river network (U.S. Geological Survey, 2006) to each of the 24 gauging sites, and then measured the reach slope and sinuosity of the reach. Reach widths— the width between river banks at each gage site—were estimated via remote sensing imagery available through the Google Earth application taken in February 2020. Percentages of developed, forested, and planted (agricultural) areas were obtained from the USGS GAGES-II dataset (Falcone, 2011). (Note that land use metrics are "static," i.e., only available at the time point when GAGES-II data were taken in 2011.)

3.3   Methodology

3.3.1 Hydraulic Geometry Parameter Estimation

To study spatial variation of the hydraulic geometry, we fit models to the entire period of field measurements to get parameter estimates for each site (see black lines in Fig. 3.2 for examples). The parameter values in Eqns. 3.1-3.3 were estimated via the nonlinear least squares (NLS) regression function in the R programming language (R core team, 2020). The residuals of each NLS regression model were examined for homoscedasticity, independence and normality using the package "nlstools" (e.g. Fig. S2). Units used in this study are m^3/s for discharge, m for depth and width, and m/s for velocity; the resulting units for a,c, and k are s/m^2, s/m^2 and m^{-3}, respectively. Channel surface water widths and mean velocities were used to fit channel Eqns. 3.1 and 3.3, respectively, while hydraulic mean depths in Eqn. 3.2 were calculated by dividing flow areas by surface water widths (after Barber & Gleason, 2018; Brinkerhoff et al., 2019; Doll et al., 2002; Shen et al., 2016).

The fitted parameters obtained via NLS did not strictly satisfy continuity (Eqn. 3.4), though nearly so (results not shown). We thus applied a normalization used in prior studies (Jowett, 1998; Lee et al., 2019; Park, 1977) to enforce continuity (Eqn. 3.5 and 3.6):

$$a_{adjusted} = \frac{a_{fitted}}{(a_{fitted}c_{fitted}k_{fitted})^{\frac{1}{3}}}, \text{ similar for } c \text{ and } k \qquad \text{Eqn. 3.5}$$

$$b_{adjusted} = \frac{b_{fitted}}{b_{fitted}+f_{fitted}+m_{fitted}}, \text{ similar for } f \text{ and } m \qquad \text{Eqn. 3.6.}$$

We also reproduced all subsequent analyses without this normalization. Results with and without normalization were nearly equivalent; results without normalization are omitted for brevity.

Eqns. 3.1 and 3.2 imply that channel cross-sectional geometry can be described by an equation of the form

$$d = \frac{c}{a^{\frac{f}{b}}} w^{\frac{f}{b}} \qquad \text{Eqn. 3.7}$$

Eqn. 3.7 shows that depth is proportional to the surface water width to the power of $\frac{f}{b}$. Prior studies have examined the value of $\frac{f}{b}$ as an indicator of channel cross sectional shape (Ferguson, 1986; Qin et al., 2020; Turowski et al., 2008). For example, width is proportional to depth when $\frac{f}{b} = 1$, implying a triangular cross section while $\frac{f}{b} = 2$ implies a parabolic form. When $b = 0$, $\frac{f}{b}$ would be infinity, implying that the wetted width does not increase with discharge, as in cases of rectangular cross section. $\frac{f}{b} < 1$ represents a convex upwards curved channel section indicative of a cut bank/point bar form with width increasing more than depth for medium-to-high discharges (See Fig.3 in Ferguson, 1986). The ratio $\frac{c}{a^{\frac{f}{b}}}$, which indicates relative bank steepness for a particular value of $\frac{f}{b}$, is absent from earlier studies. We calculated $\frac{f}{b}$ and $\frac{c}{a^{\frac{f}{b}}}$ from our AHG estimates and refer to them as "bank shape parameters."

a) Discharge vs. Wetted Width at USGS Station 50045010

b) Discharge vs. Mean Hydraulic Depth at USGS Station 50064200
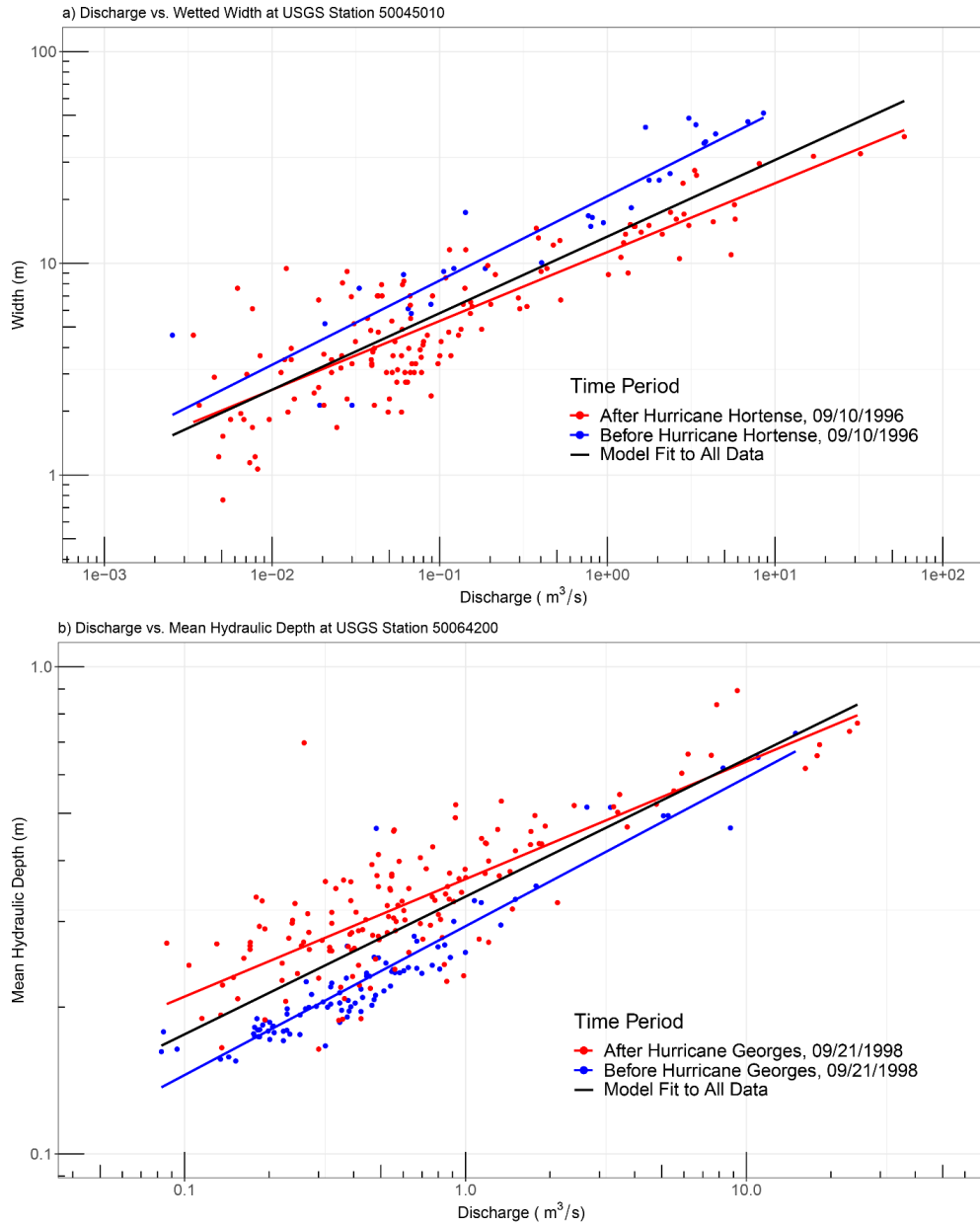
Fig. 3.2 a) Discharge vs. width at site 50045010. The black line represents the fitted nonlinear least squares model using all data available at the site since 1992. The blue and red lines correspond to the model fit only to the field measurements before and after Hurricane Hortense, respectively. b) Discharge over mean depth at site 50064200. The black line represents the nonlinear least squares model using all data available at the site

since 1990. The blue and red lines correspond to the model fit only to the field measurements before and after Hurricane Georges, respectively.

3.3.2 Watershed and River Reach Characteristics and Correlation Analyses

Upstream watershed and reach-scale characteristics were estimated to examine their relationships to AHG and AHG parameter responses to floods. Other than the characteristics introduced in the data section, we included three additional variables following Morel et al., (2019): Froude number at median discharge of all available field measurements for each site (Fr_{50}), the median width to depth ratio (WHR), and normalized active channel width ($NACW$). These are calculated as

$$Fr_{50} = \frac{Q_{50}}{g^{0.5} H_{50} W_{50}} \qquad \text{Eqn. 3.8}$$

$$WHR = \frac{W_{50}}{H_{50}} \quad \text{Eqn. 3.9}$$

$$NACW = \frac{channel\ width}{(watershed\ area)^{0.42}} \text{ Eqn. 3.10,}$$

where Q_{50} is median discharge, W_{50} and H_{50} are reach-average wetted width and depth at Q_{50}, respectively. Finally, the normalized two-year flood (calculated as the median of annual instantaneous peak flows from NWIS divided by the upstream drainage area) was included to describe the "peakiness" of a watershed's flood regime. Kendall's tau nonparametric rank correlation (Kendall, 1938b) was used to identify relationships between watershed/reach characteristics and AHG parameters.

3.3.3 AHG predictive regression models

We used a stepwise process to develop models to predict AHG parameters based on watershed and river reach characteristics. We began by creating multiple linear regression models for each AHG parameter based on all available predictors. These were reduced to final predictive models via trial and error. In order to balance model predictive power and complexity, final models were those with the highest adjusted R-squared values. Some significant variables were not used in the models due to collinearity among predictors. Following Morel et al. (2019), we took the natural log and the square root of elevation and watershed area, respectively, before considering them as predictors.

To evaluate the potential predictive power of the final regression models at similar ungaged sites in Puerto Rico, as well as to avoid overfitting, we performed leave-one-out cross-validation, which gives approximately unbiased estimates of the model's performance and is typically applied to small datasets (Cawley, 2006), to estimate the root mean square error of the predicted values of each parameter. Keeping the predictors fixed, we removed one site and retrained each model with data from the other 23 locations. We then used the trained model to predict the parameter values for the withheld site. We repeated this for all sites and then compared the predicted parameters with the observed parameter values from former steps.

3.3.4 AHG Temporal Variation Due to Tropical Cyclones

Li et al. (2020) showed that recent major TCs, primarily Hurricanes Hortense (1996), Georges (1998), and Maria (2017), caused substantial changes in river channel conveyance capacity in PR. This earlier work, however, did little to elucidate more specific geomorphic changes. AHG parameters can indeed change substantially in response to TCs (see the red and blue lines in Fig.

3.2, which show distinct AHG relationships estimated before and after major storms). We identified the largest "local" flood event—the largest annual peak streamflow value for each site—to separate the field measurements into two time series, before and after this largest local flood event. Hurricanes Hortense and Georges caused the largest flood events at six sites each, while Hurricane Maria caused the largest flood at ten others. The largest floods at the two remaining sites were caused by non-TC storms. We again followed the methodology in Section 3.3.1 to estimate AHG parameters (see Section 3.4.3) but only for periods four years before and four years after these identified flood events. We calculated "before-and-after" percentage changes in AHG parameters (including bank shape parameters) by subtracting the values after the largest flood event from the values before, and dividing the difference by the latter value. These changes were then tested for correlation with watershed and river reach characteristics using the nonparametric rank correlation mentioned in Sec. 3.3.2. We extracted the peak discharges of the local largest flood events, and divided them by the discharges of the 2-year flood at the same site to get normalized discharges of the largest local flood events. These normalized flood discharges were included as an additional characteristic in the correlation analysis specific to AHG parameter changes caused by floods.

3.4   Results

3.4.1 AHG Parameter Estimates and Correlation Tests

The power models fit reasonably well (p-values much less than 0.05) to all six parameters at all sites except for velocity at site 50064200, which yielded a p-value of 0.056 (Table S9). The average values for the exponents were 0.230, 0.394, and 0.376 for b, f and m, respectively. A

ternary plot (Fig. 3.3a) shows similar distributions of exponents from this study and from the earlier AHG studies in Puerto Rico of Lewis (1969) and Phillips & Scatena (2013). The results are also similar to those from Leopold & Maddock (1953) in the mainland midwestern United States and Leopold & Miller (1956) in mainland ephemeral rivers (results not shown). Similarly to Phillips & Scatena (2013) observations, we found that the width exponent is usually less than 0.33, with only one exception where $b = 0.344$.

The relationships between AHG parameter estimates and the various watershed and reach characteristics are tabulated in terms of Kendall's tau correlation (Table 3.1), while those of most obvious interest are shown in additional ternary plots (Fig. 3.3b-d). Upstream watershed area was found to be significantly positively (negatively) correlated with $f(m)$, while both percentage of developed area and planted area were significantly negatively (positively) correlated with $f(m)$. Average upstream watershed elevation, slope, and the percentage of forested area were found to be significant and negatively (positively) correlated with $f(m)$. No characteristics were found to be significantly associated with b, and no other characteristics were found to be significantly correlated with any exponents. Upstream watershed area, average watershed elevation, average reach width, average reach slope, WHR, Fr_{50}, and $NACW$ were also found to be significantly correlated with some coefficients (Table 3.1). The channel shape parameters $\frac{f}{b}$ and $\frac{a}{c^{\frac{f}{b}}}$ are positively and negatively correlated (at the 5% level), respectively, with average watershed elevation. Upstream watershed area is also found to be negatively correlated with $\frac{a}{c^{\frac{f}{b}}}$, while average upstream watershed slope is found to be negatively correlated with $\frac{f}{b}$, both of which are significant at the 5% level.

Table 3.1. Kendall's tau correlation results with p-values shown in parentheses. Relationships significant at the 5% level are bolded.

Watershed and River Reach Characteristics	a	c	k	b	f	m	$\dfrac{f}{b}$	$\dfrac{c}{\frac{f}{a^b}}$
Normalized Two Year Flood ($\frac{m^3}{s}/km^2$)	-0.043 (0.79)	0.27 (0.07)	-0.2 (0.17)	0.17 (0.27)	-0.1 (0.51)	0.036 (0.83)	-0.14 (0.36)	0.11 (0.48)
Watershed Area (km^2)	**0.48 (<0.001)**	**-0.5 (<0.001)**	-0.062 (0.67)	-0.018 (0.9)	**0.36 (0.014)**	**-0.36 (0.014)**	0.19 (0.19)	**-0.38 (0.009)**
Reach width (m)	**0.42 (0.004)**	-0.17 (0.27)	**-0.36 (0.013)**	0.21 (0.16)	0.2 (0.17)	-0.25 (0.087)	0.051 (0.75)	-0.18 (0.23)
Reach slope (m/m)	**-0.33 (0.023)**	0.11 (0.48)	0.19 (0.21)	-0.065 (0.68)	-0.17 (0.25)	0.17 (0.27)	-0.11 (0.48)	0.22 (0.13)
Watershed Forested Area (%)	-0.029 (0.86)	0.27 (0.07)	-0.25 (0.097)	-0.094 (0.54)	**-0.3 (0.039)**	**0.38 (0.008)**	-0.094 (0.54)	0.094 (0.54)
Watershed Developed Area (%)	0.08 (0.61)	-0.23 (0.12)	0.25 (0.087)	0.087 (0.57)	**0.51 (<0.001)**	**-0.51 (<0.001)**	0.22 (0.14)	-0.19 (0.21)
Watershed Planted Area (%)	0.11 (0.47)	-0.13 (0.39)	0.093 (0.54)	0.07 (0.65)	**0.49 (0.001)**	**-0.44 (0.004)**	0.26 (0.092)	-0.23 (0.14)
Average watershed slope	-0.072 (0.64)	0.15 (0.31)	-0.23 (0.12)	0.007 (0.98)	**-0.57 (<0.001)**	**0.54 (<0.001)**	**-0.31 (0.034)**	0.22 (0.13)
Average watershed elevation (masl)	-0.17 (0.25)	**0.3 (0.044)**	-0.22 (0.14)	0.15 (0.31)	**-0.49 (<0.001)**	**0.41 (0.004)**	**-0.36 (0.015)**	**0.41 (0.004)**
WHR	0.2 (0.17)	**-0.33 (0.026)**	-0.13 (0.39)	-0.2 (0.19)	-0.26 (0.078)	0.27 (0.07)	-0.094 (0.54)	-0.094 (0.54)
Fr_{50}	0.21 (0.16)	**-0.39 (0.007)**	0.12 (0.42)	0.087 (0.57)	0.21 (0.16)	-0.28 (0.062)	-0.043 (0.79)	-0.058 (0.71)
$NACW$ (m)	0.16 (0.29)	0.065 (0.68)	**-0.38 (0.010)**	0.27 (0.07)	-0.043 (0.79)	-0.065 (0.68)	-0.14 (0.36)	0.065 (0.68)

Sinuosity (m/m)	0.094 (0.54)	0 (1)	0.022 (0.9)	-0.058 (0.71)	0.065 (0.68)	-0.014 (0.94)	0.043 (0.79)	-0.014 (0.94)
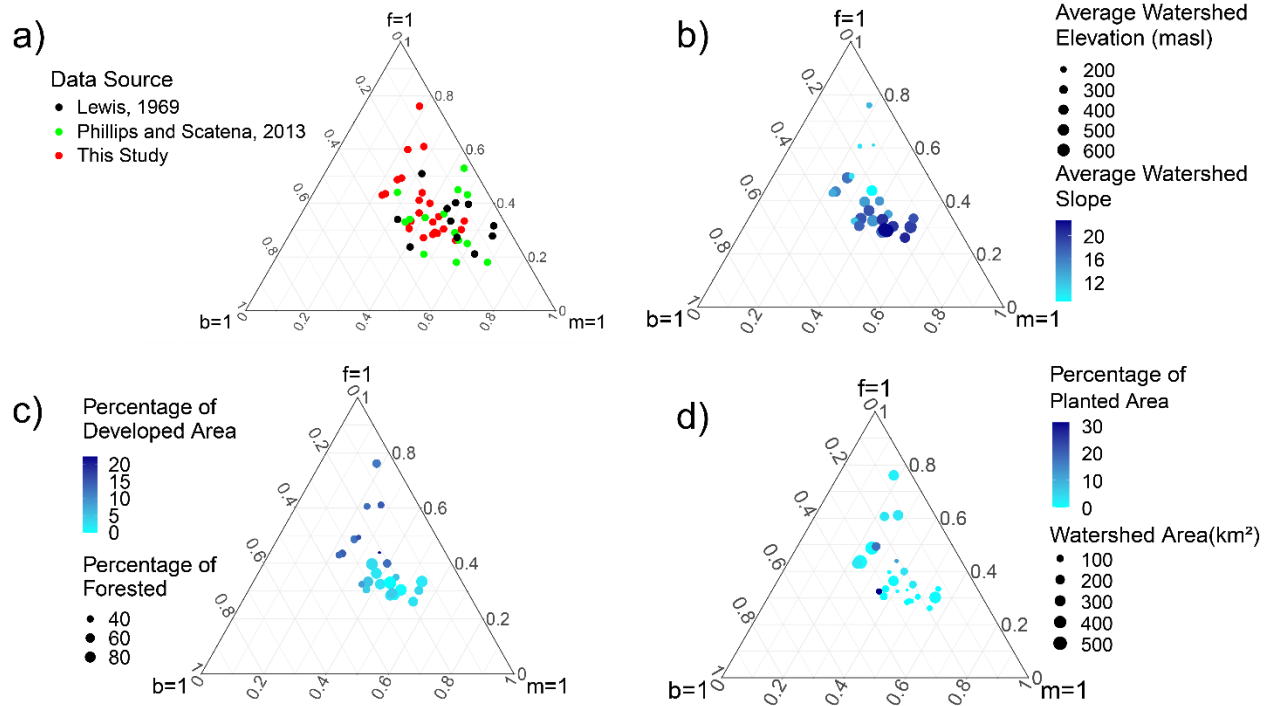
Fig. 3.3: Ternary plots showing the estimated exponents for the entire study period: a) Comparison to former studies in Puerto Rico, b) relationships with average watershed slope and elevation, c) relationships with percentages of developed and forested area, and d) relationships with percentage of planted area and watershed area.

The ratio $\frac{f}{b}$ was found to be negatively correlated (p=0.023) with average watershed elevation, indicating that higher-elevation rivers in PR tend toward more triangular and less rectangular channel cross-sectional shapes. Turowski et al. (2008) found a strong log-log relationship between the bank shape parameter $\frac{f}{b}$ and the exponent b for average parameter values in different

studies. By comparing our data with prior studies, we found that this relationship appears to hold across a wide range of studies and study locations. The range of coefficients of the models fit separately to each of the five studies shown on Fig. 4 is 0.15 - 0.33. The range of exponents is -1.42 - -1.01. The coefficient and exponent of the model fit to our data are 0.22 and -1.35, respectively, which are within the range. The model fit range also contains the equation in Turowski et al. (2008; Fig. 4, gray line; $\frac{f}{b} = (0.28 \pm 0.06)b^{-1.12 \pm 0.07}$). This confirms that in Puerto Rico, as in other locations, general, steep-banked channels lead to smaller exponent b, which is indicative of width being less adjustable, which can be caused by consolidated bank materials like cohesive soils that are common in cases of steep banks.
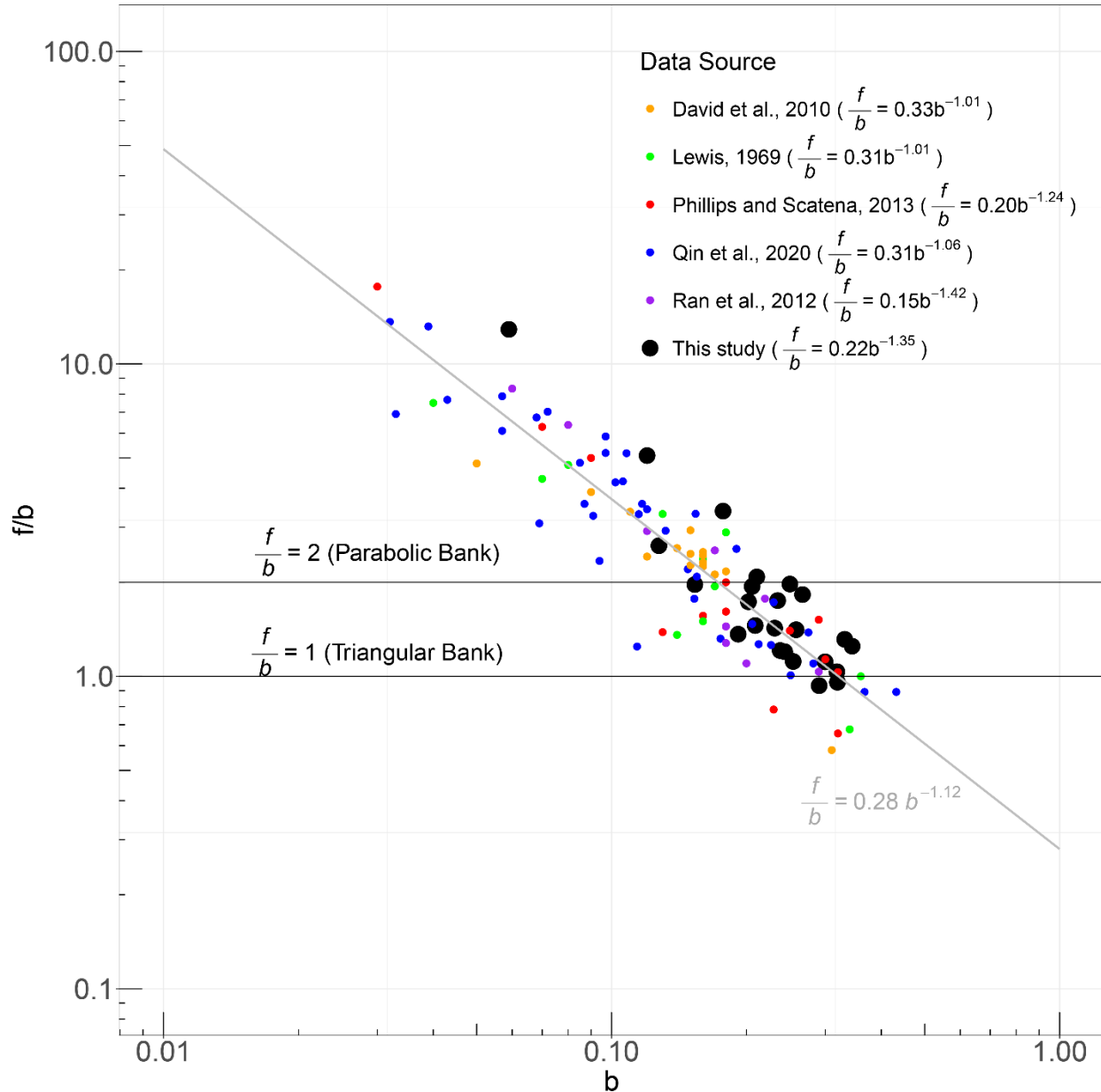
Fig. 3.4 Scatterplot of $\frac{f}{b}$ vs. b using data from multiple former studies and this study. All model fits are significant (p-values $< 10^{-3}$) Gray line shows the model fit by Turowski et al. (2008), to multiple studies. The model from Turowski et al. (2008) was fit to average values of each study, rather than whole data sets from the studies. The only common study between the five former studies shown on this plot and the studies analyzed in Turowski et al. (2008) is Lewis (1969).

3.4.2 AHG Predictive Models

The final regression models to predict AHG parameters (Section 3.3.3) are shown in Table 3.2, along with R-squared values and overall model p-values. Among the three coefficients (exponents), $k(b)$ is least well predicted, in terms of adjusted R-squared. The regression model for b is the only model that is insignificant at 5% level. When subject to leave-one-out cross validation, all regression-based models can predict parameter values with relative root mean square error (rRMSE; RMSE divided by the average parameter value) between 10% and 30%, except for the model for b, which results in 31.2%.

Table 3.2. Regression-based predictive models for AHG parameters. Predictors are: width to depth ratio at median discharge (WHR), average watershed slope (S_{ws}), average watershed elevation ($Elev_{ws}$), watershed area (A_{ws}), the percentages of developed area ($Developed$), forested area ($Forested$) and planted area ($Planted$), normalized two year flood (Q_{2yr}), reach slope (S_r), reach sinuosity ($sinuosity$), channel width (w_c), normalized active channel width ($NACW$) and Froude number at median discharge (Fr_{50}). In the leave-one-out validation, models were repeatedly fit to 23 sites, and then used to predict the remaining site's parameter. RMSEs were calculated between the leave-one-out predictions estimated values shown in Table S9; units match those of the corresponding AHG parameter. Relative RMSEs were calculated by normalizing RMSEs by the mean parameter value from Table S9 and multiplying by 100.

Model Structure	Adjusted R^2	R^2	p-value	Leave-one-out RMSE (Relative RMSE)
$a = -1.97 + 0.11WHR + 0.53\sqrt{A_{ws}} + 0.066Forested$	0.83	0.85	<0.001	3.3 (25.7%)
$c = -0.36 + 0.10log\,(Elev_{ws}) + 0.0039Planted + 0.0074Q_{2yr}$	0.55	0.61	<0.001	0.048 (18.3%)

$k = 0.66 - 0.010 S_{ws} - 0.039 NACW - 0.0039\sqrt{A_{ws}}$	0.38	0.46	0.007	0.095 (28.2%)
$b = -0.20 - 7.6e - 04 WHR + 0.095 log\,(Elev_{ws}) - 0.0015 Forested$	0.18	0.29	0.08	0.072 (31.2%)
$f = 1.18 + 0.0033 Forested + 0.015 Developed - 0.18 log\,(Elev_{ws})$	0.67	0.71	<0.001	0.073 (18.5%)
$m = 0.22 + 0.013 S_{ws} - 0.010\sqrt{A_{ws}} + 0.0013 WHR$	0.76	0.79	<0.001	0.060 (15.9%)

3.4.3 Hydraulic Geometry Response to Tropical Cyclones

We re-estimated AHG parameters for each site using two periods: four years before and after the largest local flood event (i.e., the highest single instantaneous flood peak for each site, see Sec. 3.3.4). Both the percent differences between the "before-and-after" parameter values and the absolute value of these differences were calculated. The absolute values are generally indicative of the overall tendency of a site's AHG relations to change in response to a major flood, while the real difference provides the direction of that change. The differences in the parameter values of the largest local flood event are shown in Fig. 3.5. Percent changes in parameter values are evident at most sites and for all parameters. The changes in the depth exponent f tend to be positive in the northeastern part of the island and negative in western Puerto Rico. No obvious spatial patterns were evident for other parameters.

We then computed correlations between these parameter value changes and the various watershed and river reach characteristics (Table 3.3). Fr_{50}, sinuosity, and $NACW$ are positively and significantly (at 5% level) correlated with the real percent difference of a, while $NACW$ is also negatively correlated ($p=0.034$) with the real percent difference in k. Normalized two-year flood and WHR are positively correlated with the shape coefficient $\dfrac{c}{a^{\frac{f}{b}}}$ (p-values are 0.042 and

0.03, respectively). The percentage of forested (developed) area is negatively (positively) correlated with the absolute percent difference of k, with p-values of 0.03 (0.008). The percentage of forested (developed) area is also positively (negatively) correlated with the absolute percent difference of b, with p-values of 0.003 (0.009). Watershed area, reach width, and the percentage of planted area are also significantly negatively correlated with the absolute percent difference of b. The percentage of planted area (average watershed slope) is positively (negatively) correlated with the absolute percent change of c, with $p=0.036$ ($p=0.017$).
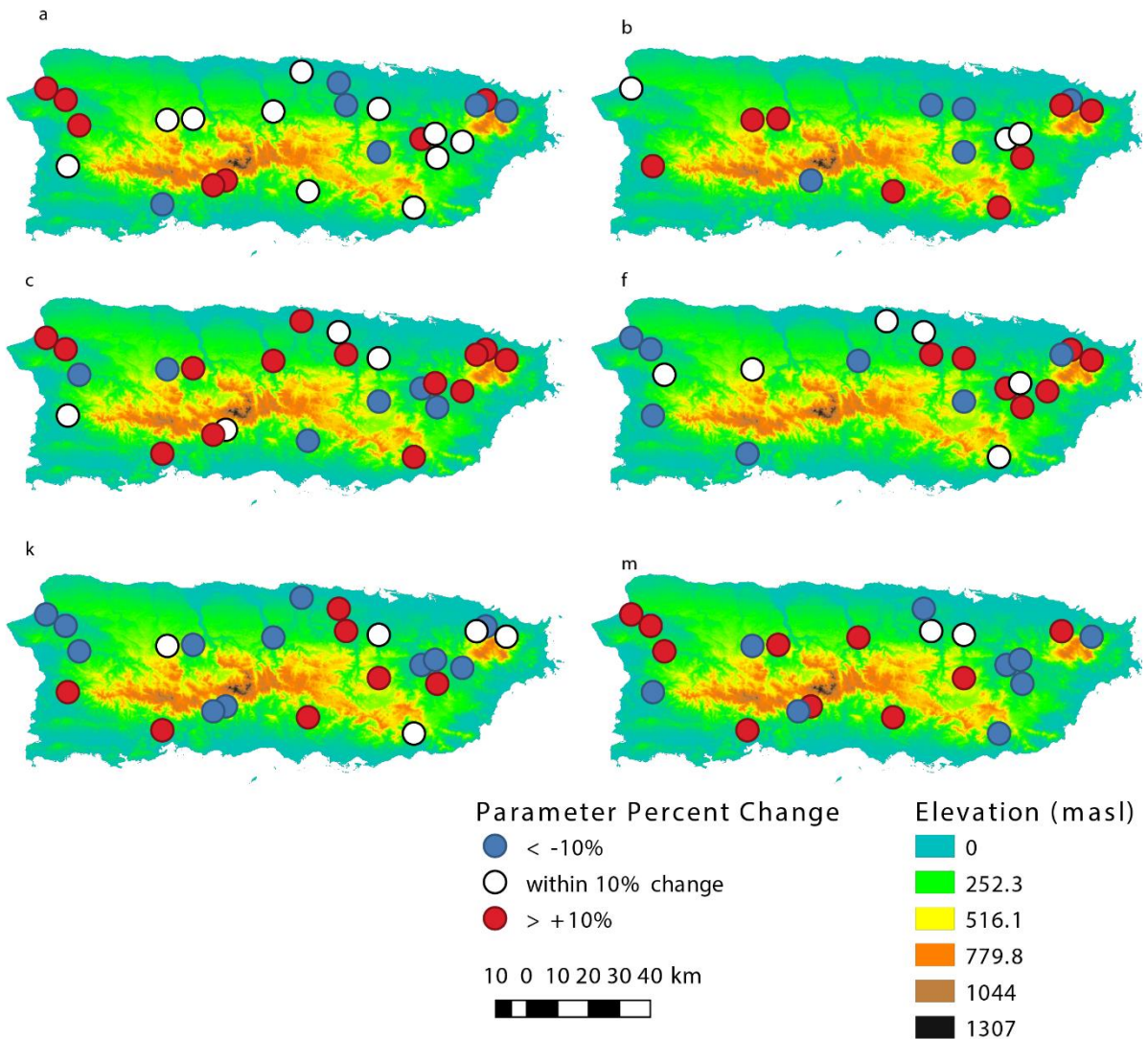
Fig. 3.5. Real percent parameter value changes of the largest flood event for all AHG parameters. Only the sites with significant model estimates for both before and after the largest flood event are shown on each panel. Number of sites shown on each panel: 24 for coefficients (a, c and k), 16 for b, 20 for f, and 21 for m. Blue dots are the sites with real parameter value decreases greater than 10%, while red dots are the sites with real parameter value increases greater than 10%. White dots are the sites within between 10% decreases and 10% increases.

Table 3.3. Kendall's Tau correlation test results of percent parameter changes caused by the largest local flood event and watershed/river reach characteristics. The values outside of the brackets are the correlations entry between the predictor and the percent parameter change, while the values inside brackets are the correlations between the predictor and the absolute value of the percent parameter change. Quantities inside parentheses are corresponding p-values; bolded results are significant at the 5% level.

Watershed and River Reach Characteristics	a (N=24)	c (N=24)	k (N=24)	b (N=16)	f (N=20)	m (N=21)	$\frac{f}{b}$ (N=13)	$\frac{c}{a^{\frac{f}{b}}}$ (N=13)
Normalized Two Year Flood ($\frac{m^3}{s}$/ km^2)	0.16 (0.29) |0.16 (0.29)|	0.17 (0.25) |0.087 (0.57)|	-0.27 (0.07) |-0.087 (0.57)|	0.23 (0.23) |0.083 (0.69)|	0.032 (0.87) |-0.063 (0.72)|	-0.17 (0.29) |-0.24 (0.14)|	-0.18 (0.44) |-0.23 (0.31)|	**0.44 (0.042)** |0.15 (0.51)|
Watershed Area (km^2)	0.083 (0.57) |-0.098 (0.5)|	-0.025 (0.86) |0.12 (0.41)|	0.0036 (0.98) |0.19 (0.21)|	-0.21 (0.26) |**-0.49 (0.0078)**|	0.1 (0.54) |0.037 (0.82)|	0.072 (0.65) |0.11 (0.49)|	0.25 (0.25) |-0.09 (0.67)|	-0.37 (0.076) |-0.039 (0.85)|
Reach width (m)	0.28 (0.062) |0.072 (0.64)|	0.13 (0.39) |0.22 (0.14)|	-0.25 (0.087) |0.087 (0.57)|	-0.22 (0.27) |**-0.4 (0.033)**|	0.22 (0.19) |0.021 (0.92)|	-0.038 (0.83) |-0.029 (0.88)|	0.31 (0.16) |-0.15 (0.51)|	-0.26 (0.25) |0.23 (0.31)|
Reach slope (m/m)	-0.043 (0.79) |0.029 (0.86)|	0 (1) | -0.13 (0.39)	-0.022 (0.9) |-0.14 (0.34)|	0.067 (0.76) |0.22 (0.27)|	-0.084 (0.63) |0.16 (0.35)|	0.086 (0.61) |-0.15 (0.35)|	-0.1 (0.68) |0.36 (0.1)|	0.1 (0.68) |0.18 (0.44)|
Watershed Forested Area (%)	0.014 (0.94) |0.12 (0.45)|	0.058 (0.71) |-0.23 (0.12)|	-0.12 (0.42) |**-0.32 (0.03)**|	0.22 (0.27) |**0.53 (0.0033)**|	-0.063 (0.72) |-0.14 (0.42)|	-0.067 (0.7) |-0.13 (0.42)|	-0.23 (0.31) |0.23 (0.31)|	0.18 (0.44) |0.1 (0.68)|
Watershed Developed Area (%)	0.036 (0.83) |-0.065 (0.68)|	0.0072 (0.98) |0.25 (0.087)|	0.014 (0.94) |**0.38 (0.0082)**|	-0.37 (0.052) |**-0.48 (0.0086)**|	0.074 (0.68) |0.084 (0.63)|	0.019 (0.93) |0.1 (0.53)|	0.36 (0.1) |0 (1)|	-0.31 (0.16) |-0.026 (0.95)|
Watershed Planted Area (%)	0.039 (0.8) |-0.078 (0.61)|	0.093 (0.54) |**0.32 (0.036)**|	-0.031 (0.84) |0.18 (0.24)|	-0.27 (0.17) |**-0.45 (0.021)**|	0.17 (0.31) |0.17 (0.31)|	0 (1) |0.01 (0.95)|	0.27 (0.21) |-0.11 (0.61)|	-0.19 (0.38) |-0.055 (0.8)|
Average watershed slope	-0.1 (0.51) |0.029 (0.86)|	-0.058 (0.71) |**-0.35 (0.017)**|	0.065 (0.68) |-0.26 (0.078)|	0.32 (0.096) |0.33 (0.079)|	-0.053 (0.77) |-0.021 (0.92)|	0.0095 (0.98) |0.076 (0.65)|	-0.31 (0.16) |0 (1)|	0.21 (0.37) |0.077 (0.77)|
Average watershed elevation (masl)	-0.072 (0.64) |0.072 (0.64)|	-0.014 (0.94) |-0.19 (0.21)|	0.065 (0.68) |-0.13 (0.39)|	0.05 (0.82) |0.27 (0.17)|	0 (1) |-0.14 (0.42)|	0 (1) |-0.0095 (0.98)|	-0.051 (0.86) |0.051 (0.86)|	0.21 (0.37) |0.28 (0.2)|
WHR	**0.31 (0.034)**	0.11 (0.48)	-0.28 (0.062)	-0.067 (0.76)	-0.16 (0.35)	0.057 (0.74)	-0.21 (0.37)	0.21 (0.37)

	|0.036 (0.83)|	|0.17 (0.27)|	|0.094 (0.54)|	|0.15 (0.45)|	|-0.23 (0.16)|	|0.12 (0.46)|	|0.051 (0.86)|	|-0.13 (0.59)|
Fr_{50}	0.072 (0.64) |-0.28 (0.062)|	0.014 (0.94) |0.029 (0.86)|	-0.065 (0.68) |-0.12 (0.45)|	0.2 (0.31) |-0.017 (0.96)|	-0.032 (0.87) |0.13 (0.46)|	0.22 (0.18) |0.25 (0.12)|	-0.26 (0.25) |-0.31 (0.16)|	**0.46 (0.03)** |-0.13 (0.59)|
$NACW$ (m)	**0.31 (0.034)** |-0.0072 (0.98)|	0.065 (0.68) |0.14 (0.36)|	-0.28 (0.062) |0.18 (0.23)|	0.033 (0.89) |-0.15 (0.45)|	0.084 (0.63) |-0.18 (0.29)|	-0.14 (0.39) |0.19 (0.24)|	0.026 (0.95) |-0.13 (0.59)|	-0.18 (0.44) |-0.21 (0.37)|
Sinuosity (m/m)	**0.3 (0.039)** |0.16 (0.29)|	0.12 (0.45) |0.23 (0.12)|	**-0.31 (0.034)** |0.014 (0.94)|	-0.22 (0.27) |-0.067 (0.76)|	0.15 (0.39) |-0.053 (0.77)|	0.0095 (0.98) |0 (1)|	0.26 (0.25) |-0.051 (0.86)|	0 (1) |0.28 (0.2)|
$\dfrac{Q_{largest}}{Q_{2yr}}$	-0.14 (0.34) |-0.22 (0.14)|	-0.17 (0.25) |-0.1 (0.51)|	0.21 (0.16) |0 (1)|	-0.1 (0.63) |0.083 (0.69)|	-0.15 (0.39) |-0.011 (0.97)|	0.2 (0.22) |0.11 (0.49)|	-0.051 (0.86) |0.21 (0.37)|	-0.21 (0.37) |-0.28 (0.2)|

3.5 Discussion

3.5.1 Comparison with other studies

All sites showed significant fit for power models, except for m at site 50064200. This could be caused by changing roughness values of the cross section over time, which controls the relationship between discharge and velocity. Changes to roughness coefficients can happen as responses to major TCs (as shown in Fig. 3.2), changing land use (Akbari et al., 2014), channel restoration (Sholtes & Doyle, 2011), or natural gradual recovery after instantaneous changes (Chen & Chiew, 2003).

The average values of the exponents b, f, m obtained in this study are 0.230, 0.394 and 0.376, respectively, which are close to Lewis (1969) and Phillips & Scatena (2013) results in Puerto Rico (Fig. 3a), Leopold and Maddock's results in the Midwest US (Leopold & Maddock, 1953), and Leopold and Miller's results in ephemeral streams in US (Leopold & Miller, 1956). The b and f values agree with the prior work in Puerto Rico (Phillips & Scatena 2013) in that width (b)

contributes a smaller component than depth (f) and velocity (m), and never exceeds one third (with only one minor exception; one site's value of b is 0.34). In 14 sites, velocity has the largest exponent, while depth has the largest exponent in the other 10 sites. Width never had the largest exponent, similar to Qin et al. (2020).

The ratio $\frac{f}{b}$ describes the shape of river banks (Ferguson, 1986), ranging from 0.93 to 12.89 in this study, with the median of 1.44. The majority of sites have ratios within or near the range 1-2, indicating that the majority of channel cross sections are either triangular or parabolic. The ratio at some sites, however, are higher, highlighting that there does exist a diversity of channel cross-sectional shapes in Puerto Rico including ones closer to rectangular.

The log-log linear relationship between the shape parameter $\frac{f}{b}$ and b are significant for both our data and a collection of parameters from former studies conducted in Puerto Rico, Colorado in the mountainous western United States, and the Yellow River in China. The fitted equations are all close to what Turowski et al. (2008) found using average values from other studies. Despite the strong log-log relationship between $\frac{f}{b}$ and b, we found that this relationship did not predict b as well as the regression-based model for that parameter (see Table 3.2; RMSE and rRMSE of b estimates based on the log-linear model are 0.61 and 265%). This may be due to the requisite log and exponential transformations. Nonetheless, the high similarity of the log-log linear relationship among different studies in highly varied geographic regions suggests the potential to estimate channel shape from the exponent b.

3.5.2 Hydraulic parameters and watershed and river reach characteristics

3.5.2.1 Exponents

The characteristics that were significantly correlated with the depth exponent f were inversely correlated with the velocity exponent m (Table 3.1), which is not unexpected due to the continuity requirement (Eqn. 3.4). These characteristics include upstream drainage area, the percentages of developed, forested, and planted area, average upstream watershed slope and elevation. Our results are consistent with Klein (1981) and Qin et al. (2020), in that depth is a greater contributor for higher discharges in large rivers (positive correlation between watershed area and f), while width contributes more in small streams (negative—but not statistically significant—correlation between upstream watershed area and b). No watershed or river reach characteristics were found to be significantly (i.e. at the 5% level) correlated with the width exponent b.

Phillips and Scatena (2013) found that while velocity has a larger exponent for rural channels in Puerto Rico, depth contributes to a larger exponent extent in urban catchments. Our correlation results agree with this finding: the percentage of developed (forested) area of a watershed is positively (negatively) correlated with the depth exponent f and negatively (positively) with the velocity exponent m. This is further supported by the significant and positive correlation between $f - m$ and percentage of developed area (Kendall's tau $= 0.54$, $p < 10^{-4}$). Cohesive banks are common in both developed and forested watersheds; with stable banks, the river channels have limited lateral adjustability (Millar and Quick, 1993; Millar, 2000). This potentially explains why land cover metrics were not significantly correlated with b. The positive correlation between f and the percentage of developed area indicates that the channels tend to adjust vertically in more developed watersheds than in more forested watersheds, which agrees

with previous research showing that channels in urbanized environments are often prone to incision (Booth, 1990; Cole et al., 2017). In forested watersheds, wood load can contribute to flow resistance and is subject to adjustments from frequent and flashy floods (Cadol and Wohl, 2013), in support of the positive correlation between m (adjustability of channel roughness) and percent forested area.

The average elevation and slope of the watersheds are highly correlated (Kendall's tau=0.58; $p<10^{-4}$), and thus yield similar correlations with f (negative) and m (positive). Ran et al. (2012) and others have concluded that mountainous bedrock channels are typically stable, meaning scour and infill are negligible. This agrees with the observations in Pike et al. (2010) that channels of higher elevation in northeastern Puerto Rico are usually more resistant to erosion due to stable river bed materials such as granite, while channels of lower elevation are usually in alluvium. This likely explains our result that higher-elevation and steeper (i.e. more mountainous) watersheds accommodate increasing discharge primarily through velocity (positive correlation with m) rather than depth (negative correlation with f). Further field studies of river bed and soil material can improve understanding of the lithologic controls on AHG parameters.

3.5.2.2 Coefficients and bank shape parameters

Average watershed elevation was found to be negatively correlated with $\frac{f}{b}$ (Kendall's tau: -0.33, $p=0.023$; Table 3.4) and positively correlated with $\frac{c}{a^{\frac{f}{b}}}$. Since most channels have forms between triangular ($\frac{f}{b} = 1$) and parabolic ($\frac{f}{b} = 2$), this correlation suggests that lower-elevation channels tend to be parabolic with a gradually-sloped banks, while the higher-elevation channels tend to

be triangular with steeper banks. This can be explained by the difference of channel substrate: higher-elevation watersheds are usually in mountainous areas with bedrock channels, while rivers in lower-elevation areas carry more alluvium which can be "shaped" into parabolic forms (Ran et al., 2012).

The coefficients in Eqns. 3.1-3.3 are unit-dependent, and are usually treated as values of width, depth or velocity when the discharge equals one unit (m^3/s in our case; Dingman & Afshari, 2018). The coefficients are general indicators of a channel's width, depth, and roughness. How these characteristics influence discharges at different flow levels is determined by exponents. For example, in Ran et al., 2012, a wide channel with highly-cohesive steep banks result in a high value of a and a relatively small value of b.

Upstream drainage area was significantly correlated with a (positive) and c (negative), and negatively but insignificantly correlated with k. This is similar to Qin et al. (2020), and suggests that channels in the larger watersheds in Puerto Rico are generally more "wide" than "deep," in terms of cross-sectional geometric controls on discharge. Reach width is significantly and positively correlated with a, confirming the interpretation of a as a scale factor for channel width (Ran et al., 2012). The significant positive correlation between reach width and k can be explained by continuity (Eqn. 3.4). Reach slope is found to be negatively significantly correlated with a, in support of that channels with greater slope have lower width to depth ratios due to less lateral adjustability of resistant bank material. The significant positive correlation between average watershed elevation and c shows that mountainous channels in Puerto Rico are usually deep, consistent with the observation mentioned above that channels at high elevations are more

likely to be triangular rather than parabolic. High values of normalized active channel width reflect wide channels relative to catchment size (by Eqn. 3.7; Morel et al., 2019), which could be indicative of increases in roughness associated with feedbacks between channel width and instream wood loading (negative correlation between normalized active channel width and k; Table 1), agreeing with former studies in that wood load increases flow resistance (Cadol & Wohl, 2013; Curran & Hession, 2013; McBride et al., 2007; McBride et al., 2008).

Coefficients are more influential when values of the variable (width, depth, and velocity) are low, while exponents are more influential for high values. To demonstrate, we considered AHG parameters together with published flood stages obtained from National Weather Service (National Oceanic and Atmospheric Administration, 2021) to predict bankfull discharges based on Eqn. 3.2. We found that on average, exponents are more influential than coefficients at determining bankfull discharge at flood stage. For example, a 1% increase in f can resulted in an average decrease in bankfull discharge of 7.1%, while a 1% increase in c gave only an average decrease of 2.9%. It should be noted, however, that few sites have direct discharge measurements near or above these flood stages (see also Li et al. 2020 for discussion on this and other limitations in the PR field measurements), so these results should be taken with a grain of salt. This calls for further data to better understand the influence of both coefficients and exponents at flood discharges.

3.5.3 Predictive Models

The leave-one-out estimates reach an acceptable level of accuracy suggested by the relative RMSE. The root mean square errors (relative RMSEs) for estimates of b, f and m are 0.072

(31.16%), 0.073 (18.48%), and 0.060 (15.94%) [-], respectively. The RMSE and p-values are generally lower, and R-squared values generally higher, than Morel's models (Morel et al., 2019), likely due to a much reduced geographic scope and thus a smaller, more homogeneous set of sites. The RMSE (relative RMSE) for coefficients a, c and k are 3.3 s/m^2 (25.67%), 0.048 s/m^2 (18.26%) and 0.095 m^{-2} (28.18%), respectively. The high root mean square of a is due to its wide range and much higher magnitude compared to other parameters. The regression models not only yielded reliable estimates of the parameters at the study sites, but show the potential to predict parameter values for ungaged sites in similar environmental settings.

3.5.4 Tropical Cyclone Effects on AHG

The normalized two-year flood is positively correlated with real (i.e., not absolute) percent change of $\frac{c}{a^{\frac{f}{b}}}$, indicating that greater "flashiness" can steepen shapes after floods, possibly as a result of channel incision (e.g., Schumm et al. 1984; Simon & Rinaldi 2006; Wallerstein & Thorne, 2004). WHR is also positively correlated with real percent change of $\frac{c}{a^{\frac{f}{b}}}$, which shows that banks in channels with flatter cross-sections erode more readily than channels with steep banks, which is likely indicative of constraints on lateral adjustability imposed by consolidated or cohesive bank materials, or vegetative root reinforcement (Millar and Quick, 1993; Millar, 2000). Sinuosity, Fr_{50}, and $NACW$ are positively correlated with the real percent change of a, showing that in meandering and wide channels and in channels with high Fr_{50}, channel widths tend to increase after floods. This is consistent with the expectation that sinuous channels are fully alluvial with laterally adjustable channel boundaries. The negative correlation between $NACW$ and real percent change of k is probably caused by continuity requirement (Eqn. 3.4).

Average watershed slope is found to be negatively correlated with absolute percent change of c, consistent with the observation from section 3.5.2 that rivers in steeper watersheds are more stable. This agrees with former research that rivers in mountainous areas are usually supply limited and have resistant boundaries that are less responsive to changing in driving forces (Montgomery & Buffington, 1997; Montgomery & MacDonald, 2002). Reach width and watershed area are negatively correlated with absolute change of b, showing that channel width's contribution to discharge is relatively more (less) stable in the larger (smaller) study watersheds and wider (narrower) channels, agreeing with Qin et al. (2020) that river stability tends to increase with watershed area. The percentage of developed (forested) area is positively (negatively) correlated with the absolute change k, indicating that flow velocity is relatively more stable in forested watersheds than in urban channels facing TC floods. Flow velocities in locations with vegetated banks and large instream roughness elements tend to be confined to narrower ranges (Zong and Nepf, 2010; Curran & Hession, 2013), thus we would expect flow velocities to experience less change in forested areas than in more developed areas. The percentage of developed (forested) area is negatively (positively) correlated with the absolute change of b, showing that the lateral adjustability is more stable in developed watersheds than in forested ones. This makes sense since urban channels are often anthropogenically confined. More data on channel boundary materials and vegetation could help future study analyze the stability of the river channels in Puerto Rico.

Li et al. (2020) found that river channels can experience both significant instant and gradual changes as responses to floods brought by TCs from a broader view focusing on channel conveyance capacity. How these conveyance capacity changes were achieved by river reaches,

however, was not discussed in that paper. We herein elaborated on how channels adjust their geometry and roughness—changes of which can result in conveyance capacity changes—and identified potential predictors that render the channel geometry and roughness changes brought by TC floods more qualitatively predictable. Future studies on the quantitative connections between AHG parameter changes and conveyance capacity change are suggested; potentially applying AHG parameter regression models to conveyance capacity estimation. This could provide practical information for flood hazard management in dynamic channel networks.

3.6   Summary and Conclusions

River cross sectional geometry plays a critical role in fluvial processes (e.g. Bennet & Bridge, 1995; Guan et al., 2016; Malkinson & Wittenberg, 2007). Power law at-a-station hydraulic geometry (AHG) formulations describing this geometry were introduced more than 60 years ago (Leopold & Maddock, 1953) and have been widely confirmed empirically and analyzed theoretically (e.g. (Andreadis et al., 2013; Barefoot et al., 2019; Dingman, 2007; Ferguson, 1986). The physical controls of AHG remain underexplored (Jia et al., 2017; Qin et al., 2020), however, especially in tropical areas which are generally less instrumented than more temperate zones.

In Puerto Rico, the intense precipitation brought by tropical cyclones (TCs) has been shown before to cause substantial changes to channel conveyance capacity via sediment redistribution (Li et al., 2020). That study failed to identify the mechanisms for such changes, however. In this study, we examine AHG at 24 stream gage sites in Puerto Rico, with a focus on understanding and modeling the upstream and river reach controls on AHG—with one goal being AHG

estimation at ungaged sites—as well as how AHG can respond to major TC-induced floods. Key findings and conclusions are summarized here:

1. AHG parameters are highly correlated with a range of watershed and river reach characteristics; these relationships can largely be understood through existing geomorphological reasoning. AHG parameter estimates in this study are similar in magnitude to former studies in Puerto Rico.

2. AHG parameters can be robustly predicted using multiple linear regression with watershed and river reach characteristics. We can reach acceptable accuracy (relative RMSEs are usually between 10% and 30%) using these models, which could be used to predict AHG parameters in similar settings where cross sectional geometry data are lacking.

3. Some sites showed distinct changes in AHG—such as narrowed and deepened channels— after large floods, the large majority of which were caused by TCs. Certain watershed and river reach characteristics, specifically upstream watershed area, average watershed slope, watershed land cover, reach width, WHR, $NACW$, and sinuosity, are predictive both of whether and how AHG parameters change in response to floods.

Chapter 4   Flood-Induced Geomorphic Change of Floodplain Extent and Depth in Puerto Rico

Adapted from: Li, Yihan, Daniel B. Wright, and Yuan Liu. "Flood-Induced Geomorphic Change of Floodplain Extent and Depth: A Case Study of Hurricane Maria in Puerto Rico", manuscript submitted to Journal of Hydrologic Engineering

4.1   Introduction

Rainfall-induced flooding from tropical cyclones (TCs) can cause devastating impacts in Puerto Rico (PR) and similar tropical island environments (Mejia Manrique et al., 2021; van Oldenborgh et al., 2017). Hurricane Maria, which made landfall in PR on 20 September 2017, caused an estimated $90 billion in damages, making it the third costliest tropical cyclone in U.S. history (National Weather Service, 2021), while the mortality rate from 20 September-31 December 2017 was 62% higher than the same period in 2016 (Kishore et al., 2018). The record-breaking rainfall rates resulted in unprecedented flooding and mudslides (Keellings & Hernández Ayala, 2019). Maria was one of the costliest hurricanes in U.S. history in terms of both economic and social damage (Rahmstorf, 2017; Rivera, 2020). The devastation also led to calls for better preparedness, in part through updated and more accurate flood hazard characterization (Santiago et al., 2020).

TC's interactions with PR's mountainous terrain have been shown to produce some of the largest flood peaks per unit watershed area in the U.S. (Smith et al., 2005) and can mobilize substantial amounts of sediment via landslides, debris flows, and channel bank failures (West et al., 2011b).

Recent work has shown that floods of about 10-year annual recurrence interval and above—which are almost always caused by TCs—can cause significant instantaneous conveyance capacity changes in PR (Li et al., 2020). That same study also found that the magnitudes of those conveyance capacity changes are comparable to peak streamflow trends over the same study period, consistent with findings in the mainland US (Slater et al., 2015b). Sediment redistribution during TCs has also been shown to reshape channels' hydraulic geometry (Li et al., 2021), particularly in lower-gradient river reaches where channel substrate is typically more erosive (Ran et al., 2012).

The delineation of floodplains (e.g. 100-year flood extent) is central to flood risk management in the United States and elsewhere (Bellomo et al., 1999; Brown, 2016; Burby, 2001; King, 2012). While there is a growing recognition that current floodplain mapping practices should be revisited in light of global warming and its impacts on extreme rainfall and runoff production (Dinh et al., 2012; Mahmoud & Gan, 2018; Oubennaceur et al., 2021; Shadmehri Toosi et al., 2020), the impacts of climate-driven geomorphic changes on floodplains have received less attention (Das & Gupta, 2021). A question that thus emerges from prior research (e.g. Li et al., 2020, 2021) into the connections between TC-induced floods and channel change in PR is: "do these connections have any implication for floodplain extent or depth?".

This study examines that question, primarily by quantifying the floodplain changes wrought by Hurricane Maria in September 2017. Flood peaks associated with Hurricane Maria constitute the record observed instantaneous discharges at many of the long-term U.S. Geological Survey (USGS) stream gage sites in PR, and caused substantial changes to channel cross-sectional geometry at many of these sites (Li et al., 2021).

Aside from the extreme nature of Hurricane Maria's flooding, one additional aspect makes it well-suited for examining geomorphic effects on floodplain mapping: two high-quality island-wide digital elevation models (DEMs) were created using aerial light detection and ranging (LiDAR)—one before Maria in 2016-2017 and one shortly after, in 2018. These two DEMs are used to develop pre-Maria and post-Maria hydraulic models for thirteen river reaches across PR. "Before and after" changes in 10-year and 100-year floodplain extents and depths were obtained from hydraulic simulations. To give some context to the magnitude of these changes, they were compared with the floodplain extent and depth changes that would result from including or excluding Hurricane Maria peak streamflow observations from the estimation of 10-year and 100-year annual peak flow quantiles for each reach.

Relevant background on the connections between major floods and subsequent floodplain mapping is provided in Section 4.2. The study area and data sources are described in Section 4.3, while the existing FEMA-approved hydraulic model setups that were adapted in this study are detailed in Section 4.4. Methodology and results are presented in Sections 4.5 and 4.6, respectively. Further discussion and conclusions are provided in Section 4.7.

4.2 Background—Floodplain Mapping and the Impacts of Major Floods

Floodplain mapping—i.e. identification of the flood extent and depth for a given flood average recurrence interval (ARI)—is central to both structural flood risk management measures such as dikes, dams, flood walls, and non-structural approaches such as land use restrictions and flood insurance (Farooq et al., 2019; Grimaldi et al., 2013; Ongdas et al., 2020). Thorough review of

floodplain mapping practice is beyond the scope of this section; see Mudashiru et al. (2021) for a more detailed explanation. Instead, this study focus on two distinct ways in which major floods can inform floodplain mapping: their potential role in "reshaping" both peak streamflow quantile estimates and channel and floodplain morphometry (i.e. geometry/topography).

Streamflow quantile estimation, also referred to as flood frequency analysis (FFA), is broadly recognized as a critical element for accurate floodplain mapping, as well as a major source of uncertainty in the process (Diehl et al., 2021; Nyaupane et al., 2018; Oubennaceur et al., 2021). FFA has been the subject of considerable theoretical and practical attention over many years (see Stedinger et al. (1993) for a review of methods, and Dawdy et al. (2012) for a review of intellectual and developments in the U.S.). The potential for fluctuations in streamflow quantile estimates stemming from additional data and methodological refinement—as well as from potential changes in land use and topography—is one reason why the Federal Emergency Management Agency (FEMA) in the U.S. is required to "assess the need to revise and update all floodplain areas and flood risk zones identified once during [a] 5-year period," an obligation that is currently far from being met (Office of Inspector General, 2017). The issue of flood quantile changes and their effects on floodplain mapping may become more pressing as evidence mounts that key flood-generating mechanisms are changing with global warming (Allan et al., 2020). Compared with other potential drivers of flood nonstationarity, the potential role of changing flood peak quantiles is well-recognized (Slater et al., 2015b; Wasko et al., 2021). Even in the absence of climate or land use change (and some statistical objections notwithstanding; Barlow et al., 2020), it is evident that recalculating quantiles in the wake of major flood events can be warranted.

Compared with updating quantile estimates, evaluation of geomorphic changes—whether induced by major floods or otherwise—can be expensive and time-consuming if it entails additional LiDAR data collection (Muhadi et al., 2020). At least in certain settings, however, such data collection can be essential. High-resolution visual remote sensing images—one taken shortly before and the other shortly after the storm—clearly illustrate the geomorphic impacts of the storm on a river reach in the vicinity of one USGS stream gage site. These images (subpanels a-b and d-e of the top and bottom panels of Fig. 4.1) clearly show channel widening and the removal of substantial amounts of vegetation. The base elevation also experienced wide-spread vertical changes (subpanels c and f in Fig. 4.1).

It should be noted that the role of large floods in shaping floodplain morphometry appears to be relatively minor, at least in temperate settings and on human (e.g. annual-decadal) timescales. This fact can be inferred from the relatively minor research attention it has received as an agent of floodplain changes compared to other factors such as urbanization and other types of land use change (Gori et al., 2019; Leopold, 1968; Marapara et al., 2021; O'Connell et al., 2007; Schober et al., 2020). The climate and hydrology of PR and other tropical environments, however, are very different from more temperate climes and less-steep river systems, both in terms of the frequency of large floods and these floods' ability to mobilize sediment. More broadly, flooding processes in tropical regions remain understudied (Khan et al., 2015; Taniwaki et al., 2017), as has the potential importance of connections between climate and flood-relevant fluvial geomorphic change (Das & Gupta, 2021; Li et al., 2020; Slater et al., 2015b).
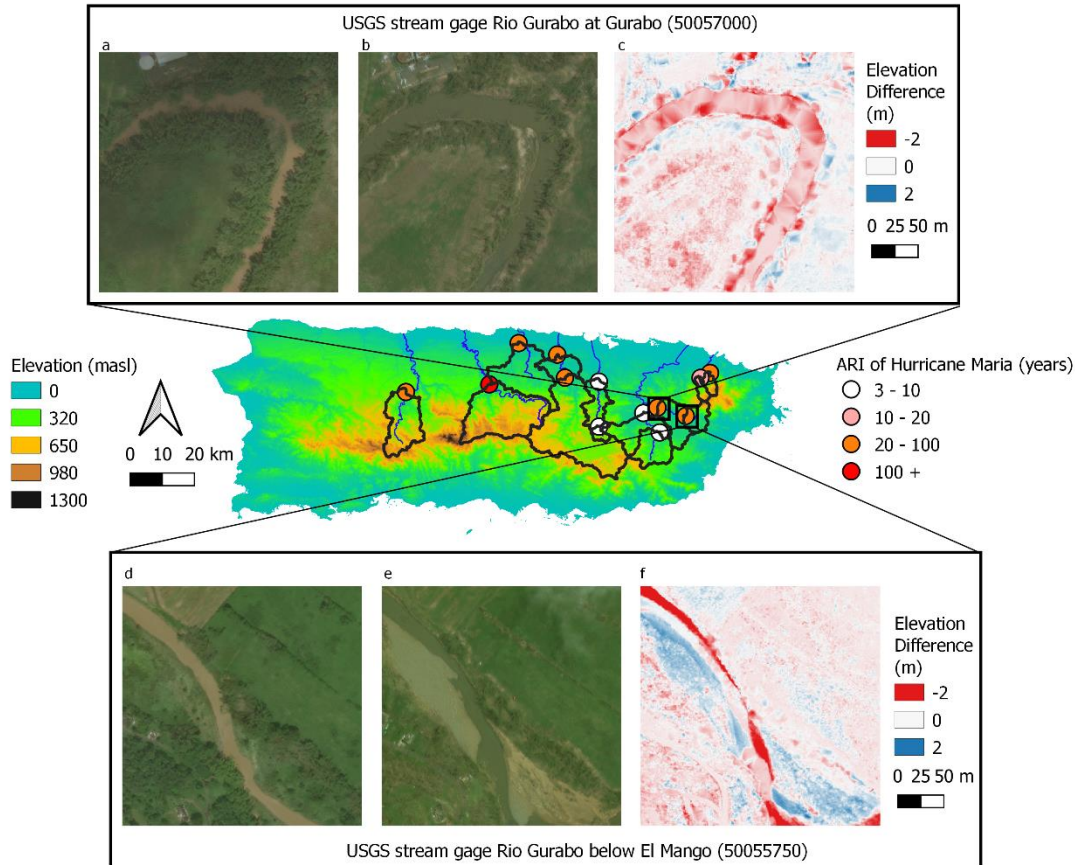
Fig. 4.1 Middle panel: Map of Puerto Rico, including USGS stream gage sites with upstream watershed boundaries, colored by Hurricane Maria average recurrence interval (ARI) estimates from LP3 using annual peak instantaneous discharge records including the peak of Hurricane Maria (see Section 4.5.1). Higher and Lower panels: High resolution satellite images taken before (panel a and d; 8 September 2017) and after (panel b and e; 24 September 2017) Hurricane Maria near the USGS stream gage Rio Gurabo at Gurabo (site 50057000, higher panel) and gage Rio Gurabo below El Mango (site 50055750, lower panel), and the land surface elevation difference between pre- and post-Maria LiDAR DEMs (panel c and f). Images in panels a and d, and b and e were obtained from Maxar Technologies (Catalog IDs 103001006F756500 and 1030010072069C00).

4.3   Study Region and Data

Puerto Rico (PR) is a 9,104 km^2 island located in the northeast Caribbean (Fig. 4.1). Elevations in the island's mountainous central portion can exceed 1300 m above sea level (masl), while the coastal lowlands have an average elevation of about 260 masl. The April-November rainy season coincides with the June-November North Atlantic TC season, and TC's contribute roughly one quarter of PR's annual precipitation (Rodgers et al., 2001). The dimensions of its rivers are usually limited by the island's aspect and east-west mountain range and range from <10 kilometers up to 50 kilometers in length (the longest being Rio de la Plata at 74 kilometers) and from <10 meters to more than 60 meters in width.

The USGS maintains historical annual instantaneous peak streamflow records for gaging stations within the National Water Information System (NWIS). These records were used to estimate 10, and 100-year peak streamflow quantiles by Log-Pearson III (LP3) quantile estimators, using L moment estimators (Hosking, 1990) in the R package "lmoments" (Asquith, 2021). Amongst other selection criteria, gaging sites with at least 20 years of peak discharge data are chosen. Sites flagged by the USGS as being located close to dams or man-made structures such as weirs were removed to avoid the influence of flow regulation and reduced channel adjustability (Reisenbüchler et al., 2019b). Thirteen sites satisfied these screening requirements (Fig. 4.1, middle panel; see Table 4.1 for site list and further details).

To study geomorphic change effects on flood mapping, two LiDAR DEMs are obtained for Puerto Rico: one made in 2016-2017 before Hurricane Maria, and one made in 2018, after Hurricane Maria, from National Oceanic and Atmospheric Administration (NOAA). The horizontal resolution of the DEM before (after) Hurricane Maria is 1 m (0.5 m). The stated

vertical accuracy of the pre-Maria (post-Maria) DEM is 9.4 cm (6.8 cm) (OCM Partners, 2021a, 2021b).

To identify potential drivers of floodplain changes by Hurricane Maria, upstream watershed and river reach characteristics were used for correlation analyses. Watershed boundaries and drainage area upstream of each stream gage were downloaded from NWIS. Watershed boundaries were then used to calculate watershed-averaged elevation and slope upstream of each gage, along with the digital elevation models (DEMs) obtained from the NOAA. Reach segments for each of the 13 gage sites were identified from the river network obtained from National Hydrography Dataset Plus (U.S. Geological Survey, 2006) for reach slope and sinuosity measurements. The sinuosity was measured as the reach length divided by the straight-line distance between the two ends of the reach. Kendall's tau nonparametric rank correlation (Kendall, 1938b) was used to examine relationships between watershed and reach characteristics and changes in floodplain extent and depth (described further in Section 4.3.3) associated with Hurricane Maria. It was unsuccessful, however, in identifying any meaningful correlations (i.e. statistically significant and consistent with geomorphic reasoning) between flood extent/depth changes and upstream watershed and river reach characteristics, and thus the results of this analysis are not shown.

Table 4.1. Summary of USGS sites, associated reach/watershed characteristics, and the ranges of Hurricane Maria average recurrence interval (ARI). The ranges of Hurricane Maria ARI were estimated using both annual peak instantaneous discharge records including and excluding the peak discharge associated with Hurricane Maria (see Section 4.5.3)

USGS Site ID	Hurricane Maria peak	# of Annual	Reach Width	Reach Slope	Sinuosity [m/m]	Upstream Watershed	Average Watershed	Average Watershed

	[m³/s] (Maria ARI [years])	Flood Peaks	[m]	[m/m]		Area [km²]	Elevation [m]	Slope [degree]
50024950	2001 (28-53)	24	30	9.7e-03	1.40	89	505	18
50035000	8037 (235-738)	74	72	1.9e-03	1.09	331	571	20
50039500	1557 (37-50)	61	10	1.5e-03	1.41	257	183	13
50045010	5094 (30-51)	30	27	9.2e-03	1.02	448	460	16
50046000	4245 (33-43)	63	26	9.0e-06	1.03	519	409	15
50047560	157 (9-11)	19	8	1.5e-02	1.24	22	438	9
50047850	259 (3-3)	38	18	4.9e-02	1.03	108	337	14
50051800	572 (5-5)	27	19	1.1e-03	1.11	106	290	14
50055000	1245 (8-9)	60	56	1.5e-04	1.22	233	260	13
50055750	691 (62-338)	29	28	2.9e-03	1.06	58	231	12
50057000	2434 (27-33)	60	31	2.6e-05	1.09	156	178	10
50063800	659 (74-174)	52	17	1.1e-02	1.38	22	434	14
50064200	495 (17-20)	43	12	2.1e-02	1.18	19	493	15

4.4   Hydraulic Models for Floodplain Mapping in Puerto Rico

One common tool for flood hazard mapping is hydraulic models which describe fluid motion and flood wave dynamics by solving mass and momentum conservation equations (Ceribasi & Ceyhunlu, 2021; Ongdas et al., 2020). One of the most widely applied models for flood simulation was developed by the U.S. Army Corps of Engineers Hydrologic Engineering Center River Analysis System (HEC-RAS; Dasallas et al., 2019), which provides both 1D and 2D simulation capabilities. Different iterations of HEC-RAS 1D have been the most commonly-used hydraulic model for floodplain mapping for FEMA National Flood Insurance Program (Afshari et al., 2018), while the newest Version 5 offers 2D capabilities (USACE., 2016). Though in principle able to provide more reliable results in complex flow settings, 2D models come with heavier computation cost and thus may not be well suited to applications with <10 m horizontal grid resolutions or in which multiple model runs are required (An et al., 2015). Steady flow modeling using 1D HEC-RAS can generate similar results as 2D modeling (Hajibayov et al., 2017) in rivers where flow directions are generally parallel to the river thalweg (Dimitriadis et al., 2016; Huţanu et al., 2020; Md Ali et al., 2015). Due to the high resolutions of the LiDAR DEMs and the large number of scenarios (i.e. two DEMs, two return levels, and 13 river reaches) in this study, most hydraulic analyses were carried out in 1D HEC-RAS, while 2D HEC-RAS was used at several sites to verify the 1D results.

1D HEC-RAS model setups were extracted from the FEMA Puerto Rico Model Inventory (FEMA Region II, 2018) for the 13 USGS gauging sites mentioned in Section 4.3 and shown in Table 4.1. These were developed by Strategic Alliance for Risk Reduction in 2018 (Strategic Alliance for Risk Reduction, 2018). These original FEMA setups are briefly described now. These HEC-RAS setups used channel/floodplain cross sectional elevations based on the pre-

Maria LiDAR DEM mentioned in Section 4.3. Each cross section was assigned a Manning's *n* value based on land cover. Notably, the original FEMA setups did not feature detailed channel bathymetry—instead, the LiDAR elevation, which is generally consistent with the water surface elevation at the time of the survey, was used as the channel bottom. This is an obvious shortcoming, and one that this study sought to mitigate, as described below in Section 4.5.2. Each cross section was provided with peak streamflow quantile estimates for recurrence intervals from 2 to 500 years, calculated from the two-parameter (drainage area and mean annual precipitation) regional regression equations published by USGS (Lopez et al., 1979; Ramos-Ginés, 1999), except for the 500-year flood (Strategic Alliance for Risk Reduction, 2018). These quantiles were adjusted using recent streamflow observations and streamflow quantile estimates from the effective coastal FEMA Flood Insurance Study (FIS) update for Puerto Rico and Municipalities were used for adjustment based on site-specific considerations (Strategic Alliance for Risk Reduction, 2018).

It should be emphasized that no attempts were made in this study to further validate or calibrate these model setups, since they presumably already complied with FEMA best practices. However, three key changes were made to the original FEMA-approved setups to better account for flood geomorphic change: 1) updating of cross-section elevations using the post-Maria LiDAR DEM; 2) the usage of at-site peak flow quantiles calculated using the methods described in Section 4.5.1; and 3) estimation of channel bathymetry as described in Section 4.5.2. The model domains were also reduced relative to the original setups—specifically restricted to the vicinity of the stream gaging stations, so that the at-site peak flow quantile estimates could be relied upon. This is described further in Section 4.5.2.

4.5   Methodology

4.5.1 Streamflow Quantile Estimation

As mentioned in Section 4.4, each cross-section within the original HEC-RAS model setups obtained from FEMA was assigned with streamflow quantile estimates from 2- to 500-years, and these estimates increased monotonically in the downstream direction within each reach. Due to limited documentation in Strategic Alliance for Risk Reduction (2018) of precisely how these were derived, it was elected to generate new at-site quantile estimates.

The Log Pearson III (LP3) distribution is widely used to model flood frequency, particularly in the United States (Griffis & Stedinger, 2007a, 2007b), and being applied to flood frequency research as well (e.g. Izinyon & Ehiorobo, 2014; Yu et al., 2019). 10- and 100-year peak streamflow for each site as LP3 quantiles using L moments (Hosking, 1990) were estimated via the R package "lmomco" (Asquith, 2021), using all available peak streamflow observations (including Hurricane Maria). All thirteen USGS gauging sites in this study experienced the peak streamflow of the 2017 water year on 20 September 2017, the same day that Hurricane Maria hit Puerto Rico. It was thus assumed that all peak flow observations on this day were caused by Hurricane Maria. To understand the significance of updating flood quantile estimates, 10- and 100-year peak streamflows were also calculated for each site using peak streamflow observations without Hurricane Maria. Reasons for doing so, and the associated results, are elaborated in Section 6.2. The ARIs of the Maria peak flows were also estimated, using the quantile function within "lmomco" (Fig. 4.1). Two sets of quantile estimates and Maria ARIs were found: the first

included the 2017 water year peak flow observations (which at all sites were caused by Maria) in the estimation, and second excluded the Maria observations.

4.5.2 DEM Correction and Terrain Generation

Due to possible non-physical differences (i.e. bias) between the two DEMs (Section 4.3), a correction process was applied. Using Google Earth, fourteen open areas across the island were identified. Areas were sought that can be assumed to not change appreciably in elevation on annual timescales—football, soccer, and baseball fields, as well as running tracks. These fields were then digitized to analyze for average elevation difference between the two LiDAR DEMs. Across these sites, the pre-Maria LiDAR was on average 7.08 cm lower than the post-Maria DEM. This difference was subtracted from the pre-Maria DEM. Further analysis of discrepancies is beyond the scope of this study.

Due to water column scattering and absorption of the signal, LiDAR-based DEMs usually depict water bodies as flat surfaces, i.e. they provide the water surface elevation rather than submerged bathymetry (Hernandez & Armstrong, 2016; Kalyanapu et al., 2013). This is the case for most USGS sites in this study, especially for the post-Maria DEM. The implication for this work is that within-channel topographic change associated with Hurricane Maria is not known and thus cannot be explicitly represented in pre- and post-Maria HEC-RAS models used in this study. During major floods, within-channel conveyance is often relatively small compared with floodplain conveyance (Bhowmik & Demissie, 1982). This is likely why, as mentioned in Section 4.4, the original FEMA models simply used the LiDAR elevations within the channels in

place of true or estimated bathymetry, which presumably extended somewhat below the LiDAR-based surface.

Inadequate treatment of channel bathymetry can nonetheless introduce unexpected errors into flood simulation results (Bhuyian et al., 2015). Multiple methods have been developed to measure or estimate channel bathymetry remotely; most of these require multispectral or hyperspectral inputs such as data from satellite and unmanned aerial vehicles (Getirana et al., 2018; He et al., 2021; Siermann et al., 2014; Thomas et al., 2021) which were unavailable in this study. Instead, this study used the DEM correction technique from Bhuyian et al. (2015), which is based only on observable channel and near-channel topography. This technique assumes that each river cross section is composed of two half-parabolic segments, the slopes of which gradually decrease to zero at the location of thalweg, where the two segments are assumed to intersect. Prior analysis of channel geometry observations have confirmed that channels at these sites are roughly parabolic (mean and median hydraulic $\frac{f}{b}$ relations of 2.5 and 1.7, respectively, straddling the parabolic relation of $\frac{f}{b} = 2.0$, see Li et al., 2021 for more details). This method has been shown to produce reasonable floodplain mapping results (Bhuyian et al., 2015, 2017).

The FEMA models obtained from FEMA generally cover long river reaches. As described in Section 4.5.1, 10-year and 100-year peak streamflow quantiles were estimated. To ensure that these were representative of realistic flood discharges within the study reaches, modeled reach lengths were restricted to the vicinity of USGS gauging sites. This was done by identifying cross sections where the original FEMA streamflow quantile estimates were within ±5% of the quantile estimate at the closest stream gage location. Areas were then "clipped" from the two

LiDAR DEMs that encompass all retained cross sections within each reach. The clipped DEMs for each reach were then used in HEC-RAS to generate new cross-sectional elevations.

4.5.3 Flood Hydraulic Simulations and Intercomparisons

HEC-RAS 1D simulations were ran using 10-year and 100-year flood quantiles (estimated with and without Hurricane Maria; Section 4.5.1) and pre- and post-Maria DEMs (Section 4.5.2) to simulate the effects on floodplain depth and extent stemming from "updating" both topography and flood quantiles. Models with different Manning's roughness values (half, double, and triple of original values) were also run to assess model sensitivity. HEC-RAS 1D simulations were also run without any modifications (i.e., using streamflow quantiles, roughness values, and cross-section geometries from the original FEMA models) for validating the former simulations. In addition, HEC-RAS 2D models were run for several sites to see if 2D results differed from 1D simulations. A 1 m grid was used with a computation interval of 1 second. Roughness values in the 2D models were interpolated from the values of the 1D cross sections.

The resulting flood depths and floodplain extents—i.e. the wetted area regardless of the inundation depth)—were compared. Holding peak flow quantiles constant, the percent change in floodplain extent after Hurricane Maria (i.e. using the post-Maria LiDAR DEM) was calculated by subtracting the extent before Hurricane Maria (i.e. using the pre-Maria LiDAR DEM) and dividing the difference by the pre-Maria extent. Flood depth changes were calculated only considering the areas that were inundated in both pre- and post-Maria models, subtracting pre-Maria simulated depths from post-Maria depths and dividing by the pre-Maria depth. The percent changes of floodplain extent and depth associated with the removal of Hurricane Maria

peak discharge observations from peak flow quantile estimates were calculated in a similar manner—by subtracting the "with-Maria" extents and depths from the "without-Maria" results and dividing by the latter.

4.6   Results

4.6.1 Geomorphic Effects of Hurricane Maria on Flood Extent and Depth

Here, simulated 10-year and 100-year flood extents and depths at the thirteen study sites resulting from the pre- and post-Maria DEMs are compared. Figs. 4.2-4.5, panels a-d show examples at two sites. As stated in Section 4.5, additional simulations were run using higher and lower roughness values, as were simulations using streamflow quantiles provided in the FEMA models rather than those estimated here. The results and conclusions drawn did not vary substantially depending on which roughness and quantile values were used, so the results of those additional simulations are omitted for brevity. Panels f of Figs. 4.2-4.5 show the flood extents resulting from the original unmodified FEMA models. Simulated floodplain extents were roughly consistent with those from the original FEMA models—compare, for example, Fig. 4.2d with 4.2f and Fig. 4.3d and 4.3f. Topographic changes—used here to represent geomorphic change (though other types of the latter are possible; see Section 4.7)—caused obvious flood extent and flood depth changes. This suggests that the refinements made to the original models did not cause undue deviations away from FEMA-sanctioned modeling practices. Two-dimensional HEC-RAS models were run at several sites to see if these geomorphic change effects on flood depend on model complexity. One- and two-dimensional models produced

similar flood extent maps (compare Figs. 4.2-4.5 panels d and e), thus supporting the decision, made for computational tractability, to focus on 1D modeling.

At USGS site 50055750 (Rio Guarabo below El Mango), the 10-year flood extent increased by 7% and the 100-year flood extent increased by 4%. The largest blue area visible in Figs. 4.2d and 4.3d was not within the pre-Maria 10- and 100-year floodplains respectively, but were predicted to see more than 5 m of flood depth in the post-Maria floodplains. This is a rather dramatic case, likely associated with a major riverbank failure; few other locations in Figs. 4.2 and 4.3 show major changes in flooded extent. Depth changes, on the other hand, are ubiquitous (Figs. 4.2c and 4.3c). For USGS site 50063800 (Rio Espiritu Santo near Rio Grande), the 10-year flood extent decreased by 5% and the 100-year flood extent decreased by 3%. The pink areas in Figs. 4.4d and 4.5d were predicted to be under water of up to 1 m depth under the pre-Maria DEM-based simulations, but outside of the 10-year and 100-year floodplains delineated using the post-Maria DEM. The flood depth increased in channel and decreased in the floodplain, likely as a result of channel scour. These two sites highlight that the "direction" of geomorphic/topographic change—floodplain expansion or contraction due to Maria's impacts—varies from place across the island.
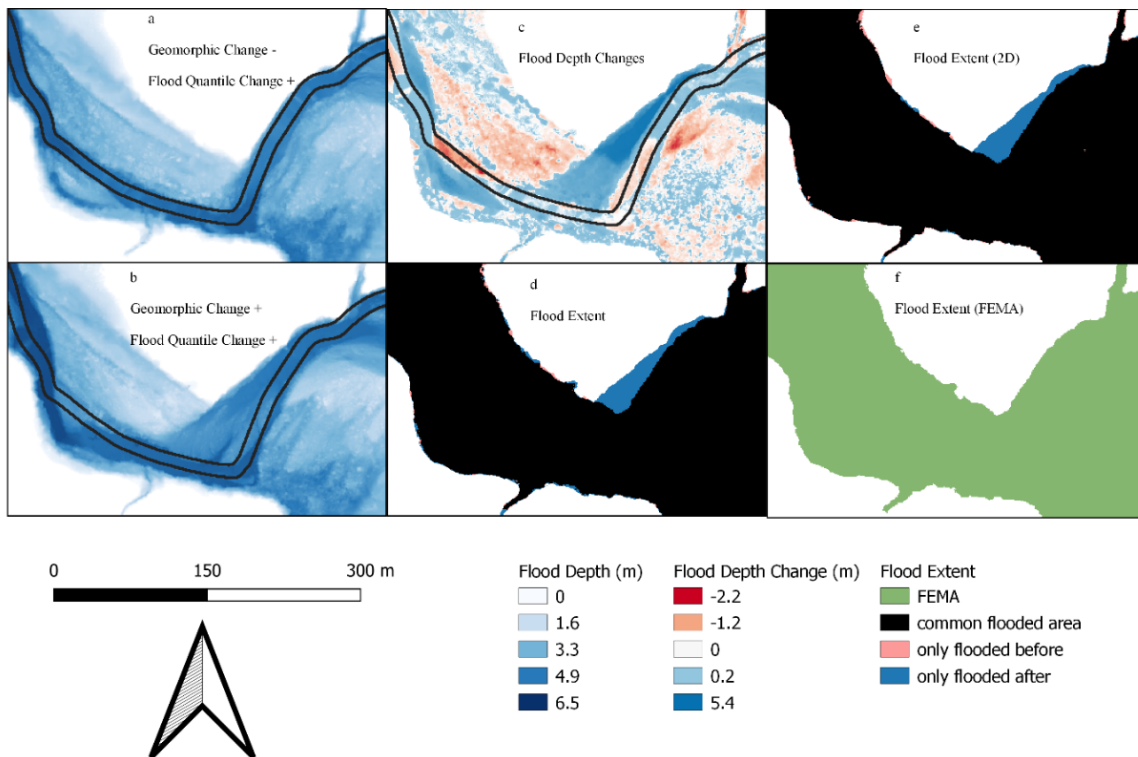
Fig. 4.2 Simulated 100-year floodplain map for Rio Guarabo below El Mango (USGS site 50055750). Panels a and b show 100-year flood depth mapping pre- and post-Maria DEMs, respectively. Panel c shows flood depth differences (pre-Maria depth subtracted from post-Maria depth). Black lines in panels a-c showed the bank lines of the river channel from the pre-Maria DEM. Panels d and e highlight pre- and post-Maria changes in floodplain extent predicted by 1D and 2D HEC-RAS. Panel f shows the 100-year flood extent created by the original 1D model obtained from FEMA.
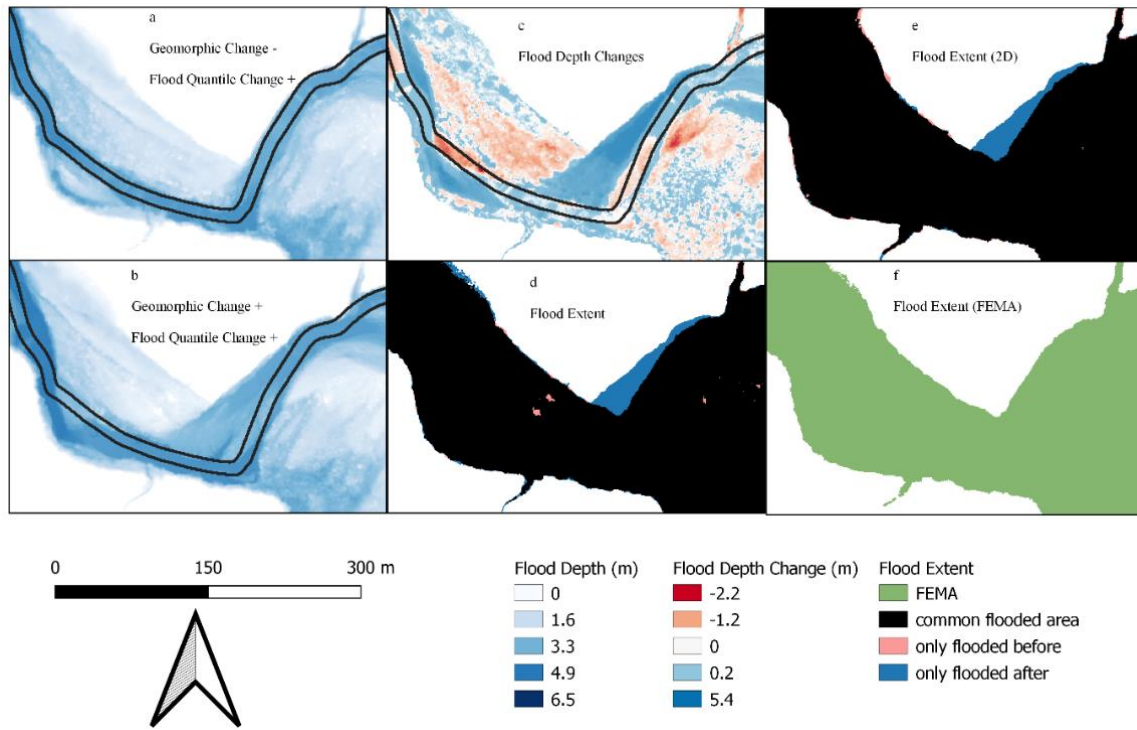
Fig. 4.3 As in Fig. 4.2, but for the 10-year flood.
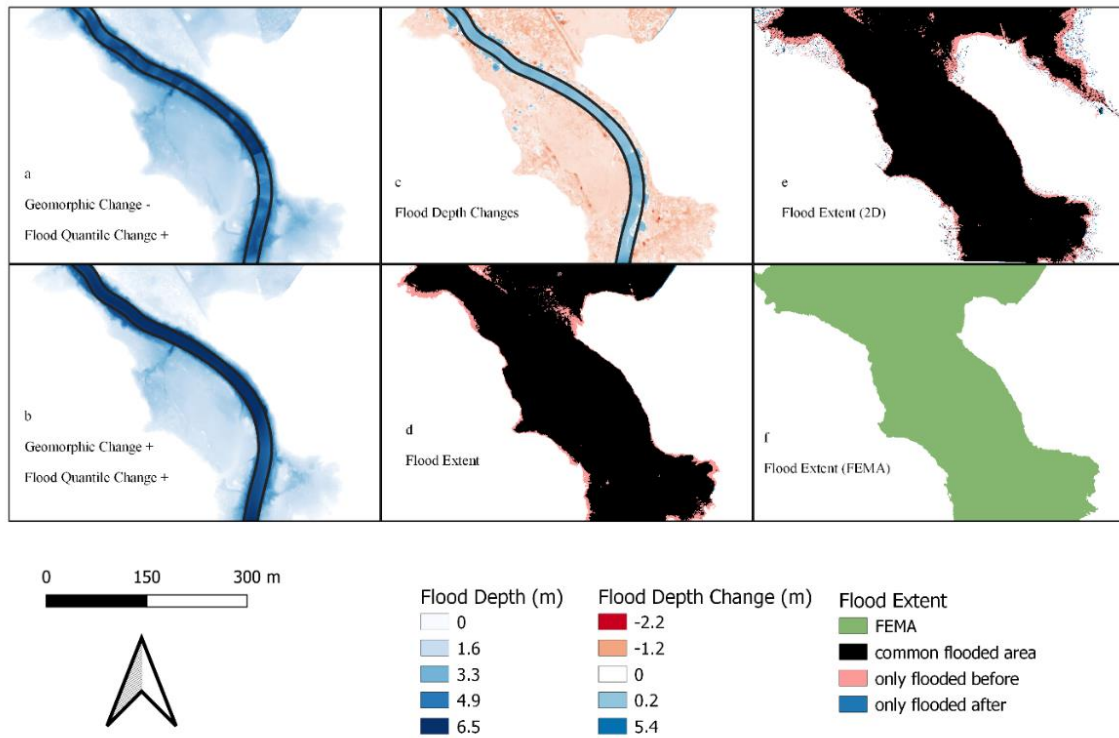
Fig. 4.4 Same as Fig. 4.2, but for the 100-year event for Rio Espiritu Santo near Rio Grande (USGS site 50063800).
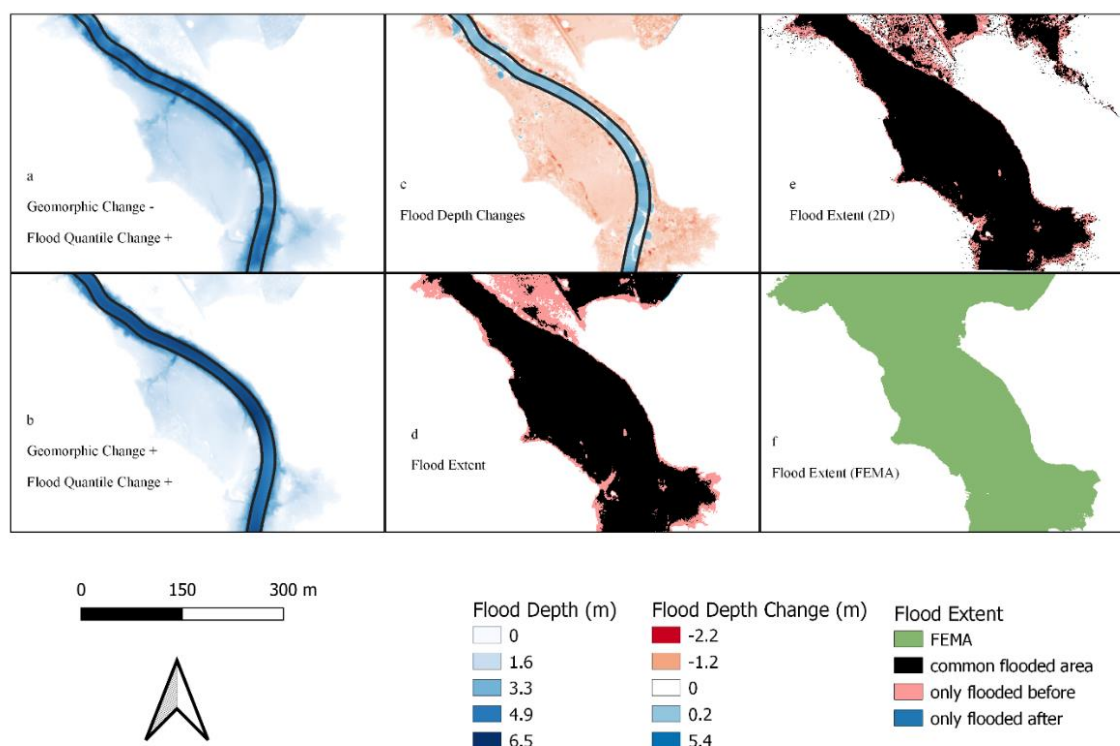
Fig. 4.5 Same as Fig. 4.2, but for the 10-year event for Rio Espiritu Santo near Rio Grande (USGS site 50063800).

Across the thirteen study sites, the flooded extent using the post-Maria DEM decreased by 1% (range: -5% to +7%) on average for 10-year floods and decreased by 0.3% (range: -3% to +4%) for 100-year floods (Table 4.2), relative to the flooded area using the pre-Maria DEM. The average absolute changes of 10-year and 100-year flood extents using the post-Maria DEM were 3% and 1%, respectively. As in the examples previously discussed, the average absolute flood depth changes were larger—5% (range: -9% to +16%) and 2% (range: -4% to +8%) for 10-year and 100-year floods, respectively. Nine sites experienced flood extent decreases for both 10-year and 100-year floods, while six (five) sites showed decreases in average flood depth for 10-year (100-year) floods. Note that the similar numbers of sites showing different directions of change

lead to average changes across sites to be near zero. The absolute values of percent change for both 10-year flooded extent and average flood depth are significantly higher than those for 100-year floods, calculated using paired t-tests ($p = 0.001$ and 0.02 for extent and depth, respectively). These results suggest that the geomorphic/topographic changes wrought by Maria had a greater influence on the extent and average depth of smaller floods and that these effects diminish at higher ARI. This is discussed further in Section 4.7.

Table 4.2. Simulated flood extent and depth changes, in percent, calculated from simulations using pre- and post-Maria LiDAR DEMs. Streamflow quantile estimates include observations of Hurricane Maria. The changes were calculated as the difference (average depth/extent simulated using pre-Maria DEM subtracted from the average depth/extent simulated using post-Maria DEM) divided by the simulated values using the pre-Maria DEM.

USGS Site Number and Name	Change in 10-y extent (%)	Change in 10-y depth (%)	Change in 100-y extent (%)	Change in 100-y depth (%)
50024950, Rio Grande de Arecibo below Utuado	-3.9	-3.7	-1.2	-2.0
50035000, Rio Grande de Manati at Ciales	-0.6	15.7	-0.1	7.6
50039500, Rio Cibuco at Vega Baja	2.3	-0.3	0.6	-1.0
50045010, Rio de La Plata below La Plata	-0.8	4.9	-0.2	1.0
50046000, Rio de La Plata at Highway 2 near Toa Alta	-1.2	0.5	-0.3	0.2
50047560, Rio de Bayamon below Lago de Cidra Dam	-2.3	0.7	-1.1	0.1
50047850, Rio de Bayamon near Bayamon	-3.7	-7.2	-1.7	-0.9
50051800, Rio Grande de Loiza at Hwy 183 San Lorenzo	-3.7	-8.7	-0.3	-2.3
50055000, Rio Grande de Loiza at Caguas	2.7	3.8	1.0	1.7
50055750, Rio Gurabo below El Mango	6.6	7.8	3.9	5.2

50057000, Rio Gurabo at Gurabo	3.5	2.2	1.8	1.4
50063800, Rio Espiritu Santo near Rio Grande	-4.6	-3.8	-2.7	-3.5
50064200, Rio Grande near El Verde	-2.6	-1.5	-0.5	0.2
Average Change	**-1.2**	**0.5**	**-0.3**	**0.2**
Average Absolute Change	**3.0**	**4.7**	**1.2**	**2.1**
Standard Deviation	**3.4**	**6.5**	**1.7**	**3.0**

4.6.2 Quantile Estimation Effects of Hurricane Maria on Flood Extent and Depth

The ARI of Hurricane Maria peak streamflow ranged from 3 to 235 years if Maria streamflows are included in that estimation, (Fig. 4.1 and Table 4.1), with a mean of 44 years. If Maria observations are excluded, these range from 3 to 738 years with a mean of 118 years. Hurricane Maria thus exceeded the 10-year event at most sites. In general, removing Hurricane Maria from the LP3 estimation resulted in decrease for both 10- and 100-year peak discharges for a majority of sites. 12 of 13 sites showed decreases in 10-year flood estimates, ranging from 1% to 18%, and the other site—where the estimated Maria ARI is 3 years—experienced an increase of 1%. On average, the 10-year flood estimates showed a decrease of 8%. 11 of 13 sites showed decreases in 100-year peak discharges, ranging from 1% to 33%, while two sites (with estimated ARIs of 3 and 5 years) experienced increases of 5% and 6% respectively (Table S10).

The streamflow quantile estimation effects on flood extent and flood depth caused by including vs. excluding Maria streamflows were not sensitive to which DEM was used, so only results using the pre-Maria DEM are provided (Table 4.3). As expected, sites that showed decreases in

streamflow quantile estimates also showed decreases in flood extent and depth. The decreases of 10-year flood extent and flood depth range from 0.4% to 8% and 0.1% to 6%, respectively, with one site showing a small 0.5% (0.4%) increase in 10-year flood extent (average depth). The decreases of 100-year flood extent and average depth range from 0.4% to 11% and from 0.1% to 17%, respectively, while two sites showed 1.5% (and 1.6%) and 1.8% (2.7%) increases in 100-year flood extent (depth). On average, flood extent decreased by 3% (4%) for 10-year (100-year) floods, while flood depth decreased by 2% (5%) for 10-year (100-year) floods. No watershed or river reach characteristics were found to be significantly correlated with either streamflow quantile estimation changes or associated flood extent or flood depth changes (results not shown). These results highlight that, contrary to the geomorphic change associated with Maria that was analyzed in the previous subsection, Maria's influence on streamflow quantile estimates is more pronounced at higher ARIs.

Table 4.3. Simulated flood extent and depth changes, in percent, from streamflow quantiles estimated including Maria streamflow observations. The percent changes were calculated as the difference (depth or extent map from records including Maria observations subtracted from the depth or extent map from records without Maria observations) divided by the corresponding values of depth or extent map from records including Maria observations. Simulations use the pre-Maria DEM.

USGS Site Number and Name	Change in 10-y extent (%)	Change in 10-y depth (%)	Change in 100-y extent (%)	Change in 100-y depth (%)
50024950, Rio Grande de Arecibo below Utuado	-3.3	-5.9	-5.8	-17.3
50035000, Rio Grande de Manati at Ciales	-2.7	-5.0	-9.0	-9.1
50039500, Rio Cibuco at Vega Baja	-3.5	-2.6	-3.7	-7.0

50045010, Rio de La Plata below La Plata	-3.1	-4.9	-8.8	-8.2
50046000, Rio de La Plata at Highway 2 near Toa Alta	-2.0	-1.7	-2.5	-3.0
50047560, Rio de Bayamon below Lago de Cidra Dam	-6.1	-5.8	-2.0	-1.9
50047850, Rio de Bayamon near Bayamon	0.5	0.4	1.5	1.6
50051800, Rio Grande de Loiza at Highway 183 San Lorenzo	-0.4	-0.3	1.8	2.7
50055000, Rio Grande de Loiza at Caguas	-0.6	-0.2	-0.4	-0.1
50055750, Rio Gurabo below El Mango	-7.6	-2.5	-10.5	-8.7
50057000, Rio Gurabo at Gurabo	-0.6	-1.2	-1.8	-2.3
50063800, Rio Espiritu Santo near Rio Grande	-2.7	-0.1	-3.1	-2.7
50064200, Rio Grande near El Verde	-3.0	-0.2	-1.1	-3.3
Average Change	**-2.7**	**-2.3**	**-3.5**	**-4.6**
Standard Deviation	**2.3**	**2.3**	**3.9**	**5.4**

4.7   Discussion and Conclusions

Using high-accuracy bias-adjusted LiDAR DEMs taken shortly before and after Hurricane Maria, flood extent (average depth) changes caused by geomorphic—i.e. floodplain topographic—changes of Hurricane Maria of up to 7% (16%) were found for the 10-year flood—with mean absolute changes of 3% (5%). Smaller changes were found for 100-year flood extents (depths): up to 4% (8%), with mean absolute changes of 1% (2%) (Table 4.2). Average floodplain depth and extent changes caused by 10-year flood events are of higher values than changes caused by 100-year flood events. This can be caused by the larger margin areas associated with 100-year

flood events where floodplain depth and extent changes are less. When Hurricane Maria observations are removed from the records, flood extent (depth) decreases by up to 8% (6%) for the 10-year event. Somewhat larger "quantile effect" changes of 11% (17%) for flood extent were found for the 100-year event (Table 4.3). This suggests that, at least in the sites examined here, geomorphic change—an understudied phenomenon, and imperfectly represented here by topographic changes wrought by Maria—as a result of major floods can be an important contributor to the temporal evolution of floodplains. It is also conceivable that the magnitude of geomorphic change could be higher elsewhere in Puerto Rico; changes were only evaluated in the vicinity of USGS stream gage sites, which are generally situated in locations of high channel stability.

The estimated ARI of Hurricane Maria was greater than 10-year for most sites (9 or 10 out of 13, depending on how the ARI was estimated [Table 4.1]). Thus there is general agreement with Li et al. (2020) that in PR, floods of roughly 10-year ARI and above can cause meaningful channel geomorphic change. More broadly, these findings (e.g., Fig. 4.2-4.5) confirm former studies that flood hazard can change in response to changes in channel conveyance capacity and channel morphology (e.g., Guan et al., 2016; Li et al., 2020, 2021; Slater, 2016; Wyżga, 1997). Changes in topography were the only type of geomorphic change captured in this study. In reality, a wider variety of changes can occur during and after major floods. Subpanels a and b, and d and f of Fig. 4.1, for example, shows substantial land cover change in the vicinity of the pictured channel, including trees felled by Hurricane Maria potentially increasing woody debris. Such changes can alter channel roughness and thus conveyance capacity (e.g., Kalyanapu, 2009), as can alteration of the channel substrate due to scour or deposition. Furthermore, major TCs such as Maria are

multi-hazard events. Maria, for example, caused substantial erosion and deposition along PR's beaches, with most suffering a loss of beach elevation (Barreto-Orta et al., 2019). Hurricanes can also hasten the decline of coral reefs (Gardner et al., 2005), which are believed to protect low-latitude coastal areas against floods (Ferrario et al., 2014). Study co-author Wright has observed that major floods often cause substantial sediment deposition in the vicinity of river mouths in other Caribbean islands, with the potential to dramatically reduce conveyance and increase flood potential over the "final stretch" where rivers feed into the ocean. Thus river channel and floodplain geomorphic change can be added to an already long list of riverine and coastal flood issues that can be influenced by TCs. An important issue with all these modes of change is how quickly—if at all—the affected environments can return to their pre-storm state. For example, Li et al. (2020) showed that channel conveyance capacity in PR undergoes a multiyear period of "recovery" toward prestorm quasi-equilibrium conditions. It would be challenging to extend this type of analysis to floodplain change due to the need for multiple high-accuracy LiDAR surveys over multiple decades.

Using climate change attribution techniques, Patricola & Wehner (2018) showed that Maria's rainfall was enhanced by recent climate warming, consistent with the general agreement around the tendency of TC rainfall to increase, especially in the tropical belt (Scoccimarro et al., 2017). With increasing rainfall intensity of TCs, channels and floodplains in PR and similar environments may experience more frequent or larger changes than those experienced historically.

Comparison between Sections 4.6.1 and 4.6.2 of geomorphic changes and "quantile update" changes suggests that geomorphic/topographic change due to major floods should be considered

as FEMA or other agencies assess flood map updating needs. The results also add to recent arguments (e.g. Naylor et al., 2017; Nones, 2019; Slater et al., 2015, 2019) that connections between climate, geomorphology, and floods may be an overlooked aspect of climate change-flood connections. However, the cost of acquiring and processing accurate and high-resolution terrain models frequently could hinder them being updated for the purpose of flood management, especially in some developing countries (Muhadi et al., 2020). Potential solutions to this issue include: 1.) confining the terrain models to be updated only within the area with high flood risk so tools such as LiDAR -carrying unmanned aerial vehicles could be more cost-effective, 2.) creating models to interpolate widespread geomorphological changes from smaller samples (e.g. Muñoz-Salinas et al., 2008), and 3.) conducting cost-benefit analyses based on potential economic risks of over or underprediction of floodplain after geomorphic changes.

Chapter 5   The Evolution of Social Perceptions of and Socioeconomic Responses to Tropical Cyclones in the Greater Caribbean

The majority of the chapter is synthesized from of the book Sea of Storms (Schwartz, 2015), with other resources explicitly.

5.1   Introduction

Chapters 2 and 3 focus on the temporal evolution of natural riverine systems in response to tropical cyclone (TC) rainfall-induced flooding, ultimate resulting in Chapter 4 in changes to abrupt alteration of flood hazard due to intense TC flooding. Chapter 2 further highlights how these systems gradually recover from storms. This chapter attempts to draw some broad parallels between the temporal evolution of these natural systems and how Caribbean people and institutions have responded to and understood TCs. Hurricanes affected the Caribbean region long before the first evidence of human habitation. People and institutions in the Caribbean archipelago have long sought to understand the causes of the hurricanes, seeking practical ways to deal with difficult conditions after hurricanes, and processing past experiences for potential prevention from damages of future hurricanes.

Before the physical processes of hurricanes started to be understood in early 19th century, they were usually assumed to have supernatural causes due to peoples' powerlessness in the face of their unpredictability and destructive forces. They were usually believed to be summoned either by wrathful or malevolent gods, in both cases as punishment for evil or immoral behaviors of people (McNeill, 2003; Pádua, 2010). Lacking scientifically-rooted methods, people also sought

ways to predict storms and protect themselves from them. Prayer and ritual played important roles, but humans also learned to read natural signs warning of the coming hurricanes from the past. A reddish sun, a strong odor from the sea, a rapid change of the wind direction from east to west, and the disappearance of insects were believed to indicate a hurricane's approach (Abbad, 1866). These experiences were passed on as social and cultural genes from generation to generation. Scientific developments gradually unveiled the relationships among natural parameters such as air pressure, temperature, wind, and precipitation. The knowledge promotes the idea that it was the natural interactions among these elements that caused the hurricanes, and thus humans should not bear responsibility for their happening (Kislow, 2008). However, as scholars and scientists furthered research in environmental sciences, climatology, meteorology, hydrology, and many other related fields, they came to agree that anthropological activities like fossil fuel usage and land cover / land use changes indeed affected the frequency and intensity of such natural hazards. This perspective again put responsibility back on humans for the severity of hurricanes' impacts (Pielke, 2013).

As scientific explanations and predictions developed, people and institutions sought ways to organize to minimize the damage. Early European colonial empires would send governments, which were composed mainly by royal families and the nobility, would send little more than nominal donations and expressions of sympathy to the survivors. Colonial governments developed more sophisticated relief policies, often for the benefit of particular races and classes with an aim to maintain the long-term profitability of the islands. With progress on human rights and the rise of democracy in the region in the 20th century, governments' reactions to hurricanes became more comprehensive, including forecasting and land use planning before hurricanes

along with rescuing and rebuilding afterwards. As will be seen, however, longstanding issues of race and class remain.

This chapter expands the focus on Puerto Rico in the former chapters to a broader Caribbean. While there are different definitions of the "Caribbean," this chapter specifically refers to the islands and not continental America. In this chapter, we will focus on changing understanding of divine providence and nature explanations of TCs, evolving social risk, and different roles of government evolved throughout the social and economic development of the Caribbean region. We close with a case study of Hurricane Maria in Puerto Rico, linking back to the focus of the former chapters. The chapter briefly summarizes the current state of understanding of and social responses to hurricanes, and the future directions that Hurricane Maria pointed out for local society. The majority of the chapter is synthesized from Sea of Storms (Schwartz, 2015), with other resources explicitly.

5.2   A Quasi-Cyclical Explanation of Hurricane Occurrence: From Religion to Science

Indigenous Caribbean peoples like the Taíno and Carib feared and respected the destructive power of TCs and often deified them. While islanders presumably dreaded the powers of these deities due to potential damage to agriculture, they also tried to alleviate the hazards through practical experience. Rows of trees were planted as windbreaks to protect the villages. Root crops like yucca, malanga, and yautia were favored by people in the Greater Antilles because of their great resistance to windstorm damage. The deification of hurricanes also shows that the indigenous people have already learned the circling behaviors, seasonality and both destructive

and creative nature of hurricanes. Taíno ceramic representations of a wind god, for example, shows a round face with spiraling arms pointing in opposite directions. This suggests that the Taíno perceived the circulatory nature of the hurricane winds around an eye, which was not established by Western science until the mid-nineteenth century (Ortiz, 2005). They remembered the occasions of the great hurricanes, and marked time in their communal ceremonial dances. Although believed to bring the destruction of floods, tidal surges, and high winds, TCs were also believed to renew the earth and bring life-giving waters by the indigenous people, a lesson later confirmed by colonial agriculturalists. These practices, together with the providential explanations, helped people adjust their annual social and economic cycle to frequent hurricanes. For example, the Caribs also recognized the seasonal nature of the TCs and integrated them into the cycle of their wars. Preparations for their raiding season against the Taíno each year began when constellation Ursa Minor appeared following the summer solstice, and the raids were carried out principally from late September to December when the TC season had largely subsided.

Similarly, natural disasters were also ascribed to the Judeo-Christian God during the region's colonial period. Starting in the 16th century, when European powers started to expand their influence in the area, their familiarity with hurricanes grew. Unlike drought, floods, earthquakes or other catastrophes to which there were plenty of biblical references, hurricanes were "new" disasters, unmentioned by ancient natural philosophers and cosmographers in Europe before colonization of the Caribbean. Early colonial observers attempted to reconcile theological explanations with their own experiences. As the European economic, social and political dominance grew, Christianity also took hold over the Caribbean area. Spanish governors in the

Caribbean suggested that hurricanes had become less intense and frequent ever since the Eucharist saved the Indians from ignorance and idolatry. Though the explanations might not be reasonable in today's view, it is possible that there was the coincidence of the introduction of Eucharist to Hispaniola by Spaniards and a lower TC activity phase of the El Niño Southern Oscillation, which potentially facilitated broad acceptance of Christianity by indigenous people.

Despite differing religious views, early European immigrants did appreciate and absorb the local experience of indigenous peoples facing hurricanes. They formed the idea that humans were not entirely powerless in the face of hurricanes and floods. They adjusted building styles to survive hurricanes better by learning from the local huts, and learned how to read the signs of hurricanes' coming. These experiences fascinated European observers as they believed that local communities were capable of hurricane prediction, and observers gradually found that God's intervention might not be the only way of explaining the causes of hurricanes. In particular, if the hurricanes were brought by God to correct people's evil deeds, then why did hurricanes come to the region each year in the same season?

During the age of the Enlightenment, peoples' perceptions and understanding of hurricanes made rapid progress. Regular observation and measurement of natural phenomena had gained many advocates, including within institutions like the Royal Society of London. During the period, scientific instruments like thermometers and barometers began to come into use. It was often observed that a drop in barometric pressure indicates stormy weather, and thus the barometric readings were thought to be useful even though the physics behind the observations were not totally understood. The first barometers arrived in Barbados in 1677, and local officials began recordkeeping of climatic conditions and measurements. The records, reported to the Royal

Society after a devastating hurricane hit Barbados before Martinique and Santo Domingo, were the first barometer readings of a tropical depression. Meticulous and sometimes obsessively detailed weather diaries, though some scientific institutions found them inapplicable and incapable of prediction or prevention, showed the mainstream scientific interests in hurricanes and the early attempts of science to understand hurricanes, and the belief that results would be beneficial. This recordkeeping has continued, with most islands' administrations featuring meteorological and hydrological services.

A large hurricane hit the eastern Caribbean area in August 1831, causing severe floods that took thousands of lives and caused enormous damage in many islands, such as Barbados and St. Vincent. This experience greatly motivated scientists and general public to learn more about the hurricanes, and that year marked the beginning of major advances in understanding and analysis of hurricanes. Early discoveries included that hurricane winds rotate around a central axis and that the speed of translation is independent of the speed of the surrounding winds. Additional work revealed insights into the relationships between rising heat and effects of convection on storm strength. Scientific debates about hurricane behavior occasionally became intense. Noticeably from these debates, however, were discussions of the role of providence and sin, showing a significant conceptual departure from earlier colonial and indigenous interpretations. New technology such as anemometers in the form of a wheel with cups to measure wind speed were invented. Statistics also became a tool that was applied to post-disaster situations for gathering information on the damage and loss calculation. The invention of steamships, telegraph and the oceanic cables made transcontinental and transatlantic communication of the hurricane conditions more efficient. Ethnological studies also began to study the deep-rooted racial

prejudice that negative habits like sloth can be associated with a particular race, thus going some way towards encouraging people to work together to plan for and recover from hurricanes and floods. Human frailties were quite separate from explanations of hurricanes during this time.

The rise of multidisciplinary science and technology in the 20th century led to growing convictions that hurricanes might be controlled or managed. Observation aircraft started to fly into and above storms, radar allowed distant observation of the weather, high-altitude weather balloons were used to get information on wind currents, and eventually weather satellites provided routine observation. Recorded data not only increased in volume but also in accuracy and consistency. These improvements greatly increased the accuracy of hurricane predictions and decreased associated potential hazards. For a time, the notion emerged that humans might be able to even prevent or control hurricanes. As understanding deepened, however, the scientific community started to realize that, rather than moving towards control of hurricanes, human actions and policies were actually exacerbating TC impacts. Urbanization, population concentration, agricultural expansion, and commercial area development not only increased the economic and social risks from hurricanes and other storms, but also caused direct ecological effects such as contraction of wetlands which add to the physical damage caused by hurricanes. Furthermore, while records showed that even though hurricane frequency stayed the same between 1975 and 2005, the proportion reaching Category 4 or 5 status doubled (Pielke Jr. et al., 2005; Shepherd & Knutson, 2007; Webster et al., 2005). This phenomenon is usually believed by the mainstream scientific community not to be a natural one, but to result from global warming, the root cause of which is the use of fossil fuels. Thus, current belief once again places responsibility for the devastation of hurricanes on human behavior.

5.3   Social Influence and Institution's Role

As hurricanes left geomorphic changes on river channels and floodplains (Chapters 2-4), they also left marks on society which could then influence future risks. Hurricanes' effects change interactions among people—how people organize themselves at different levels, communicate with each other, allocate resources and build communities, and how governments manage post-disaster relief and rebuilding. We turn here to how institutions reacted to and in some cases were created by hurricanes, and how in turn those institutions' actions affected future risks.

Social influences of hurricanes have been pervasive in the Caribbean. They can be as simple as increased risks for misplaced agricultural or commercial areas in flood-prone zones, and there are also examples of hurricanes directly influencing reforms such as trade policies, revolutions, and even emancipation and abolition of slavery. Take, for example, the islands that experienced multiple TCs in August 1780. As a relief policy, the Spanish government temporarily allowed the trade of foodstuffs with foreigners in its colonies such as Puerto Rico. The British Parliament responded to the appeals from Jamaica and Barbados, which had suffered tremendous losses during the TC season, with a huge amount of relief grant out of the fear of rebellion (Burnard, 2012). The hurricanes exacerbated poor living conditions for the slaves, who suffered most among all social classes. This led to discussion of slaves' conditions, with some arguing that it was not just simply the hurricanes that mattered, but also a structural situation inherent in slavery system. With increasing criticisms of the conditions of slaves, movements of abolition and emancipation were under way (e.g., Dickson, 2017; Luster, 1995) .

Governments are the natural destination that people turn to for help and relief after natural disasters in the 21ˢᵗ century. However, governments didn't always assume this level of responsibility. The Spanish crown started to be interested in hurricane hazards in the several decades after discovery by Columbus in 1492. Along with demographic information of each administrative district in the new territories, the crown also ordered local officials to keep an inventory of information on hydrography and hurricane occurrences. However, these early interests from the government were not out of care for common people, but for the purpose of controlling and making the area profitable, including by planning agriculture, navigation, and commerce around the hurricane season. City councils and the royal appointed governors were the first institutions to respond to natural disasters in the Spanish Caribbean colonies. Appointed by the crown and representative only of elite interests, their responses usually prioritized hurricane effects on the routes and patterns of transatlantic commerce. They usually appealed to the crown for economic concessions, such as tax relief and exemption, debt foreclosure extension and exemption, and support for more black slaves to help the planter class on the island.

The economic and political evolution of the Caribbean were influential on hurricane risks, sometimes turning the natural phenomena into human disasters. Export-oriented plantation agriculture tended to concentrate populations near islands' coasts or on lowlands near rivers and streams that could provide waterpower and facilitate transportation, but which also placed such activities in the way of flooding. It was recognized, however, that not all effects of hurricanes were negative. Large harvests often followed hurricanes, now understood as being due to hurricane-induced seed dispersal and nutrient transport. Only large planters were generally able to take advantage of such restorative effects of the hurricanes, however, since smaller owners

were often forced to sell their properties to larger planters to cope with immediate food shortages, housing loss, and disease. This stimulated the concentration of land through a transformation from small scale farms to larger plantations that focused only on a few export crops such as sugar and coffee. This concentration brought high profits in "quiet" years, but made the islands particularly vulnerable to food shortages and starvation after hurricanes.

Hurricanes usually came in the season of harvesting sugar and a number of other crops, thus there was always a risk that the last year's investment and labor might be in vain. Under increased hurricane risks brought by plantation expansion and population concentration, Indians and slaves—which made up the most of the islands' populations—could barely benefit from any of the aforementioned relief policies such as tax exemption. On top of limited relief support, these people, together with small proprietors, were sometimes recruited by governments to clear the roads at their own expense or face punishment and fines. It was thus the poorest citizens, not the government, that bore much of the direct responsibility for rebuilding. Together with food shortages, these struggles brought people together across cultural, ethnic, and social boundaries to exchange food and other resources, to provide the labor force for rebuilding, for organized prayer, and for other religious rites in hopes of protecting against hurricanes and floods. Donations to charities, usually organized by churches, were also a key element of recovery. The missing role of governments in disaster response sewed a growing discontent in the colonies that was exacerbated with each additional storm. Struggling with the commercial objectives and by mercantilist competition with European rivals, by the 18th century, colonial governments realized that they needed to assume more responsibility and take a more active role in disaster relief and rebuilding. Tax relief was extended to smaller planters, and trading food with other

islands—including those under control of other European crowns—was allowed after hurricanes to mitigate food shortages. Governments also started to organize donation efforts in their home countries. They propagandized the importance of the islands in newspapers after major TCs, and called for large-scale donation subscriptions. Although many policies still aimed primarily at maximizing islands' extractable productivity, colonial governments had assumed more responsibility under the realization that this productivity depended in part on islands' ability to recover from storms.

As hurricanes brought people together and then pushed responsibility onto governments, they also could intensify social divisions. Complaints grew around the unequal distribution of recovery resources due to social class, age, gender, race or religion. Relief funds tended to go to the hands of those privileged individuals such as large proprietors. Large houses on stable and safe land, which were usually owned by the upper class, were usually designed as shelters to accommodate refugees who lost their homes during hurricanes. ideas of racial segregation, however, led to unwillingness to provide such aid to many victims. Under the devastation of natural disasters and social discrimination, one option left to the lower and slave classes was revolution. Jamaica experienced a serious revolt in 1760 following a storm, while similar breakdown was also reported in Barbados, where the rebellion took place in heavily damaged Bridgetown. In Haiti, immediately after a TC hit in August 1791, a slave revolt overthrew French colonization and turned the island in to an independent country. Governments soon realized the economic costs of these social disturbances, and together with the awakening of modern humanitarian during the Enlightenment, the elite and upper class discussed the human rights of slaves and free people of color, the largest component of local population, and started to make

concessions to them. Natural hurricanes finally facilitated the "social hurricanes" which brought emancipation and slave abolition to the era. With such changes, Caribbean societies started to mitigate the disparities in wealth and rights of different race, class, and civil status, and witnessed more cooperation that would decrease hurricane and flood risks to common people. Following the Santa Ana Hurricane which hit Puerto Rico in 1825, for example, Captain Sir Thomas Cochrane expressed his personal sympathy and sent 100 pesos to the governor of Puerto Rico to be distributed to the poor communities. In St. Vincent after a TC in 1831, slaves demonstrated willingness to cooperate in the post-storm recovery even though they were the most affected group and now their masters didn't have the power to enforce their obedience due to the lack of troops or constabulary on the island (S. D. Smith, 2012). These examples demonstrate growing sympathy and affinity at the individual level among royal administrators, plantation owners and slaves.

With a strong interest in decreasing hurricane and flood risks, governments also realized that post-disaster relief was insufficient. Financial, organizational, and political support were provided to researchers in related meteorological fields to understand, predict, and try to reduce the magnitude of the hurricanes. Progress in multiple scientific disciplines in the 20th century empowered the governments to take pre-hurricane activities to reduce hurricane hazards and risks. Current governments have a large complement of tools ranging from flood risk mapping, regional planning, hurricane prediction and real-time tracking, to disaster rescuing, apportioning relief funds, and other supporting policies to not only save lives but also try to maintain living standards. Though major progress has been made towards bringing all people together to rebuild

homes in the aftermath, systemic racism in the region and beyond still impedes recovery from TCs (Rodriguez-Díaz & Lewellen-Williams, 2020).

5.4   Hurricane Maria in Puerto Rico

The role of the U.S. government in Puerto Rico embodies how modern governments cope with hurricane risks. Immediately following the transfer of government from Spain in 1899, Puerto Rico was hit by Hurricane San Ciriaco. While some tax revenues were returned from Congress to Puerto Rico and the military organized rebuilding, a slow response, unfair distribution of relief, and suppression of pro-Spanish elements strained Puerto Rico's new relationship with the U.S. The government learned from the lessons of Hurricane San Ciriaco when, in 1932, the Category 4 Hurricane San Ciprián came in the shadow of the Great Depression. Although in a severe economic crisis, Congress provided Puerto Rico with both direct aid from Washington and appropriations for the Red Cross to organize relief efforts. Later, the creation of the Federal Emergency Management Agency (FEMA) provided comprehensive hurricane risk management, from pre-disaster planning to post-disaster relief. It reflected a growing concern for hurricane victims and resolution of the government to do something in the wake of natural disasters. With these policies and changes, Puerto Rico seemed to be placed in good hands. Fortunately, although hurricanes were never absent from the island, Puerto Rico didn't experience another Category 4 or greater hurricane until Maria in 2017.

Hurricane Maria made landfall on 20 September 2017. Immediately before Maria, official forecasts did predict its rapid intensification. However, Hurricane Maria encountered favorable conditions that made it grow much faster and stronger than both models' and forecasters'

expectations. It claimed around 3,000 lives (Carlos et al., 2018), led to the departure of 200,000 more for the mainland (Lugo, 2019), deprived many residents of reliable electricity for almost a year, greatly increased mortality rates, and caused roughly $90 billion in damage on the island (National Weather Service, 2021). In the aftermath, two questions haunted people's minds: Why was it so severe? And what can be done to reduce future risks?

The severe damage was potentially intensified through lack of planning. Although FEMA created flood hazard maps for Puerto Rico, those maps can be out of date, lacking necessary updates about both hydrological and geomorphological information (see Chapter 4). Relief grants of over $12 billion from FEMA and $20 billion from the US Department of Housing and Urban Development were committed. Support was provided to clear roads, rebuild houses, restore electricity, and provide food and other daily necessities. Then-President Trump also made a personal visit to the Island. However, much of this response was too slow to meet the urgent needs (Willison et al., 2019), and some was only forthcoming under pressure from the public (Farber, 2018). Not all disaster supplied made their way to local communities due to potential political corruption (Romo & Florido, 2020), and, as in earlier storms, Hurricane Maria once again reveals unfairness in the distribution of preparation and relief through the boundaries between different social classes, races, genders and religions (García-López, 2018; Rodriguez-Díaz & Lewellen-Williams, 2020; Willison et al., 2019).

5.5   Summary

The history of the evolving providential and scientific understandings and socioeconomic structures showed that much like the riverine systems examined in Chapters 2-4, human

reactions to hurricanes show elements of both cyclical and adaptive behavior. Advances in scientific and socioeconomic methods in principle provide many more options to reduce hurricanes' impacts. Nonetheless, longstanding and intertwined social tensions and competing economic priorities resurface in the days and years after major storms. The balance of these human forces with the winds and rains of future hurricanes are likely to continue to shape the lives of Caribbean peoples in ways that will continue to echo those of the past in key ways.

Chapter 6   Conclusions and Future Directions

6.1   Conclusions

Although river channels can adjust to climate (Shugar et al., 2017) and land cover change (Mulahasan et al., 2017) on interannual to multidecadal scales (Slater et al., 2019), the roles of both instantaneous and short-term (i.e. up to several years) changes in this process of adjustment have received relatively little attention. Nearly instantaneous changes of both conveyance capacity and hydraulic geometry can result from the mobilization of sediment during major floods. These channel geomorphic changes caused during floods may in turn affect future flood hazards.

In Chapter 2, we found that short-term conveyance capacity change in Puerto Rico is widespread and can be comparable in magnitude to those of long-term peak streamflow change. TCs, which are predicted to intensify in a warming climate, not only cause the largest floods in Puerto Rico but are also critical drivers of conveyance capacity changes. We found that floods of about 10-year recurrence intervals are capable of causing such changes; this frequency is likely substantially higher than in more temperate settings.

In Chapter 3, AHG parameters were found to change after major hurricanes. Significant watershed and river reach characteristics were found to predict both AHG parameters and their changes after major hurricanes. Regression models were built with the significant characteristics, and the predictions reached an acceptable accuracy. The models can be used to predict AHG

parameters for ungaged sites, which would provide the critical geometry and roughness information in hydrologic and hydraulic studies.

In Chapter 4, hydraulic model simulations using pre- and post-storm digital terrain models showed that flood extent and depth underwent substantial changes after Hurricane Maria. This suggests that the fluvial geomorphic changes identified in chapter 2 and 3 will result in flood hazard changes in Puerto Rico. This in turn suggests that flood management institutions should consider the need for additional topographic data collection and new floodplain mapping in the wake of a record-breaking flood event.

Chapter 5 attempts to draw parallels between the TC-induced fluvial geomorphic evolution of river systems in the Caribbean and the time evolution social and economic systems in response to hurricanes in the region. Beginning in prehistory and continuing in the early colonial period, hurricanes were thought to be punishments meted out by deities to punish certain behaviors or action. This view gradually gave way to science-based observation and understanding. Socioeconomic systems have gradually and episodically developed coping strategies, policies, and technologies that can in principle decrease hurricane hazards and risks. Recurring class, racial, and economic tensions, however, continue to impede resilience to cyclones, while ongoing land use change and other planning failures, together with climate change—particularly intensification of tropical cyclone strength—has led to a renewed sense of hurricanes as being a result of human behavior.

6.2   Future Directions

This dissertation reveals that there are geomorphic changes associated with major hurricanes that can result in flood hazard changes. At the same time, it raises—but does not answer—additional questions. These could guide future research directions that would provide better understanding of the mechanisms behind these changes. It is worth noting here that while this research made extensive use of various observational datasets, an overarching limitation of the work is that no primary data was collected. It is probable that future progress in this area would require the collection of site-specific data throughout the research process, as opposed to the approach used here of "mining" existing datasets.

One potential future research direction centers around the long-term recovery behavior of the channels. After the instantaneous channel conveyance changes caused by hurricanes, it was shown in Chapter 2 that most channels would undergo a quasi-equilibrium "recovery" of conveyance, i.e. fully or partially revert back to its pre-storm state. The rate and the extent of the recovery are important for understanding flood hazard trends. This could not be examined in Chapter 4 due to the limited number (namely, one pre-storm and one post-storm) of digital terrain models needed to predict floodplain extent and depth. Longer-term collection of terrain and bathymetric information would be needed to examine post-storm recover. Attention should also be paid to other relevant characteristics such as channel substrates and vegetation loading which can also affect conveyance through roughness.

The channel cross sectional shape parameter $\frac{c}{a^{\frac{f}{b}}}$ was introduced in Chapter 3 for the first time, it describes the steepness of the banks for a given form determined by $\frac{f}{b}$. In practice, these parameters can be used by comparing with channel shapes to validate the results of AHG from

discharge records, and AHG parameters can be used as a proxy to monitor channel shape for underexplored reaches, together with remote sensing technologies. It was also found that data of different parts of the globe generally agreed on the log-log linear relationship between $\frac{f}{b}$ and b, with similar intercepts and slopes. Future studies about whether there are theoretical and physical controls behind that could further hydraulic geometry understanding.

The only geomorphic changes we considered in Chapter 4 were terrain elevation. However, high-resolution satellite images suggested that other than terrain changes, different land cover (e.g., fallen forests) may result in substantial roughness changes, which will add to flood hazard changes. A more comprehensive examination of the geomorphic changes could help flood risk managers to develop more accurate flood maps. Future studies can associate the more accurate flood hazards with social, economic, or environmental valuations. This association would yield maps of flood risks—which could embed societal and economic impacts—rather than just flood hazards, which only considers the physical reach of floods. Information on flood risks for different regions can be overlaid on local maps of race, class and economic groups. The adverse effects of the disasters can be analyzed to reveal if different groups suffered equally, and how existing socioeconomic, racial, class, and other inequalities affect the vulnerability to TCs and ability to recover. Together with other information like pollution distribution critical infrastructure, these comparisons could add to environmental justice studies and help ensure equitable pre-disaster urban planning and post-disaster relief distribution.

Climate change effects on riverine flood hazards were found to be of similar magnitudes as geomorphic effects caused by TCs. However, this dissertation only looks at the climate change

effects on flood peak discharges, and using relatively short records. Most climate models predicted decreases in future TC frequencies, but increases in strongest storm intensities and rainfall rates. It is also predicted that sea level rise, from climate change, will probably contribute to storm surge risks (T. R. Knutson et al., 2010; Walsh et al., 2016a). It should be noted that these effects from climate change can influence flood hazards and risks. Future studies of these dimensions of climate change will help illustrate more comprehensive effects of TCs on flood hazards and risks.

References

Abbad, I. (1866). *Historia geográfica, civil y natural de la Isla de San Juan Bautista de Puerto Rico*. Imp. y Librería de Acosta.

Afshari, S., Tavakoly, A. A., Rajib, M. A., Zheng, X., Follum, M. L., Omranian, E., & Fekete, B. M. (2018). Comparison of new generation low-complexity flood inundation mapping tools with a hydrodynamic model. *Journal of Hydrology*, *556*, 539–556. https://doi.org/10.1016/j.jhydrol.2017.11.036

Ahmad, R., Scatena, F. N., & Gupta, A. (1993). Morphology and sedimentation in Caribbean montane streams: Examples from Jamaica and Puerto Rico. *Sedimentary Geology*, *85*(1–4), 157–169. https://doi.org/10.1016/0037-0738(93)90080-O

Akbari, A., Mozafari, G., Fanodi, M., & Hemmesy, M. S. (2014). Impact of Landuse Change on River Floodplain Using Public Domain Hydraulic Model. *Modern Applied Science*, *8*(5), 80. https://doi.org/10.5539/mas.v8n5p80

Allan, R. P., Barlow, M., Byrne, M. P., Cherchi, A., Douville, H., Fowler, H. J., Gan, T. Y., Pendergrass, A. G., Rosenfeld, D., Swann, A. L. S., Wilcox, L. J., & Zolina, O. (2020). Advances in understanding large-scale responses of the water cycle to climate change. *Annals of the New York Academy of Sciences*, *1472*(1), 49–75. https://doi.org/10.1111/nyas.14337

An, H., Yu, S., Lee, G., & Kim, Y. (2015). Analysis of an open source quadtree grid shallow water flow solver for flood simulation. *Quaternary International*, *384*, 118–128. https://doi.org/10.1016/j.quaint.2015.01.032

Andreadis, K. M., Schumann, G. J.-P., & Pavelsky, T. (2013). A simple global river bankfull width and depth database: Data and Analysis Note. *Water Resources Research*, *49*(10), 7164–7168. https://doi.org/10.1002/wrcr.20440

Arnone, E., Dialynas, Y. G., Noto, L. V., & Bras, R. L. (2016). Accounting for soil parameter uncertainty in a physically based and distributed approach for rainfall-triggered landslides: Soil Parameter Uncertainty in Distributed Landslide Analysis. *Hydrological Processes*, *30*(6), 927–944. https://doi.org/10.1002/hyp.10609

Asquith, W. H. (2021). *lmomco—L-moments, censored L-moments, trimmed L-moments, L-comoments, and many distributions*.

Barber, C. A., & Gleason, C. J. (2018). Verifying the prevalence, properties, and congruent hydraulics of at-many-stations hydraulic geometry (AMHG) for rivers in the continental United States. *Journal of Hydrology*, *556*, 625–633. https://doi.org/10.1016/j.jhydrol.2017.11.038

Barefoot, E., Pavelsky, T. M., Allen, G. H., Zimmer, M. A., & McGlynn, B. L. (2019). Temporally Variable Stream Width and Surface Area Distributions in a Headwater Catchment. *Water Resources Research*, *55*(8), 7166–7181. https://doi.org/10.1029/2018WR023877

Barlow, A. M., Sherlock, C., & Tawn, J. (2020). Inference for extreme values under threshold-based stopping rules. *Journal of the Royal Statistical Society: Series C (Applied Statistics)*, *69*(4), 765–789. https://doi.org/10.1111/rssc.12420

Barreto-Orta, M., Méndez-Tejeda, R., Rodríguez, E., Cabrera, N., Díaz, E., & Pérez, K. (2019). *State of the beaches in Puerto Rico after Hurricane Maria (2017)*. *87*(1), 8.

Bayazit, M., & Önöz, B. (2007). To prewhiten or not to prewhiten in trend analysis? *Hydrological Sciences Journal*, *52*(4), 611–624. https://doi.org/10.1623/hysj.52.4.611

Bellomo, D., Pajak, M. J., & Sparks, J. (1999). Coastal Flood Hazards and the National Flood Insurance Program. *Journal of Coastal Research*, *28*, 7.

Bennet, S. J., & Bridge, J. S. (1995). The Geometry and Dynamics of Low-Relief Bed Forms in Heterogeneous Sediment in a Laboratory Channel, and their Relationship to Water Flow and Sediment Transport. *SEPM Journal of Sedimentary Research*, *Vol. 65A*. https://doi.org/10.1306/D4268013-2B26-11D7-8648000102C1865D

Best, H., McNamara, J. P., & Liberty, L. (2005). Association of Ice and River Channel Morphology Determined Using Ground-penetrating Radar in the Kuparuk River, Alaska. *Arctic, Antarctic, and Alpine Research*, *37*(2), 157–162. https://doi.org/10.1657/1523-0430(2005)037[0157:AOIARC]2.0.CO;2

Bhowmik, N. G., & Demissie, M. (1982). Carrying Capacity of Flood Plains. *Journal of the Hydraulics Division*, *108*(3), 443–452. https://doi.org/10.1061/JYCEAJ.0005839

Bhuyian, Md. N. M., Kalyanapu, A., & Hossain, F. (2017). Evaluating Conveyance-Based DEM Correction Technique on NED and SRTM DEMs for Flood Impact Assessment of the 2010 Cumberland River Flood. *Geosciences*, *7*(4), 132. https://doi.org/10.3390/geosciences7040132

Bhuyian, Md. N. M., Kalyanapu, A. J., & Nardi, F. (2015). Approach to Digital Elevation Model Correction by Improving Channel Conveyance. *Journal of Hydrologic Engineering*, *20*(5), 04014062. https://doi.org/10.1061/(ASCE)HE.1943-5584.0001020

Booth, D. B. (1990). STREAM-CHANNEL INCISION FOLLOWING DRAINAGE-BASIN URBANIZATION. *Journal of the American Water Resources Association*, *26*(3), 407–417. https://doi.org/10.1111/j.1752-1688.1990.tb01380.x

Bridge, J. S. (1993). The interaction between channel geometry, water flow, sediment transport and deposition in braided rivers. *Geological Society, London, Special Publications*, *75*(1), 13–71. https://doi.org/10.1144/GSL.SP.1993.075.01.02

Brinkerhoff, C. B., Gleason, C. J., & Ostendorf, D. W. (2019). Reconciling at-a-Station and at-Many-Stations Hydraulic Geometry Through River-Wide Geomorphology. *Geophysical Research Letters*, *46*(16), 9637–9647. https://doi.org/10.1029/2019GL084529

Brown, J. T. (2016). *Introduction to FEMA's National Flood Insurance Program (NFIP)*. Congressional Research Service.

Bulmer-Thomas, V. (2012). *The economic history of the Caribbean since the Napoleonic wars*. Cambridge University Press.

Burby, R. J. (2001). Flood insurance and floodplain management: The US experience. *Environmental Hazards*, *3*(3), 111–122. https://doi.org/10.3763/ehaz.2001.0310

Burnard, T. (2012). Harvest Years? Reconfigurations of Empire in Jamaica, 1756–1807. *The Journal of Imperial and Commonwealth History*, *40*(4), 533–555. https://doi.org/10.1080/03086534.2012.724234

Carlos, S.-B., Goldman, A., Andrade, E., Barrett, N., Colon-Ramos, U., Edberg, M., Garcia-Meza, A., Goldman, L., Roess, A., Sandberg, J., & Zeger, S. (2018). *Ascertainment of the estimated excess mortality from hurricane Maria in Puerto Rico.*

Cawley, G. C. (2006). Leave-One-Out Cross-Validation Based Model Selection Criteria for Weighted LS-SVMs. *The 2006 IEEE International Joint Conference on Neural Network Proceedings*, 1661–1668. https://doi.org/10.1109/IJCNN.2006.246634

Ceribasi, G., & Ceyhunlu, A. I. (2021). Generation of 1D and 2D flood maps of Sakarya river passing through Geyve district of Sakarya city in Turkey. *Natural Hazards*, *105*(1), 631–642. https://doi.org/10.1007/s11069-020-04327-8

Chen, X., & Chiew, Y.-M. (2003). Response of Velocity and Turbulence to Sudden Change of Bed Roughness in Open-Channel Flow. *Journal of Hydraulic Engineering*, *129*(1), 35–43. https://doi.org/10.1061/(ASCE)0733-9429(2003)129:1(35)

Chen, Y. R., & Chu, P.-S. (2014). Trends in precipitation extremes and return levels in the Hawaiian Islands under a changing climate: CHANGES IN PRECIPITATION EXTREMES AND RETURN PERIODS IN HAWAII. *International Journal of Climatology*, *34*(15), 3913–3925. https://doi.org/10.1002/joc.3950

Clark, J. J., & Wilcock, P. R. (2000a). Effects of land-use change on channel morphology in northeastern Puerto Rico. *Geological Society of America Bulletin*, 15.

Clark, J. J., & Wilcock, P. R. (2000b). Effects of land-use change on channel morphology in northeastern Puerto Rico. *Geological Society of America Bulletin*, *112*(12), 1763–1777. https://doi.org/10.1130/0016-7606(2000)112<1763:EOLUCO>2.0.CO;2

Clarke, R. T. (2013). How should trends in hydrological extremes be estimated?: Trends in Hydrological Extremes. *Water Resources Research*, *49*(10), 6756–6764. https://doi.org/10.1002/wrcr.20485

Dai, S. B., & Lu, X. X. (2010a). Sediment deposition and erosion during the extreme flood events in the middle and lower reaches of the Yangtze River. *Quaternary International*, *226*(1–2), 4–11. https://doi.org/10.1016/j.quaint.2010.01.026

Dai, S. B., & Lu, X. X. (2010b). Sediment deposition and erosion during the extreme flood events in the middle and lower reaches of the Yangtze River. *Quaternary International*, *226*(1–2), 4–11. https://doi.org/10.1016/j.quaint.2010.01.026

Daly, C., Helmer, E. H., & Quiñones, M. (2003). Mapping the climate of Puerto Rico, Vieques and Culebra: CLIMATE MAPPING. *International Journal of Climatology*, *23*(11), 1359–1381. https://doi.org/10.1002/joc.937

Das, S., & Gupta, A. (2021). Multi-criteria decision based geospatial mapping of flood susceptibility and temporal hydro-geomorphic changes in the Subarnarekha basin, India. *Geoscience Frontiers*, *12*(5), 101206. https://doi.org/10.1016/j.gsf.2021.101206

Dasallas, L., Kim, Y., & An, H. (2019). Case Study of HEC-RAS 1D–2D Coupling Simulation: 2002 Baeksan Flood Event in Korea. *Water*, *11*(10), 2048. https://doi.org/10.3390/w11102048

David, G. C. L., Wohl, E., Yochum, S. E., & Bledsoe, B. P. (2010). Controls on at-a-station hydraulic geometry in steep headwater streams, Colorado, USA. *Earth Surface Processes and Landforms*, *35*(15), 1820–1837. https://doi.org/10.1002/esp.2023

Dawdy, D. R., Griffis, V. W., & Gupta, V. K. (2012). Regional Flood-Frequency Analysis: How We Got Here and Where We Are Going. *Journal of Hydrologic Engineering*, *17*(9), 953–959. https://doi.org/10.1061/(ASCE)HE.1943-5584.0000584

Diakakis, M., Deligiannakis, G., Katsetsiadou, K., & Lekkas, E. (2015a). Hurricane Sandy mortality in the Caribbean and continental North America. *Disaster Prevention and Management*, *24*(1), 132–148. https://doi.org/10.1108/DPM-05-2014-0082

Diakakis, M., Deligiannakis, G., Katsetsiadou, K., & Lekkas, E. (2015b). Hurricane Sandy mortality in the Caribbean and continental North America. *Disaster Prevention and Management: An International Journal*, *24*(1), 132–148. https://doi.org/10.1108/DPM-05-2014-0082

Dickson, WILLIAM. G. (2017). *LETTERS ON SLAVERY*. HANSEBOOKS.

Diehl, R. M., Gourevitch, J. D., Drago, S., & Wemple, B. C. (2021). Improving flood hazard datasets using a low-complexity, probabilistic floodplain mapping approach. *PLOS ONE*, *16*(3), e0248683. https://doi.org/10.1371/journal.pone.0248683

Dimitriadis, P., Tegos, A., Oikonomou, A., Pagana, V., Koukouvinos, A., Mamassis, N., Koutsoyiannis, D., & Efstratiadis, A. (2016). Comparative evaluation of 1D and quasi-2D hydraulic models based on benchmark and real-world applications for uncertainty assessment in flood mapping. *Journal of Hydrology*, *534*, 478–492. https://doi.org/10.1016/j.jhydrol.2016.01.020

Dingman, S. L. (2007). Analytical derivation of at-a-station hydraulic–geometry relations. *Journal of Hydrology*, *334*(1–2), 17–27. https://doi.org/10.1016/j.jhydrol.2006.09.021

Dingman, S. L., & Afshari, S. (2018). Field verification of analytical at-a-station hydraulic-geometry relations. *Journal of Hydrology*, *564*, 859–872. https://doi.org/10.1016/j.jhydrol.2018.07.020

Dinh, Q., Balica, S., Popescu, I., & Jonoski, A. (2012). Climate change impact on flood hazard, vulnerability and risk of the Long Xuyen Quadrangle in the Mekong Delta. *International*

Journal of River Basin Management, *10*(1), 103–120. https://doi.org/10.1080/15715124.2012.663383

Doll, B. A., Wise-Frederick, D. E., Buckner, C. M., Wilkerson, S. D., Harman, W. A., Smith, R. E., & Spooner, J. (2002). HYDRAULIC GEOMETRY RELATIONSHIPS FOR URBAN STREAMS THROUGHOUT THE PIEDMONT OF NORTH CAROLINA. *Journal of the American Water Resources Association*, *38*(3), 641–651. https://doi.org/10.1111/j.1752-1688.2002.tb00986.x

Doyle, M. W., & Shields, F. D. (2000). Incorporation of bed texture into a channel evolution model. *Geomorphology*, *34*(3–4), 291–309. https://doi.org/10.1016/S0169-555X(00)00014-3

Eckner, A. (2012). *A Framework for the Analysis of Unevenly Spaced Time Series Data*. 45.

Falcone, J. A., Carlisle, D. M., Wolock, D. M., & Meador, M. R. (2010a). GAGES: A stream gage database for evaluating natural and altered flow conditions in the conterminous United States: ***Ecological Archives* E091-045** . *Ecology*, *91*(2), 621–621. https://doi.org/10.1890/09-0889.1

Falcone, J. A., Carlisle, D. M., Wolock, D. M., & Meador, M. R. (2010b). GAGES: A stream gage database for evaluating natural and altered flow conditions in the conterminous United States: ***Ecological Archives* E091-045** . *Ecology*, *91*(2), 621–621. https://doi.org/10.1890/09-0889.1

Farber, D. A. (2018). Response and Recovery after Maria: Lessons for Disaster Law and Policy. *SSRN Electronic Journal*. https://doi.org/10.2139/ssrn.3174466

Farooq, M., Shafique, M., & Khattak, M. S. (2019). Flood hazard assessment and mapping of River Swat using HEC-RAS 2D model and high-resolution 12-m TanDEM-X DEM

(WorldDEM). *Natural Hazards*, *97*(2), 477–492. https://doi.org/10.1007/s11069-019-03638-9

FEMA Region II. (2018). *Puerto Rico Model Inventory*. https://www.arcgis.com/apps/webappviewer/index.html?id=e860313f550d487c88b360dd7da52d19

Ferguson, R. I. (1986). Hydraulics and hydraulic geometry. *Progress in Physical Geography: Earth and Environment*, *10*(1), 1–31. https://doi.org/10.1177/030913338601000101

Ferrario, F., Beck, M. W., Storlazzi, C. D., Micheli, F., Shepard, C. C., & Airoldi, L. (2014). The effectiveness of coral reefs for coastal hazard risk reduction and adaptation. *Nature Communications*, *5*(1), 3794. https://doi.org/10.1038/ncomms4794

Fitzpatrick, F. A., & Knox, J. C. (2000). SPATIAL AND TEMPORAL SENSITIVITY OF HYDROGEOMORPHIC RESPONSE AND RECOVERY TO DEFORESTATION, AGRICULTURE, AND FLOODS. *Physical Geography*, *21*(2), 89–108. https://doi.org/10.1080/02723646.2000.10642701

García-López, G. A. (2018). The Multiple Layers of Environmental Injustice in Contexts of (Un)natural Disasters: The Case of Puerto Rico Post-Hurricane Maria. *Environmental Justice*, *11*(3), 101–108. https://doi.org/10.1089/env.2017.0045

Gardner, T. A., Côté, I. M., Gill, J. A., Grant, A., & Watkinson, A. R. (2005). HURRICANES AND CARIBBEAN CORAL REEFS: IMPACTS, RECOVERY PATTERNS, AND ROLE IN LONG-TERM DECLINE. *Ecology*, *86*(1), 174–184. https://doi.org/10.1890/04-0141

Gellis, A. (1993). The effects of hurricane hugo on suspended-sediment loads, Lago loíza Basin, Puerto Rico. *Earth Surface Processes and Landforms*, *18*(6), 505–517. https://doi.org/10.1002/esp.3290180604

Getirana, A., Jung, H. C., & Tseng, K.-H. (2018). Deriving three dimensional reservoir bathymetry from multi-satellite datasets. *Remote Sensing of Environment*, *217*, 366–374. https://doi.org/10.1016/j.rse.2018.08.030

Gleason, C. J., & Smith, L. C. (2014). Toward global mapping of river discharge using satellite images and at-many-stations hydraulic geometry. *Proceedings of the National Academy of Sciences*, *111*(13), 4788–4791. https://doi.org/10.1073/pnas.1317606111

Gori, A., Blessing, R., Juan, A., Brody, S., & Bedient, P. (2019). Characterizing urbanization impacts on floodplain through integrated land use, hydrologic, and hydraulic modeling. *Journal of Hydrology*, *568*, 82–95. https://doi.org/10.1016/j.jhydrol.2018.10.053

Goudarzi, M. A., Cocard, M., Santerre, R., & Woldai, T. (2013). GPS interactive time series analysis software. *GPS Solutions*, *17*(4), 595–603. https://doi.org/10.1007/s10291-012-0296-2

Griffis, V. W., & Stedinger, J. R. (2007a). Log-Pearson Type 3 Distribution and Its Application in Flood Frequency Analysis. I: Distribution Characteristics. *Journal of Hydrologic Engineering*, *12*(5), 482–491. https://doi.org/10.1061/(ASCE)1084-0699(2007)12:5(482)

Griffis, V. W., & Stedinger, J. R. (2007b). Log-Pearson Type 3 Distribution and Its Application in Flood Frequency Analysis. II: Parameter Estimation Methods. *Journal of Hydrologic Engineering*, *12*(5), 492–500. https://doi.org/10.1061/(ASCE)1084-0699(2007)12:5(492)

Grimaldi, S., Petroselli, A., Arcangeletti, E., & Nardi, F. (2013). Flood mapping in ungauged basins using fully continuous hydrologic–hydraulic modeling. *Journal of Hydrology*, *487*, 39–47. https://doi.org/10.1016/j.jhydrol.2013.02.023

Guan, M., Carrivick, J. L., Wright, N. G., Sleigh, P. A., & Staines, K. E. H. (2016a). Quantifying the combined effects of multiple extreme floods on river channel geometry and on flood hazards. *Journal of Hydrology*, *538*, 256–268. https://doi.org/10.1016/j.jhydrol.2016.04.004

Guan, M., Carrivick, J. L., Wright, N. G., Sleigh, P. A., & Staines, K. E. H. (2016b). Quantifying the combined effects of multiple extreme floods on river channel geometry and on flood hazards. *Journal of Hydrology*, *538*, 256–268. https://doi.org/10.1016/j.jhydrol.2016.04.004

Hajdukiewicz, H., Wyżga, B., Mikuś, P., Zawiejska, J., & Radecki-Pawlik, A. (2016). Impact of a large flood on mountain river habitats, channel morphology, and valley infrastructure. *Geomorphology*, *272*, 55–67. https://doi.org/10.1016/j.geomorph.2015.09.003

Hajibayov, F., Ozkul, B. D., & Terzi, F. (2017). *Floodplain Modeling and Mapping Using The Geographical Information Systems (GIS) and Hec-RAS/Hec-GeoRAS Applications. Case of Edirne, Turkey.* 9.

Hannaford, J., & Buys, G. (2012). Trends in seasonal river flow regimes in the UK. *Journal of Hydrology*, *475*, 158–174. https://doi.org/10.1016/j.jhydrol.2012.09.044

Harvey, A. M. (2007). Differential recovery from the effects of a 100-year storm: Significance of long-term hillslope–channel coupling; Howgill Fells, northwest England. *Geomorphology*, *84*(3–4), 192–208. https://doi.org/10.1016/j.geomorph.2006.03.009

Hatcher, K. L., & Jones, J. A. (2013). Climate and Streamflow Trends in the Columbia River Basin: Evidence for Ecological and Engineering Resilience to Climate Change. *Atmosphere-Ocean*, *51*(4), 436–455. https://doi.org/10.1080/07055900.2013.808167

Hawley, R. J., MacMannis, K. R., & Wooten, M. S. (2013). Bed coarsening, riffle shortening, and channel enlargement in urbanizing watersheds, northern Kentucky, USA. *Geomorphology*, *201*, 111–126. https://doi.org/10.1016/j.geomorph.2013.06.013

He, J., Lin, J., Ma, M., & Liao, X. (2021). Mapping topo-bathymetry of transparent tufa lakes using UAV-based photogrammetry and RGB imagery. *Geomorphology*, *389*, 107832. https://doi.org/10.1016/j.geomorph.2021.107832

Heritage, G. L., Large, A. R. G., Moon, B. P., & Jewitt, G. (2004a). Channel hydraulics and geomorphic effects of an extreme flood event on the Sabie River, South Africa. *CATENA*, *58*(2), 151–181. https://doi.org/10.1016/j.catena.2004.03.004

Heritage, G. L., Large, A. R. G., Moon, B. P., & Jewitt, G. (2004b). Channel hydraulics and geomorphic effects of an extreme flood event on the Sabie River, South Africa. *CATENA*, *58*(2), 151–181. https://doi.org/10.1016/j.catena.2004.03.004

Hernandez, W., & Armstrong, R. (2016). Deriving Bathymetry from Multispectral Remote Sensing Data. *Journal of Marine Science and Engineering*, *4*(1), 8. https://doi.org/10.3390/jmse4010008

Hosking, J. R. M. (1990). L-Moments: Analysis and Estimation of Distributions Using Linear Combinations of Order Statistics. *Journal of the Royal Statistical Society: Series B (Methodological)*, *52*(1), 105–124. https://doi.org/10.1111/j.2517-6161.1990.tb01775.x

Huang, Q., Long, D., Du, M., Zeng, C., Qiao, G., Li, X., Hou, A., & Hong, Y. (2018). Discharge estimation in high-mountain regions with improved methods using multisource remote

sensing: A case study of the Upper Brahmaputra River. *Remote Sensing of Environment*, *219*, 115–134. https://doi.org/10.1016/j.rse.2018.10.008

Huţanu, E., Mihu-Pintilie, A., Urzica, A., Paveluc, L. E., Stoleriu, C. C., & Grozavu, A. (2020). Using 1D HEC-RAS Modeling and LiDAR Data to Improve Flood Hazard Maps Accuracy: A Case Study from Jijia Floodplain (NE Romania). *Water*, *12*(6), 1624. https://doi.org/10.3390/w12061624

Izinyon, O., & Ehiorobo, J. (2014). L-moments approach for flood frequency analysis of river Okhuwan in Benin-Owena River basin in Nigeria. *Nigerian Journal of Technology*, *33*(1), 10. https://doi.org/10.4314/njt.v33i1.2

Jia, Y., Yi, Y., Li, Z., Wang, Z., & Zheng, X. (2017). Integrating hydraulic equivalent sections into a hydraulic geometry study. *Journal of Hydrology*, *552*, 407–420. https://doi.org/10.1016/j.jhydrol.2017.06.039

Jowett, I. G. (1998). Hydraulic geometry of New Zealand rivers and its use as a preliminary method of habitat assessment. *Regulated Rivers: Research & Management: An International Journal Devoted to River Research and Management*, *14.5*, 451–466. https://doi.org/10.1002/(SICI)1099-1646(1998090)14:5<451::AID-RRR512>3.0.CO;2-1

Kale, V. S., & Hire, P. S. (2004). Effectiveness of monsoon floods on the Tapi River, India: Role of channel geometry and hydrologic regime. *Geomorphology*, *57*(3–4), 275–291. https://doi.org/10.1016/S0169-555X(03)00107-7

Kalyanapu, A. J. (2009). *Effect of land use-based surface roughness on hydrologic model output*. 22.

Kalyanapu, A. J., Hossain, A. K. M. A., Kim, J., Yigzaw, W., Hossain, F., & Shum, C. K. (2013). Toward a Methodology to Investigate the Downstream Flood Hazards on the American

River due to Changes in Probable Maximum Flood due to Effects of Artificial Reservoir Size and Land-Use/Land-Cover Patterns. *Earth Interactions*, *17*(24), 1–24. https://doi.org/10.1175/2012EI000496.1

Keellings, D., & Hernández Ayala, J. J. (2019). Extreme Rainfall Associated With Hurricane Maria Over Puerto Rico and Its Connections to Climate Variability and Change. *Geophysical Research Letters*, *46*(5), 2964–2973. https://doi.org/10.1029/2019GL082077

Kendall, M. G. (1938a). A New Measure of Rank Correlation. *Biometrika*, *30*(1/2), 14.

Kendall, M. G. (1938b). A New Measure of Rank Correlation. *Biometrika*, *30*(1/2), 81. https://doi.org/10.2307/2332226

Khan, M. M. H., Bryceson, I., Kolivras, K. N., Faruque, F., Rahman, M. M., & Haque, U. (2015). Natural disasters and land-use/land-cover change in the southwest coastal areas of Bangladesh. *Regional Environmental Change*, *15*(2), 241–250. https://doi.org/10.1007/s10113-014-0642-8

King, R. O. (2012). *National Flood Insurance Program: Background, Challenges, and Financial Status* (Vol. 40650). Congressional Research Service.

Kishore, N., Marqués, D., Mahmud, A., Kiang, M. V., Rodriguez, I., Fuller, A., Ebner, P., Sorensen, C., Racy, F., Lemery, J., Maas, L., Leaning, J., Irizarry, R. A., Balsari, S., & Buckee, C. O. (2018). Mortality in Puerto Rico after Hurricane Maria. *New England Journal of Medicine*, *379*(2), 162–170. https://doi.org/10.1056/NEJMsa1803972

Kislow, P. V. (2008). *Hurricanes: Background, history and bibliography*. Nova Science Publishers.

Klein, M. (1981). Drainage area and the variation of channel geometry downstream. *Earth Surface Processes and Landforms*, *6*(6), 589–593. https://doi.org/10.1002/esp.3290060608

Knighton, D., & Wharton. (2014). *Fluvial Forms and Processes: A New Perspective* (2nd ed.). Routledge. https://doi.org/10.4324/9780203784662

Knutson, T., Camargo, S. J., Chan, J. C. L., Emanuel, K., Ho, C.-H., Kossin, J., Mohapatra, M., Satoh, M., Sugi, M., Walsh, K., & Wu, L. (2020). Tropical Cyclones and Climate Change Assessment: Part II: Projected Response to Anthropogenic Warming. *Bulletin of the American Meteorological Society*, *101*(3), E303–E322. https://doi.org/10.1175/BAMS-D-18-0194.1

Knutson, T. R., McBride, J. L., Chan, J., Emanuel, K., Holland, G., Landsea, C., Held, I., Kossin, J. P., Srivastava, A. K., & Sugi, M. (2010). Tropical cyclones and climate change. *Nature Geoscience*, *3*(3), 157–163. https://doi.org/10.1038/ngeo779

Konrad, C., Berge, H., Fuerstenberg, R., Steff, K., Olsen, T., & Guyenet, J. (2011). Channel Dynamics in the Middle Green River, Washington, from 1936 to 2002. *Northwest Science*, *85*(1), 1–14. https://doi.org/10.3955/046.085.0101

Kossin, J. P. (2018). A global slowdown of tropical-cyclone translation speed. *Nature*, *558*(7708), 104–107. https://doi.org/10.1038/s41586-018-0158-3

Krapesch, G., Hauer, C., & Habersack, H. (2011a). Scale orientated analysis of river width changes due to extreme flood hazards. *Natural Hazards and Earth System Sciences*, *11*(8), 2137–2147. https://doi.org/10.5194/nhess-11-2137-2011

Krapesch, G., Hauer, C., & Habersack, H. (2011b). Scale orientated analysis of river width changes due to extreme flood hazards. *Natural Hazards and Earth System Science*, *11*(8), 2137–2147. https://doi.org/10.5194/nhess-11-2137-2011

Landsea, C. W., & Franklin, J. L. (2013). Atlantic Hurricane Database Uncertainty and Presentation of a New Database Format. *Monthly Weather Review*, *141*(10), 3576–3592. https://doi.org/10.1175/MWR-D-12-00254.1

Larsen, M. C., & Román, A. S. (2001). Mass wasting and sediment storage in a small montane watershed: An extreme case of anthropogenic disturbance in the humid tropics. In J. M. Dorava, D. R. Montgomery, B. B. Palcsak, & F. A. Fitzpatrick (Eds.), *Water Science and Application* (Vol. 4, pp. 119–138). American Geophysical Union. https://doi.org/10.1029/WS004p0119

Lee, L., Lees, M., & Ridenour, G. S. (2019). Multi-Interval Data Mining of At-A-Station Hydraulic Geometry to Quantify Temporal Stability. *2019 IEEE 10th Annual Information Technology, Electronics and Mobile Communication Conference (IEMCON)*, 0501–0508. https://doi.org/10.1109/IEMCON.2019.8936151

Leopold, L. B. (1968). *Hydrology for Urban Land Planning: A Guidebook on the Hydrologic Effects of Urban Land Use*. US Government Printing Office.

Leopold, L. B., & Maddock, T. (1953). *The hydraulic geometry of stream channels and some physiographic implications* (Vol. 252). US Government Printing Office.

Leopold, L. B., & Miller, J. P. (1956). *Ephemeral streams—Hydraulic factors and their relation to the drainage net* (Vol. 282). US Government Printing Office.

Leopold, L. B., Wolman, M. G., & Miller, J. P. (1964). *Fluvial processes in geomorphology*. Freeman.

Lewis, L. A. (1969). SOME FLUVIAL GEOMORPHIC CHARACTERISTICS OF THE MANATI BASIN, PUERTO RICO. *Annals of the Association of American Geographers*, *59*(2), 280–293. https://doi.org/10.1111/j.1467-8306.1969.tb00671.x

Li, Y., Wright, D. B., & Bledsoe, B. P. (2021). *Watershed Controls and Tropical Cyclone-Induced Changes in River Hydraulic Geometry in Puerto Rico* [Preprint]. Hydrology. https://doi.org/10.1002/essoar.10508930.1

Li, Y., Wright, D. B., & Byrne, P. K. (2020). The Influence of Tropical Cyclones on the Evolution of River Conveyance Capacity in Puerto Rico. *Water Resources Research*, *56*(9). https://doi.org/10.1029/2020WR027971

Lopez, M. A., Colon-Dieppa, E., & Cobb, E. D. (1979). *Floods in Puerto Rico, magnitude and frequency*. https://doi.org/10.3133/wri78141

López-Marrero, T., & Yarnal, B. (2010a). Putting adaptive capacity into the context of people's lives: A case study of two flood-prone communities in Puerto Rico. *Natural Hazards*, *52*(2), 277–297. https://doi.org/10.1007/s11069-009-9370-7

López-Marrero, T., & Yarnal, B. (2010b). Putting adaptive capacity into the context of people's lives: A case study of two flood-prone communities in Puerto Rico. *Natural Hazards*, *52*(2), 277–297. https://doi.org/10.1007/s11069-009-9370-7

López-Moreno, J. I., Beguería, S., & García-Ruiz, J. M. (2006). Trends in high flows in the central Spanish Pyrenees: Response to climatic factors or to land-use change? *Hydrological Sciences Journal*, *51*(6), 1039–1050. https://doi.org/10.1623/hysj.51.6.1039

Lorenzo-Lacruz, J., Vicente-Serrano, S. M., López-Moreno, J. I., Morán-Tejeda, E., & Zabalza, J. (2012). Recent trends in Iberian streamflows (1945–2005). *Journal of Hydrology*, *414–415*, 463–475. https://doi.org/10.1016/j.jhydrol.2011.11.023

Lugo, A. E. (2019). *Social-Ecological-Technological Effects of Hurricane María on Puerto Rico: Planning for Resilience under Extreme Events* (1st ed. 2019). Springer International Publishing : Imprint: Springer. https://doi.org/10.1007/978-3-030-02387-4

Luster, R. E. (1995). *The amelioration of the slaves in the British Empire, 1790-1833*. P. Lang.

Magilligan, F. J., Buraas, E. M., & Renshaw, C. E. (2015). The efficacy of stream power and flow duration on geomorphic responses to catastrophic flooding. *Geomorphology*, *228*, 175–188. https://doi.org/10.1016/j.geomorph.2014.08.016

Mahmoud, S. H., & Gan, T. Y. (2018). Urbanization and climate change implications in flood risk management: Developing an efficient decision support system for flood susceptibility mapping. *Science of The Total Environment*, *636*, 152–167. https://doi.org/10.1016/j.scitotenv.2018.04.282

Malkinson, D., & Wittenberg, L. (2007). Scaling the effects of riparian vegetation on cross-sectional characteristics of ephemeral mountain streams—A case study of Nahal Oren, Mt. Carmel, Israel. *CATENA*, *69*(2), 103–110. https://doi.org/10.1016/j.catena.2006.04.026

Mallakpour, I., & Villarini, G. (2016). A simulation study to examine the sensitivity of the Pettitt test to detect abrupt changes in mean. *Hydrological Sciences Journal*, *61*(2), 245–254. https://doi.org/10.1080/02626667.2015.1008482

Mann, H. B. (1945). Nonparametric Tests Against Trend. *Econometrica*, *13*(3), 245. https://doi.org/10.2307/1907187

Marapara, T. R., Jackson, B. M., Hartley, S., & Maxwell, D. (2021). Disentangling the factors that vary the impact of trees on flooding (a review). *Water and Environment Journal*, *35*(2), 514–529. https://doi.org/10.1111/wej.12647

Masterman, R., & Thorne, C. R. (1992). Predicting Influence of Bank Vegetation on Channel Capacity. *Journal of Hydraulic Engineering*, *118*(7), 1052–1058. https://doi.org/10.1061/(ASCE)0733-9429(1992)118:7(1052)

McNeill, J. R. (2003). Observations on the Nature and Culture of Environmental History. *History and Theory*, *42*(4), 5–43. https://doi.org/10.1046/j.1468-2303.2003.00255.x

Md Ali, A., Solomatine, D. P., & Di Baldassarre, G. (2015). Assessing the impact of different sources of topographic data on 1-D hydraulic modelling of floods. *Hydrology and Earth System Sciences*, *19*(1), 631–643. https://doi.org/10.5194/hess-19-631-2015

Mejia Manrique, S. A., Harmsen, E. W., Khanbilvardi, R. M., & González, J. E. (2021). Flood Impacts on Critical Infrastructure in a Coastal Floodplain in Western Puerto Rico during Hurricane María. *Hydrology*, *8*(3), 104. https://doi.org/10.3390/hydrology8030104

Menne, M. J., Durre, I., Vose, R. S., Gleason, B. E., & Houston, T. G. (2012). An Overview of the Global Historical Climatology Network-Daily Database. *Journal of Atmospheric and Oceanic Technology*, *29*(7), 897–910. https://doi.org/10.1175/JTECH-D-11-00103.1

Millar, R. G., & Quick, M. C. (1993). Effect of Bank Stability on Geometry of Gravel Rivers. *Journal of Hydraulic Engineering*, *119*(12), 1343–1363. https://doi.org/10.1061/(ASCE)0733-9429(1993)119:12(1343)

Moknatian, M., & Piasecki, M. (2019). Lake Volume Data Analyses: A Deep Look into the Shrinking and Expansion Patterns of Lakes Azuei and Enriquillo, Hispaniola. *Hydrology*, *7*(1), 1. https://doi.org/10.3390/hydrology7010001

Montgomery, D. R., & Buffington, J. M. (1997). Channel-reach morphology in mountain drainage basins. *Geological Society of America Bulletin*, 16.

Montgomery, D. R., & MacDonald, L. H. (2002). DIAGNOSTIC APPROACH TO STREAM CHANNEL ASSESSMENT AND MONITORING. *Journal of the American Water Resources Association*, *38*(1), 1–16. https://doi.org/10.1111/j.1752-1688.2002.tb01530.x

Morel, M., Booker, D. J., Gob, F., & Lamouroux, N. (2020a). Intercontinental predictions of river hydraulic geometry from catchment physical characteristics. *Journal of Hydrology*, *582*, 124292. https://doi.org/10.1016/j.jhydrol.2019.124292

Morel, M., Booker, D. J., Gob, F., & Lamouroux, N. (2020b). Consistent Theoretical and Empirical Predictions of at-a-Station Hydraulic Geometry Exponents in Stream Reaches. *Water Resources Research*, *56*(10). https://doi.org/10.1029/2020WR027242

Morel, M., Tamisier, V., Pella, H., Booker, D. J., Navratil, O., Piégay, H., Gob, F., & Lamouroux, N. (2019). Revisiting the drivers of at-a-station hydraulic geometry in stream reaches. *Geomorphology*, *328*, 44–56. https://doi.org/10.1016/j.geomorph.2018.12.007

Mudashiru, R. B., Sabtu, N., Abustan, I., & Balogun, W. (2021). Flood hazard mapping methods: A review. *Journal of Hydrology*, *603*, 126846. https://doi.org/10.1016/j.jhydrol.2021.126846

Muhadi, N. A., Abdullah, A. F., Bejo, S. K., Mahadi, M. R., & Mijic, A. (2020). The Use of LiDAR-Derived DEM in Flood Applications: A Review. *Remote Sensing*, *12*(14), 2308. https://doi.org/10.3390/rs12142308

Mulahasan, S., Stoesser, T., & McSherry, R. (2017). Effect of Floodplain Obstructions on the Discharge Conveyance Capacity of Compound Channels. *Journal of Irrigation and Drainage Engineering*, *143*(11), 04017045. https://doi.org/10.1061/(ASCE)IR.1943-4774.0001240

Muñoz-Salinas, E., Renschler, C. S., Palacios, D., & Namikawa, L. M. (2008). Updating channel morphology in digital elevation models: Lahar assessment for Tenenepanco-Huiloac Gorge, Popocatépetl volcano, Mexico. *Natural Hazards*, *45*(2), 309–320. https://doi.org/10.1007/s11069-007-9162-x

National Oceanic and Atmospheric Administration. (2021). *National Weather Service*.

National Weather Service. (2021). *Costliest U.S. Tropical Cyclones Tables Updated*. https://www.ncdc.noaa.gov/billions/dcmi.pdf

Naylor, L. A., Spencer, T., Lane, S. N., Darby, S. E., Magilligan, F. J., Macklin, M. G., & Möller, I. (2017). Stormy geomorphology: Geomorphic contributions in an age of climate extremes: Stormy Geomorphology. *Earth Surface Processes and Landforms*, *42*(1), 166–190. https://doi.org/10.1002/esp.4062

Neuhold, C., Stanzel, P., & Nachtnebel, H. P. (2009). Incorporating river morphological changes to flood risk assessment: Uncertainties, methodology and application. *Natural Hazards and Earth System Sciences*, *9*(3), 789–799. https://doi.org/10.5194/nhess-9-789-2009

Nones, M. (2019). Dealing with sediment transport in flood risk management. *Acta Geophysica*, *67*(2), 677–685. https://doi.org/10.1007/s11600-019-00273-7

Nugent, A. D., & Rios-Berrios, R. (2018). Factors Leading to Extreme Precipitation on Dominica from Tropical Storm Erika (2015). *Monthly Weather Review*, *146*(2), 525–541. https://doi.org/10.1175/MWR-D-17-0242.1

Nyaupane, N., Bhandari, S., Rahaman, Md. M., Wagner, K., Kalra, A., Ahmad, S., & Gupta, R. (2018). Flood Frequency Analysis Using Generalized Extreme Value Distribution and Floodplain Mapping for Hurricane Harvey in Buffalo Bayou. *World Environmental and Water Resources Congress 2018*, 364–375. https://doi.org/10.1061/9780784481400.034

Obeysekera, J., & Salas, J. D. (2016). Frequency of Recurrent Extremes under Nonstationarity. *Journal of Hydrologic Engineering*, *21*(5), 04016005. https://doi.org/10.1061/(ASCE)HE.1943-5584.0001339

OCM Partners. (2019). 2016–2017 USGS Lidar DEM: Puerto Rico. *Charleston, SC: NOAA National Centers for Environmental Information*. https://www.fisheries.noaa.gov/inport/item/55314

OCM Partners. (2021a). *2016—2017 USGS Lidar DEM: Puerto Rico*. https://www.fisheries.noaa.gov/inport/item/55314

OCM Partners. (2021b). *2018 USGS Lidar DEM: Post Hurricane Maria—Puerto Rico*. https://www.fisheries.noaa.gov/inport/item/60105

O'Connell, P. E., Ewen, J., O'Donnell, G., & Quinn, P. (2007). Is there a link between agricultural land-use management and flooding? *Hydrology and Earth System Sciences*, *11*(1), 96–107. https://doi.org/10.5194/hess-11-96-2007

Office of Inspector General. (2017). *FEMA needs to improve management of its flood mapping programs.* https://www.documentcloud.org/documents/4066233-OIG-17-110-Sep17.html

Ogden, F. L. (2016a). Evidence of equilibrium peak runoff rates in steep tropical terrain on the island of Dominica during Tropical Storm Erika, August 27, 2015. *Journal of Hydrology*, *542*, 35–46. https://doi.org/10.1016/j.jhydrol.2016.08.041

Ogden, F. L. (2016b). Evidence of equilibrium peak runoff rates in steep tropical terrain on the island of Dominica during Tropical Storm Erika, August 27, 2015. *Journal of Hydrology*, *542*, 35–46. https://doi.org/10.1016/j.jhydrol.2016.08.041

Ongdas, N., Akiyanova, F., Karakulov, Y., Muratbayeva, A., & Zinabdin, N. (2020). Application of HEC-RAS (2D) for Flood Hazard Maps Generation for Yesil (Ishim) River in Kazakhstan. *Water*, *12*(10), 2672. https://doi.org/10.3390/w12102672

Ortiz, F. (2005). *El huracán: Su mitología y sus símbolos* (2a ed). Fondo de Cultura Económica.

Oubennaceur, K., Chokmani, K., Gauthier, Y., Ratte-Fortin, C., Homayouni, S., & Toussaint, J.-P. (2021). Flood Risk Assessment under Climate Change: The Petite Nation River Watershed. *Climate*, *9*(8), 125. https://doi.org/10.3390/cli9080125

Pádua, J. A. (2010). As bases teóricas da história ambiental. *Estudos Avançados*, *24*(68), 81–101. https://doi.org/10.1590/S0103-40142010000100009

Pall, P., Aina, T., Stone, D. A., Stott, P. A., Nozawa, T., Hilberts, A. G. J., Lohmann, D., & Allen, M. R. (2011). Anthropogenic greenhouse gas contribution to flood risk in England and Wales in autumn 2000. *Nature*, *470*(7334), 382–385. https://doi.org/10.1038/nature09762

Palm, R., & Hodgson, M. E. (1993a). Natural Hazards in Puerto Rico. *Geographical Review*, *83*(3), 280. https://doi.org/10.2307/215730

Palm, R., & Hodgson, M. E. (1993b). Natural Hazards in Puerto Rico. *Geographical Review*, *83*(3), 280. https://doi.org/10.2307/215730

Park, C. C. (1977). World-wide variations in hydraulic geometry exponents of stream channels: An analysis and some observations. *Journal of Hydrology*, *33*(1–2), 133–146. https://doi.org/10.1016/0022-1694(77)90103-2

Patricola, C. M., & Wehner, M. F. (2018). Anthropogenic influences on major tropical cyclone events. *Nature*, *563*(7731), 339–346. https://doi.org/10.1038/s41586-018-0673-2

Pettitt, A. N. (1979). A Non-Parametric Approach to the Change-Point Problem. *Applied Statistics*, *28*(2), 126. https://doi.org/10.2307/2346729

Phillips, C. B., & Jerolmack, D. J. (2016). Self-organization of river channels as a critical filter on climate signals. *Science*, *352*(6286), 694–697. https://doi.org/10.1126/science.aad3348

Phillips, C. B., & Scatena, F. N. (2013). Reduced channel morphological response to urbanization in a flood-dominated humid tropical environment: REDUCED CHANNEL MORPHOLOGICAL RESPONSE TO URBANIZATION. *Earth Surface Processes and Landforms*, *38*(9), 970–982. https://doi.org/10.1002/esp.3345

Pielke, R. A. (2013). *The Hurricane* (0 ed.). Routledge. https://doi.org/10.4324/9781315822679

Pielkejr, R. A., Landsea, C., Mayfield, M., Layer, J., & Pasch, R. (2005). HURRICANES AND GLOBAL WARMING. *Bulletin of the American Meteorological Society 86*, *11*, 1571–1575.

Pike, A. S., Scatena, F. N., & Wohl, E. E. (2010). Lithological and fluvial controls on the geomorphology of tropical montane stream channels in Puerto Rico. *Earth Surface Processes and Landforms*, *35*(12), 1402–1417. https://doi.org/10.1002/esp.1978

Ponce, V. M. (1989). *Engineering hydrology: Principles and practices* (Vol. 640). Prentice Hall.

Pya, N., & Wood, S. N. (2015). Shape constrained additive models. *Statistics and Computing*, *25*(3), 543–559. https://doi.org/10.1007/s11222-013-9448-7

Qin, C., Wu, B., Wang, Y., Fu, X., Xue, Y., Li, D., Li, M., & Zhang, Y. (2020). Dynamic variability of at-a-station hydraulic-geometry for mountain rivers in the southeast Qinghai-Tibet Plateau: The cases of Yalong River and upper Jinsha River. *CATENA*, *194*, 104723. https://doi.org/10.1016/j.catena.2020.104723

R core team. (2020). *R: A language and environment for statistical computing.* (4.0.3) [Computer software]. R Foundation for Statistical Computing. https://www.R-project.org/

Rahmstorf, S. (2017). Rising hazard of storm-surge flooding. *Proceedings of the National Academy of Sciences*, *114*(45), 11806–11808. https://doi.org/10.1073/pnas.1715895114

Ramos-Ginés, O. (1999). *Estimation of magnitude and frequency of floods for streams in Puerto Rico: New empirical models*. https://doi.org/10.3133/wri994142

Ramos-Scharrón, C. E., Torres-Pulliza, D., & Hernández-Delgado, E. A. (2015). Watershed- and island wide-scale land cover changes in Puerto Rico (1930s–2004) and their potential effects on coral reef ecosystems. *Science of The Total Environment*, *506–507*, 241–251. https://doi.org/10.1016/j.scitotenv.2014.11.016

Ran, L., Wang, S., & Lu, X. X. (2012). Hydraulic geometry change of a large river: A case study of the upper Yellow River. *Environmental Earth Sciences*, *66*(4), 1247–1257. https://doi.org/10.1007/s12665-011-1336-x

Reid, D. E., Hickin, E. J., & Babakaiff, S. C. (2010). Low-flow hydraulic geometry of small, steep mountain streams in southwest British Columbia. *Geomorphology*, *122*(1–2), 39–55. https://doi.org/10.1016/j.geomorph.2010.05.012

Reisenbüchler, M., Bui, M. D., Skublics, D., & Rutschmann, P. (2019a). An integrated approach for investigating the correlation between floods and river morphology: A case study of the Saalach River, Germany. *Science of The Total Environment*, *647*, 814–826. https://doi.org/10.1016/j.scitotenv.2018.08.018

Reisenbüchler, M., Bui, M. D., Skublics, D., & Rutschmann, P. (2019b). An integrated approach for investigating the correlation between floods and river morphology: A case study of

the Saalach River, Germany. *Science of The Total Environment*, *647*, 814–826. https://doi.org/10.1016/j.scitotenv.2018.08.018

Ritter, D. F., Kochel, R. C., & Miller, J. R. (2006). *Process geomorphology* (4. ed., [Reissued]). Waveland Press.

Rivera, F. I. (2020). Puerto Rico's population before and after Hurricane Maria. *Population and Environment*, *42*(1), 1–3. https://doi.org/10.1007/s11111-020-00356-4

Robert, A., Roy, A. G., & Serres, B. (1992). Changes in velocity profiles at roughness transitions in coarse grained channels. *Sedimentology*, *39*(5), 725–735. https://doi.org/10.1111/j.1365-3091.1992.tb02149.x

Rodgers, E. B., Adler, R. F., & Pierce, H. F. (2001). Contribution of Tropical Cyclones to the North Atlantic Climatological Rainfall as Observed from Satellites. *JOURNAL OF APPLIED METEOROLOGY*, *40*, 16.

Rodríguez, H. (1997). A Socioeconomic Analysis of Hurricanes in Puerto Rico: An Overview of Disaster Mitigation and Preparedness. In H. F. Diaz & R. S. Pulwarty (Eds.), *Hurricanes* (pp. 121–143). Springer Berlin Heidelberg. https://doi.org/10.1007/978-3-642-60672-4_7

Rodriguez-Díaz, C. E., & Lewellen-Williams, C. (2020). Race and Racism as Structural Determinants for Emergency and Recovery Response in the Aftermath of Hurricanes Irma and Maria in Puerto Rico. *Health Equity*, *4*(1), 232–238. https://doi.org/10.1089/heq.2019.0103

Romo, V., & Florido, A. (2020, January 20). Political Unrest In Puerto Rico After Discovery Of Unused Hurricane Aid. *National Public Radio*. https://www.npr.org/2020/01/20/797996503/political-unrest-in-puerto-rico-after-discovery-of-unused-hurricane-aid

Santiago, L., Flores, D., & Hong, C.-Y. (2020). The impact of extreme weather events on community risk planning and management: The case of San Juan, Puerto Rico after hurricane Maria. *Urbe. Revista Brasileira de Gestão Urbana*, *12*, e20190062. https://doi.org/10.1590/2175-3369.012.e20190062

Schober, B., Hauer, C., & Habersack, H. (2020). Floodplain losses and increasing flood risk in the context of recent historic land use changes and settlement developments: Austrian case studies. *Journal of Flood Risk Management*, *13*(3). https://doi.org/10.1111/jfr3.12610

Schwartz, S. B. (2015). *Sea of storms: A history of hurricanes in the greater Caribbean from Columbus to Katrina*. Princeton University Press.

Scoccimarro, E., Villarini, G., Gualdi, S., Navarra, A., Vecchi, G., Walsh, K., & Zhao, M. (2017). Tropical Cyclone Rainfall Changes in a Warmer Climate. In J. M. Collins & K. Walsh (Eds.), *Hurricanes and Climate Change*. Springer International Publishing. http://link.springer.com/10.1007/978-3-319-47594-3

Sen, P. K. (1968). *Estimates of the Regression Coefficient Based on Kendall's Tau*. 12.

Shadmehri Toosi, A., Doulabian, S., Ghasemi Tousi, E., Calbimonte, G. H., & Alaghmand, S. (2020). Large-scale flood hazard assessment under climate change: A case study. *Ecological Engineering*, *147*, 105765. https://doi.org/10.1016/j.ecoleng.2020.105765

Shen, C., Wang, S., & Liu, X. (2016). Geomorphological significance of at-many-stations hydraulic geometry: Physical Interpretations of AMHG. *Geophysical Research Letters*, *43*(8), 3762–3770. https://doi.org/10.1002/2016GL068364

Shepherd, J. M., & Knutson, T. (2007). The Current Debate on the Linkage Between Global Warming and Hurricanes: Global warming and hurricanes. *Geography Compass*, *1*(1), 1–24. https://doi.org/10.1111/j.1749-8198.2006.00002.x

Sholtes, J. S., & Doyle, M. W. (2011). Effect of Channel Restoration on Flood Wave Attenuation. *Journal of Hydraulic Engineering*, *137*(2), 196–208. https://doi.org/10.1061/(ASCE)HY.1943-7900.0000294

Sholtes, J. S., Yochum, S. E., Scott, J. A., & Bledsoe, B. P. (2018). Longitudinal variability of geomorphic response to floods. *Earth Surface Processes and Landforms*, *43*(15), 3099–3113. https://doi.org/10.1002/esp.4472

Shugar, D. H., Clague, J. J., Best, J. L., Schoof, C., Willis, M. J., Copland, L., & Roe, G. H. (2017). River piracy and drainage basin reorganization led by climate-driven glacier retreat. *Nature Geoscience*, *10*(5), 370–375. https://doi.org/10.1038/ngeo2932

Siermann, J., Harvey, C., Morgan, G., & Heege, T. (2014). Satellite Derived Bathymetry and Digital Elevation Models (DEM). *IPTC 2014: International Petroleum Technology Conference*. IPTC 2014: International Petroleum Technology Conference, Doha, Qatar,. https://doi.org/10.3997/2214-4609-pdb.395.IPTC-17346-MS

Sievers, G. L. (1978). Weighted Rank Statistics for Simple Linear Regression. *Journal of the American Statistical Association*, *73*(363), 628–631. https://doi.org/10.1080/01621459.1978.10480067

Simon, A. (1990). *Sediment discharge from a montane basin, Puerto Rico: Implications of erosion processes and rates In the humid tropics*. 13.

Slater, L. J. (2016). To what extent have changes in channel capacity contributed to flood hazard trends in England and Wales?: Effects of Changing Channel Capacity on Flooding in

England and Wales. *Earth Surface Processes and Landforms*, *41*(8), 1115–1128. https://doi.org/10.1002/esp.3927

Slater, L. J., Khouakhi, A., & Wilby, R. L. (2019a). River channel conveyance capacity adjusts to modes of climate variability. *Scientific Reports*, *9*(1), 12619. https://doi.org/10.1038/s41598-019-48782-1

Slater, L. J., Khouakhi, A., & Wilby, R. L. (2019b). River channel conveyance capacity adjusts to modes of climate variability. *Scientific Reports*, *9*(1), 12619. https://doi.org/10.1038/s41598-019-48782-1

Slater, L. J., Singer, M. B., & Kirchner, J. W. (2015a). Hydrologic versus geomorphic drivers of trends in flood hazard. *Geophysical Research Letters*, *42*(2), 370–376. https://doi.org/10.1002/2014GL062482

Slater, L. J., Singer, M. B., & Kirchner, J. W. (2015b). Hydrologic versus geomorphic drivers of trends in flood hazard. *Geophysical Research Letters*, *42*(2), 370–376. https://doi.org/10.1002/2014GL062482

Smith, J. A., Sturdevant-Rees, P., Baeck, M. L., & Larsen, M. C. (2005a). Tropical cyclones and the flood hydrology of Puerto Rico: TROPICAL CYCLONES AND FLOOD HYDROLOGY OF PUERTO RICO. *Water Resources Research*, *41*(6). https://doi.org/10.1029/2004WR003530

Smith, J. A., Sturdevant-Rees, P., Baeck, M. L., & Larsen, M. C. (2005b). Tropical cyclones and the flood hydrology of Puerto Rico: TROPICAL CYCLONES AND FLOOD HYDROLOGY OF PUERTO RICO. *Water Resources Research*, *41*(6). https://doi.org/10.1029/2004WR003530

Smith, L. C., Alsdorf, D. E., Magilligan, F. J., Gomez, B., Mertes, L. A. K., Smith, N. D., & Garvin, J. B. (2000a). Estimation of erosion, deposition, and net volumetric change caused by the 1996 Skeiðarársandur jökulhlaup, Iceland, from Synthetic Aperture Radar Interferometry. *Water Resources Research*, *36*(6), 1583–1594. https://doi.org/10.1029/1999WR900335

Smith, L. C., Alsdorf, D. E., Magilligan, F. J., Gomez, B., Mertes, L. A. K., Smith, N. D., & Garvin, J. B. (2000b). Estimation of erosion, deposition, and net volumetric change caused by the 1996 Skeiðarársandur jökulhlaup, Iceland, from Synthetic Aperture Radar Interferometry. *Water Resources Research*, *36*(6), 1583–1594. https://doi.org/10.1029/1999WR900335

Smith, S. D. (2012). Storm Hazard and Slavery: The Impact of the 1831 Great Caribbean Hurricane on St Vincent. *Environment and History*, *18*(1), 97–123. https://doi.org/10.3197/096734012X13225062753660

Staffler, H., Pollinger, R., Zischg, A., & Mani, P. (2008). Spatial variability and potential impacts of climate change on flood and debris flow hazard zone mapping and implications for risk management. *Natural Hazards and Earth System Sciences*, *8*(3), 539–558. https://doi.org/10.5194/nhess-8-539-2008

Stedinger, J. R., Vogel, R. M., & Foufoula-Georgiou, E. (1993a). Frequency Analysis of Extreme Events. In D. R. Maidment (Ed.), *Handbook of Hydrology*. New York: McGraw-Hill.

Stedinger, J. R., Vogel, R. M., & Foufoula-Georgiou, E. (1993b). *Frequency Analysis of Extreme Events* (D. R. Maidment, Ed.). McGraw-Hill.

Stewardson, M. (2005). Hydraulic geometry of stream reaches. *Journal of Hydrology*, *306*(1–4), 97–111. https://doi.org/10.1016/j.jhydrol.2004.09.004

Strategic Alliance for Risk Reduction. (2018). *Puerto Rico Advisory Data and Products—Post-Hurricanes Irma and Maria*. http://cedd.pr.gov/fema/wp-content/uploads/2018/06/Puerto_Rico_Advisory_Report_2018.05.23_Final_English.pdf

Su, T., Wang, S., Mei, Y., & Shao, W. (2015). Comparison of channel geometry changes in Inner Mongolian reach of the Yellow River before and after joint operation of large upstream reservoirs. *Journal of Geographical Sciences*, *25*(8), 930–942. https://doi.org/10.1007/s11442-015-1211-x

Surian, N. (1999). *Channel changes due to river regulation: The case of the Piave River, Italy*. 17.

Taniwaki, R. H., Piggott, J. J., Ferraz, S. F. B., & Matthaei, C. D. (2017). Climate change and multiple stressors in small tropical streams. *Hydrobiologia*, *793*(1), 41–53. https://doi.org/10.1007/s10750-016-2907-3

Thomas, N., Pertiwi, A. P., Traganos, D., Lagomasino, D., Poursanidis, D., Moreno, S., & Fatoyinbo, L. (2021). Space-Borne Cloud-Native Satellite-Derived Bathymetry (SDB) Models Using ICESat-2 And Sentinel-2. *Geophysical Research Letters*, *48*(6). https://doi.org/10.1029/2020GL092170

Turowski, J. M., Hovius, N., Wilson, A., & Horng, M.-J. (2008). Hydraulic geometry, river sediment and the definition of bedrock channels. *Geomorphology*, *99*(1–4), 26–38. https://doi.org/10.1016/j.geomorph.2007.10.001

U.S. Geological Survey. (2006). *National Hydrography Dataset (version 01_05)*. https://nhdplus.com/NHDPlus/ NHDPlusV1_21.php

U.S. Geological Survey. (2021a). *Peak Streamflow for the Nation*. https://nwis.waterdata.usgs.gov/usa/nwis/peak

U.S. Geological Survey. (2021b). *Streamflow Measurements for the Nation*. https://waterdata.usgs.gov/nwis/measurements

USACE. (2016). *HEC-RAS River Analysis System Hydraulic Reference Manual. Version 5.0*. Hydrol. Eng. Cent.(HEC), US Army Corps Eng.

van Oldenborgh, G. J., van der Wiel, K., Sebastian, A., Singh, R., Arrighi, J., Otto, F., Haustein, K., Li, S., Vecchi, G., & Cullen, H. (2017). Attribution of extreme rainfall from Hurricane Harvey, August 2017. *Environmental Research Letters*, *12*(12), 124009. https://doi.org/10.1088/1748-9326/aa9ef2

Walsh, K. J. E., McBride, J. L., Klotzbach, P. J., Balachandran, S., Camargo, S. J., Holland, G., Knutson, T. R., Kossin, J. P., Lee, T., Sobel, A., & Sugi, M. (2016a). Tropical cyclones and climate change. *WIREs Climate Change*, *7*(1), 65–89. https://doi.org/10.1002/wcc.371

Walsh, K. J. E., McBride, J. L., Klotzbach, P. J., Balachandran, S., Camargo, S. J., Holland, G., Knutson, T. R., Kossin, J. P., Lee, T., Sobel, A., & Sugi, M. (2016b). Tropical cyclones and climate change: Tropical cyclones and climate change. *Wiley Interdisciplinary Reviews: Climate Change*, *7*(1), 65–89. https://doi.org/10.1002/wcc.371

Wang, L., Sichangi, A. W., Zeng, T., Li, X., Hu, Z., & Genanu, M. (2019). New methods designed to estimate the daily discharges of rivers in the Tibetan Plateau. *Science Bulletin*, *64*(7), 418–421. https://doi.org/10.1016/j.scib.2019.03.015

Wang, S., Hassan, M. A., & Xie, X. (2006). Relationship between suspended sediment load, channel geometry and land area increment in the Yellow River Delta. *CATENA*, *65*(3), 302–314. https://doi.org/10.1016/j.catena.2006.01.003

Wasko, C., Westra, S., Nathan, R., Orr, H. G., Villarini, G., Villalobos Herrera, R., & Fowler, H. J. (2021). Incorporating climate change in flood estimation guidance. *Philosophical Transactions of the Royal Society A: Mathematical, Physical and Engineering Sciences*, *379*(2195), 20190548. https://doi.org/10.1098/rsta.2019.0548

Webster, P. J., Holland, G. J., Curry, J. A., & Chang, H.-R. (2005). Changes in Tropical Cyclone Number, Duration, and Intensity in a Warming Environment. *Science*, *309*(5742), 1844–1846. https://doi.org/10.1126/science.1116448

West, A. J., Lin, C.-W., Lin, T.-C., Hilton, R. G., Liu, S.-H., Chang, C.-T., Lin, K.-C., Galy, A., Sparkes, R. B., & Hovius, N. (2011a). Mobilization and transport of coarse woody debris to the oceans triggered by an extreme tropical storm. *Limnology and Oceanography*, *56*(1), 77–85. https://doi.org/10.4319/lo.2011.56.1.0077

West, A. J., Lin, C.-W., Lin, T.-C., Hilton, R. G., Liu, S.-H., Chang, C.-T., Lin, K.-C., Galy, A., Sparkes, R. B., & Hovius, N. (2011b). Mobilization and transport of coarse woody debris to the oceans triggered by an extreme tropical storm. *Limnology and Oceanography*, *56*(1), 77–85. https://doi.org/10.4319/lo.2011.56.1.0077

Willison, C. E., Singer, P. M., Creary, M. S., & Greer, S. L. (2019). Quantifying inequities in US federal response to hurricane disaster in Texas and Florida compared with Puerto Rico. *BMJ Global Health*, *4*(1), e001191. https://doi.org/10.1136/bmjgh-2018-001191

Wiman, J., & Almstedt, A. E. (1997). Hydrodynamics, erosion and heat transfer in a pressurized fluidized bed: Influence of pressure, fluidization velocity, particle size and tube bank

geometry. *Chemical Engineering Science*, *52*(16), 2677–2695. https://doi.org/10.1016/S0009-2509(97)00096-1

Wu, W., & He, Z. (2009). Effects of vegetation on flow conveyance and sediment transport capacity. *International Journal of Sediment Research*, *24*(3), 247–259. https://doi.org/10.1016/S1001-6279(10)60001-7

Wuebbles, D. J., Fahey, D. W., Hibbard, K. A., Dokken, D. J., Stewart, B. C., & Maycock, T. K. (2017). *Climate Science Special Report: Fourth National Climate Assessment, Volume I*. U.S. Global Change Research Program. https://doi.org/10.7930/J0J964J6

Wyżga, B. (1997). Methods for studying the response of flood flows to channel change. *Journal of Hydrology*, *198*(1–4), 271–288. https://doi.org/10.1016/S0022-1694(96)03289-1

Ye, B., Yang, D., & Kane, D. L. (2003). Changes in Lena River streamflow hydrology: Human impacts versus natural variations: CHANGES IN LENA RIVER STREAMFLOW. *Water Resources Research*, *39*(7). https://doi.org/10.1029/2003WR001991

Yeh, C.-F., Wang, J., Yeh, H.-F., & Lee, C.-H. (2015). Spatial and Temporal Streamflow Trends in Northern Taiwan. *Water*, *7*(12), 634–651. https://doi.org/10.3390/w7020634

Yochum, S. E., Sholtes, J. S., Scott, J. A., & Bledsoe, B. P. (2017). Stream power framework for predicting geomorphic change: The 2013 Colorado Front Range flood. *Geomorphology*, *292*, 178–192. https://doi.org/10.1016/j.geomorph.2017.03.004

Yousefi, S., Mirzaee, S., Keesstra, S., Surian, N., Pourghasemi, H. R., Zakizadeh, H. R., & Tabibian, S. (2018). Effects of an extreme flood on river morphology (case study: Karoon River, Iran). *Geomorphology*, *304*, 30–39. https://doi.org/10.1016/j.geomorph.2017.12.034

Yu, G., Wright, D. B., Zhu, Z., Smith, C., & Holman, K. D. (2019). Process-based flood frequency analysis in an agricultural watershed exhibiting nonstationary flood seasonality. *Hydrology and Earth System Sciences*, *23*(5), 2225–2243. https://doi.org/10.5194/hess-23-2225-2019

Yuan, Y., Jiang, Y., Taguas, E. V., Mbonimpa, E. G., & Hu, W. (2015). Sediment loss and its cause in Puerto Rico watersheds. *SOIL*, *1*(2), 595–602. https://doi.org/10.5194/soil-1-595-2015

Zhang, W., Wang, W., Zheng, J., Wang, H., Wang, G., & Zhang, J. (2015). Reconstruction of stage–discharge relationships and analysis of hydraulic geometry variations: The case study of the Pearl River Delta, China. *Global and Planetary Change*, *125*, 60–70. https://doi.org/10.1016/j.gloplacha.2014.12.004

Zhang, W., Yan, Y., Zheng, J., Li, L., Dong, X., & Cai, H. (2009). Temporal and spatial variability of annual extreme water level in the Pearl River Delta region, China. *Global and Planetary Change*, *69*(1–2), 35–47. https://doi.org/10.1016/j.gloplacha.2009.07.003

Zischg, A. P., Hofer, P., Mosimann, M., Röthlisberger, V., Ramirez, J. A., Keiler, M., & Weingartner, R. (2018). Flood risk (d)evolution: Disentangling key drivers of flood risk change with a retro-model experiment. *Science of The Total Environment*, *639*, 195–207. https://doi.org/10.1016/j.scitotenv.2018.05.056

Appendix
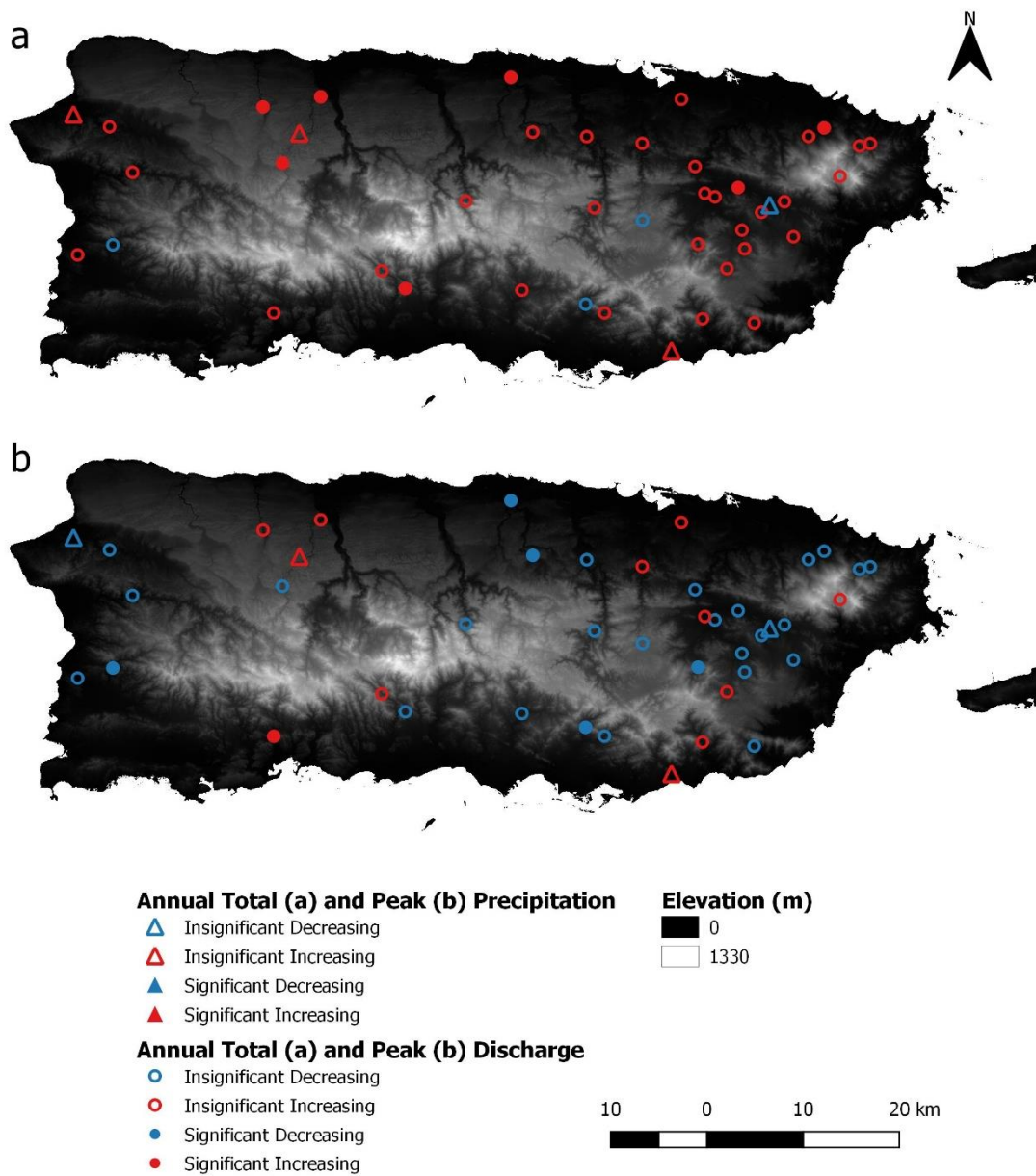
Fig. S1. (a) Annual total precipitation and discharge trend using the M-K test. (b) Annual maximum three-day average precipitation trend analyses using the M-K test. Statistical significance is determined at the 5% level.

Residuals

Standardized Residuals

Autocorrelation

Normal Q–Q Plot of Standardized Residuals
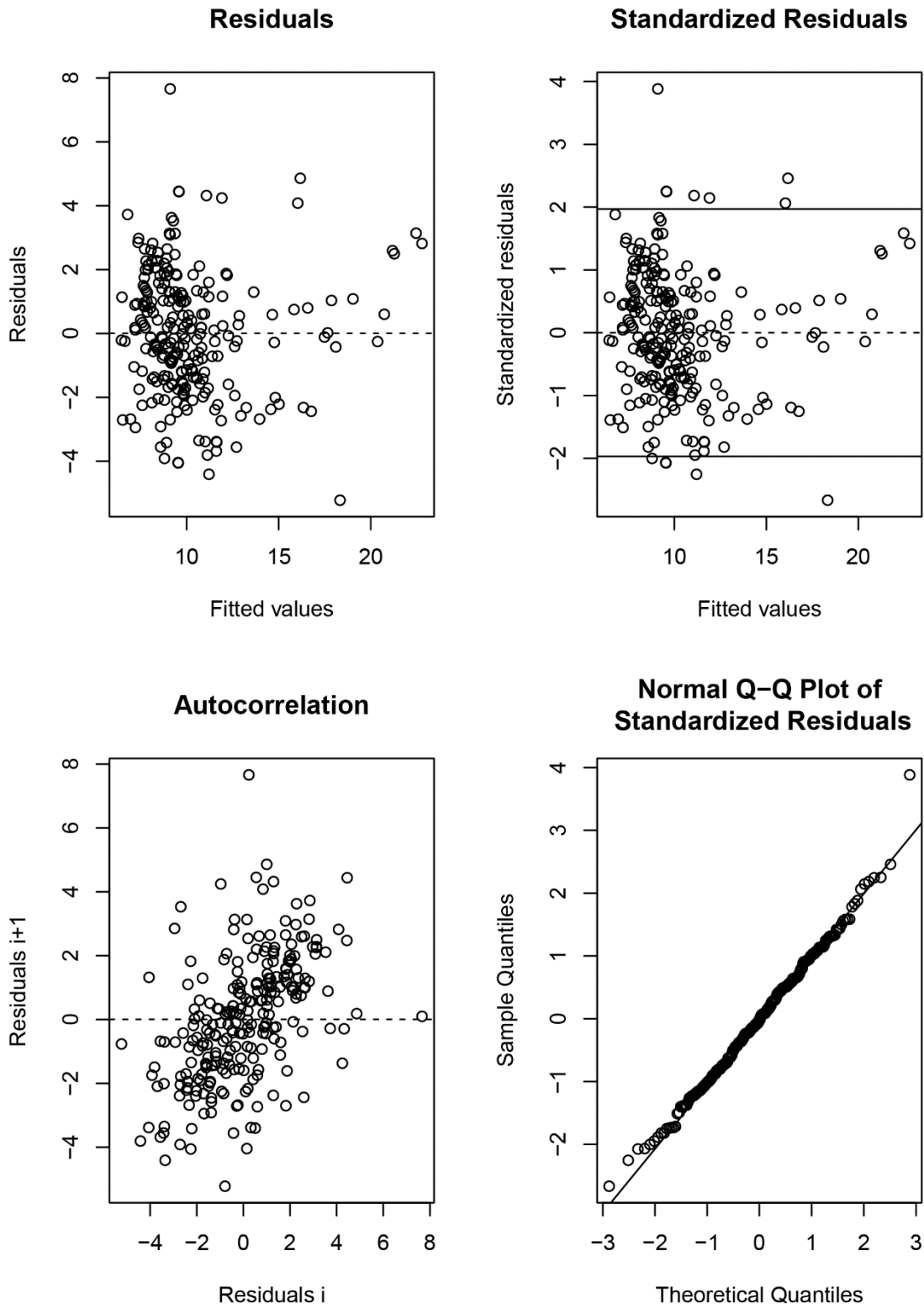
Fig. S2 Regression diagnostic plots for width model at site 50064200.

Table S1. Details on the 39 USGS stream gages involved in the research. Sites 50043800, 50055225, and 50067000 are not included in the GAGES-II dataset (Falcone et al., 2010) and thus lack land use information. Information on mean elevation and slope for 50014800 were not available through NWIS or GAGES-II. The "record length" in the last column refers to the period in which both daily discharge and field measurements data are available for each site.

USGS Site Number	Watershed Area [km^2]	Developed Area [%]	Forested Area [%]	Mean Elevation [masl]	Mean Slope [%]	Start/End Year (Record Length [years])
50014800	75	6	59	N/A	N/A	1984-2015 (32)
50028000	48	3	68	564	16	1960-2016 (57)
50028400	58	2	72	501	18	1969-2016 (38)
50034000	43	2	53	727	22	1970-2016 (41)
50038320	39	12	44	238	13	1970-2016 (47)
50039500	257	12	52	183	13	1959-2016 (58)
50043800	284	N/A	N/A	527	16	1989-2016 (28)
50045010	448	12	46	460	16	1989-2017 (29)
50047560	22	22	24	438	9	1991-2016 (17)
50047850	108	13	50	337	14	1965-2016 (35)
50049100	39	65	21	76	7	1970-2016 (40)
50050900	16	1	46	379	15	1978-2016 (39)
50051310	26	1	39	284	13	1978-2016 (39)
50051800	106	5	38	290	14	1990-2016 (27)
50053025	19	7	59	426	20	1990-2016 (27)
50055000	233	13	38	260	13	1945-2016 (58)
50055225	43	N/A	N/A	222	12	1991-2016 (26)
50055750	58	8	34	231	12	1990-2016 (26)
50056400	42	19	23	163	9	1960-2016 (47)
50057000	156	16	28	178	10	1960-2016 (57)
50058350	20	22	52	181	14	1990-2017 (28)
50063800	22	3	91	434	14	1967-2016 (49)

50064200	19	2	75	493	15	1967-2016 (41)
50065500	18	0	100	499	20	1968-2016 (40)
50067000	10	N/A	N/A	307	17	1980-2015 (36)
50075000	3	0	100	698	14	1946-2016 (49)
50081000	17	7	42	226	11	1960-2016 (39)
50090500	14	1	93	294	17	1971-2017 (40)
50092000	47	0	85	447	20	1966-2016 (51)
50100200	26	6	67	496	22	1971-2015 (28)
50100450	43	2	75	478	22	1989-2015 (27)
50106100	113	4	45	408	18	1987-2016 (30)
50112500	25	1	83	582	24	1964-2016 (53)
50113800	31	1	80	649	23	1989-2016 (28)
50124200	49	2	64	401	21	1981-2016 (36)
50136400	47	2	87	369	18	1986-2016 (31)
50138000	311	13	59	201	13	1975-2017 (43)
50144000	244	2	78	460	18	1963-2015 (53)
50147800	184	13	37	152	10	1968-2017 (50)

Table S2. Correlation analysis between annual peak discharge change (normalized by upstream drainage area) and watershed characteristics. Bolded values are significant at the 5% level.

Watershed Characteristic	Pearson (p-value)	Kendall's Tau (p-value)
Slope	0.10 (0.57)	0.15 (0.20)
Elevation	0.09 (0.61)	0.08 (0.48)
Normalized 2-Year Flood	**-0.54 (0.0004)**	-0.17 (0.14)
Developed Area	0.10 (0.56)	-0.16 (0.17)
Forested Area	0.01 (0.95)	0.19 (0.12)

Upstream Drainage Area	0.14 (0.42)	0.05 (0.68)

Table S3. Correlation analysis between long-term conveyance capacity changes and watershed characteristics.

Watershed Characteristic	Pearson (p-value)	Kendall's Tau (p-value)
Slope	0.16(0.35)	0.07 (0.53)
Elevation	0.07 (0.68)	0.05 (0.69)
Normalized 2-Year Flood	-0.22 (0.18)	-0.21 (0.07)
Developed Area	0.14 (0.42)	0.15 (0.20)
Forested Area	-0.02 (0.90)	-0.04 (0.78)
Upstream Drainage Area	-0.06 (0.70)	0.02 (0.87)

Table S4. Correlation analysis between instantaneous conveyance capacity changes and watershed characteristics using 10-year, 5-year, and 20-year recurrence interval flood thresholds. Values significant at the 5% level are in bold.

Watershed Characteristic	Pearson (10-year) (p-value)	Pearson (5-year) (p-value)	Pearson (20-year) (p-value)	Kendall's Tau (10-year) (p-value)	Kendall's Tau (5-year) (p-value)	Kendall's Tau (20-year) (p-value)
Normalized discharge of the flood event	**-0.23** **(0.03)**	**-0.19** **(0.01)**	-0.31 (0.06)	0.03 (0.63)	0.002 (0.95)	-0.17 (0.13)
Slope	0.09 (0.41)	0.08 (0.25)	0.16 (0.34)	0.10 (0.18)	0.08 (0.11)	0.16 (0.18)
Normalized 2-Year Flood	0.01 (0.94)	0.07 (0.33)	-0.11 (0.51)	0.11 (0.13)	0.07 (0.17)	0.02 (0.86)

Elevation	-0.13 (0.24)	-0.05 (0.51)	-0.08 (0.62)	-0.03 (0.67)	-0.02 (0.75)	0.07 (0.57)
Developed Area	0.15 (0.16)	0.16 (0.11)	0.12 (0.48)	-0.06 (0.44)	-0.08 (0.12)	-0.04 (0.78)
Forested Area	-0. 06 (0.56	-0.04 (0.59)	-0.11 (0.53)	0.05 (0.50)	0.03 (0.51)	0.05 (0.71)
Upstream Drainage Area	0.02 (0.82)	-0.05 (0.53)	0.05 (0.77)	-0.10 (0.17)	**-0.11** **(0.03)**	-0.08 (0.46)

Table S5. Correlation analysis results between instantaneous volatility and watershed characteristics, using 10-year, 5-year, and 20-year recurrence interval flood thresholds.

Watershed characteristic	Pearson (10-year) (p-value)	Pearson (5-year) (p-value)	Pearson (20-year) (p-value)	Kendall's Tau (10-year) (p-value)	Kendall's Tau (5-year) (p-value)	Kendall's Tau (20-year) (p-value)
Slope	-0.09 (0.59)	-0.10 (0.54)	-0.11 (0.52)	-0.06 (0.58)	-0.12 (0.28)	0.001 (1)
Elevation	-0.06 (0.73)	-0.08 (0.63)	-0.01 (0.97)	-0.07 (0.57)	-0.106 (0.42)	-0.01 (0.96)
Normalized 2-Year Flood	-0.03 (0.84)	-0.01 (0.95)	-0.05 (0.75)	0.09 (0.45)	0.10 (0.41)	0.06 (0.60)
Developed Area	-0.04 (0.83)	-0.05 (0.77)	0.02 (0.90)	-0.11 (0.34)	-0.09 (0.46)	-0.14 (0.23)
Forested Area	0.09 (0.60)	0.11 (0.53)	0.05 (0.77)	0.04 (0.72)	0.06 (0.64)	0.07 (0.54)
Upstream Drainage Area	-0.17 (0.32)	-0.18 (0.27)	-0.19 (0.27)	-0.17 (0.13)	-0.19 (0.09)	-0.19 (0.08)

Table S6. Correlation analysis results between gradual volatility and watershed characteristics, 10-year, 5-year, and 20-year recurrence interval flood thresholds.

Watershed Characteristic	Pearson (10-year) (p-value)	Pearson (5-year) (p-value)	Pearson (20-year) (p-value)	Kendall's Tau (10-year) (p-value)	Kendall's Tau (5- year) (p-value)	Kendall's Tau (20-year) (p-value)
Slope	-0.03 (0.84)	-0.04 (0.80)	-0.01 (0.94)	-0.06 (0.60)	-0.12 (0.30)	-0.04 (0.75)
Elevation	-0.08 (0.62)	-0.10 (0.53)	-0.08 (0.62)	-0.08 (0.48)	-0.09 (0.42)	-0.08 (0.52)
Normalized 2-Year Flood	0.003 (0.98)	0.04 (0.82)	0.01 (0.94)	0.07 (0.57)	0.11 (0.35)	0.03 (0.78)
Developed Area	-0.11 (0.53)	-0.17 (0.32)	-0.08 (0.62)	-0.11 (0.35)	-0.09 (0.44)	-0.12 (0.30)
Forested Area	0.17 (0.33)	0.16 (0.34)	0.18 (0.28)	0.05 (0.70)	0.02 (0.86)	0.03 (0.82)
Upstream Drainage Area	-0.16 (0.35)	-0.21 (0.21)	-0.16 (0.35)	-0.16 (0.15)	-0.18 (0.11)	-0.15 (0.19)

Table S7. Correlation analysis between total volatility and watershed characteristics, using 10-year, 5-year, and 20-year recurrence interval flood thresholds.

Watershed Characteristic	Pearson (10-year) (p-value)	Pearson (5-year) (p-value)	Pearson (20 year) (p-value)	Kendall's Tau (10-year) (p-value)	Kendall's Tau (5-year) (p-value)	Kendall's Tau (20-year) (p-value)
Slope	-0.06 (0.72)	-0.08 (0.65)	-0.06 (0.73)	-0.06 (0.64)	0.12 (0.30)	-0.04 (0.73)
Elevation	-0.07 (0.67)	-0.09 (0.58)	-0.05 (0.77)	-0.07 (0.55)	-0.10 (0.40)	-0.08 (0.50)
Normalized 2-Year Flood	-0.01 (0.93)	0.01 (0.94)	-0.02 (0.91)	-0.07 (0.57)	0.09 (0.44)	0.02 (0.84)
Developed Area	-0.07 (0.67)	0.11 (0.53)	-0.04 (0.83)	-0.10 (0.38)	-0.10 (0.39)	-0.11 (0.35)
Forested Area	0.13 (0.44)	0.14 (0.42)	0.13 (0.46)	0.05 (0.69)	0.04 (0.76)	0.03 (0.82)
Upstream Drainage Area	-0.16 (0.33)	-0.20 (0.24)	-0.17 (0.30)	-0.15 (0.18)	-0.19 (0.09)	-0.15 (0.18)

Table S8. Summary of 24 sites in Chapter 3

Site	Largest Flood Date	Largest Flood Discharge (m³/s)	Channel Width (m)	Reach Slope (m/m)	Sinuosity	Fr_{50}
50024950	9/22/1998	2162	29.5	0.0097	1.3994	0.6539
50028000	9/22/1998	665	11.1	0.0151	1.1318	0.2472
50035000	9/20/2017	8037	71.9	0.0019	1.0849	0.3670
50039500	9/20/2017	1557	10.4	0.0015	1.4138	0.5679
50045010	9/10/1996	5575	27.3	0.0092	1.0169	0.0641
50046000	9/10/1996	4528	26.1	8.84E-06	1.0263	1.0078
50047560	9/10/1996	425	8.4	0.0151	1.2385	0.1951
50047850	9/10/1996	1840	18.1	0.0491	1.0260	0.3506
50051800	9/10/1996	1607	19.1	0.0011	1.1111	0.2773
50055000	9/10/1996	2349	56.1	0.0001	1.2205	0.4388
50055750	9/20/2017	691	27.7	0.0029	1.0589	0.4252
50057000	9/20/2017	2434	31.	2.57E-05	1.0845	0.2798
50063800	9/20/2017	659	16.9	0.0110	1.3751	0.3357
50064200	9/21/1998	623	11.9	0.0206	1.1768	0.2444
50065500	5/10/2014	566	10.2	0.0195	1.4004	0.1660
50092000	9/21/1998	1593	11.1	0.0361	1.0432	0.3700
50106100	9/20/2017	1528	5.1	0.0375	1.0438	0.2962
50113800	9/20/2017	475	14.5	0.0013	1.2571	0.1762

50114900	9/21/1998	283	7.3	0.0305	1.2523	0.5638
50124200	10/26/2012	674	2.9	0.0096	1.0159	0.1750
50136400	9/22/1998	685	9.0	0.0025	1.3229	0.2717
50144000	9/20/2017	5236	60.1	0.0052	2.8782	0.4275
50147800	9/20/2017	1531	25.9	0.1685	1.0110	0.5622
50148890	9/20/2017	2094	12.6	0.0020	1.4745	0.3665

Table S8. continued

Site	Developed	Forested	Planted	Q2yr	Watershed Area (km2)	Mean Elevation (masl)
50024950	4.98	70.15	0.11	321	89	505
50028000	2.74	68.14	0.00	151	48	564
50035000	3.48	54.36	0.44	470	331	571
50039500	11.98	51.60	1.76	131	257	183
50045010	12.29	45.80	0.52	829	448	460
50046000	14.60	44.32	0.87	538	519	409
50047560	22.32	23.64	11.29	15	22	438
50047850	12.98	49.56	3.38	183	108	337
50051800	5.20	38.29	2.54	297	106	290
50055000	13.48	37.65	2.87	645	233	260
50055750	8.37	34.31	31.01	142	58	231

50057000	16.17	27.98	17.63	460	156	178
50063800	2.98	90.79	0.00	210	22	434
50064200	2.19	74.89	0.60	132	19	493
50065500	0.00	99.86	0.00	291	18	499
50092000	0.36	85.21	0.00	134	47	447
50106100	4.44	44.80	0.00	82	113	408
50113800	0.86	80.11	0.00	70	31	649
50114900	4.32	72.29	0.00	32	19	626
50124200	2.38	63.96	0.00	68	49	401
50136400	1.89	86.81	0.00	96	47	369
50144000	2.02	77.76	0.48	402	244	460
50147800	12.98	36.85	2.71	693	184	152
50148890	14.72	37.97	2.79	277	247	136

Table S9. Estimates of Hydraulic Geometry Parameters for 24 USGS Sites in Chapter 3 in Puerto Rico

Site	a	c	k	b	f	m
50024950	13.51(<1e-10)	0.23(<1e-10)	0.33(<1e-10)	0.3(<1e-10)	0.33(<1e-10)	0.37(<1e-10)
50028000	8.54(<1e-10)	0.29(<1e-10)	0.4(<1e-10)	0.25(<1e-10)	0.28(<1e-10)	0.46(<1e-10)
50035000	34.47(<1e-10)	0.23(<1e-10)	0.13(<1e-10)	0.15(<1e-10)	0.3(<1e-10)	0.54(<1e-10)

50039500	15.62(<1e-10)	0.11(<1e-10)	0.6(<1e-10)	0.059(0.00011)	0.76(<1e-10)	0.18(<1e-10)
50045010	14.016(<1e-10)	0.3(<1e-10)	0.23(<1e-10)	0.27(<1e-10)	0.49(<1e-10)	0.25(<1e-10)
50046000	12.79(<1e-10)	0.28(<1e-10)	0.28(<1e-10)	0.33(<1e-10)	0.44(<1e-10)	0.23(<1e-10)
50047560	5.38(<1e-10)	0.37(<1e-10)	0.5(<1e-10)	0.21(<1e-10)	0.44(<1e-10)	0.35(<1e-10)
50047850	11.34(<1e-10)	0.27(<1e-10)	0.33(<1e-10)	0.21(<1e-10)	0.4(<1e-10)	0.39(<1e-10)
50051800	15.18(<1e-10)	0.27(<1e-10)	0.25(<1e-10)	0.2(<1e-10)	0.35(<1e-10)	0.45(<1e-10)
50055000	12.13(<1e-10)	0.25(<1e-10)	0.33(<1e-10)	0.34(<1e-10)	0.43(<1e-10)	0.23(<1e-10)
50055750	11.56(<1e-10)	0.28(<1e-10)	0.31(<1e-10)	0.33(<1e-10)	0.32(<1e-10)	0.35(<1e-10)
50057000	12.55(<1e-10)	0.26(<1e-10)	0.31(<1e-10)	0.25(<1e-10)	0.49(<1e-10)	0.26(<1e-10)
50063800	12.56(<1e-10)	0.34(<1e-10)	0.23(<1e-10)	0.26(<1e-10)	0.4(<1e-10)	0.35(<1e-10)
50064200	9.6(<1e-10)	0.3(<1e-10)	0.35(0.001)	0.27(<1e-10)	0.32(<1e-10)	0.41(0.056)
50065500	11.75(<1e-10)	0.37(<1e-10)	0.23(<1e-10)	0.23(<1e-10)	0.33(<1e-10)	0.44(<1e-10)
50092000	11.68(<1e-10)	0.32(<1e-10)	0.27(<1e-10)	0.21(<1e-10)	0.3(<1e-10)	0.49(<1e-10)
50106100	10.81(<1e-10)	0.2(<1e-10)	0.47(8.3e-08)	0.32(<1e-10)	0.31(<1e-10)	0.38(0.001)
50113800	11.71(<1e-10)	0.3(<1e-10)	0.29(<1e-10)	0.24(<1e-10)	0.29(<1e-10)	0.47(<1e-10)
50114900	7.029(<1e-10)	0.27(<1e-10)	0.52(<1e-10)	0.24(<1e-10)	0.29(<1e-10)	0.46(<1e-10)
50124200	12.19(<1e-10)	0.25(<1e-10)	0.33(<1e-10)	0.19(<1e-10)	0.26(<1e-10)	0.55(<1e-10)
50136400	10.86(<1e-10)	0.27(<1e-10)	0.35(<1e-10)	0.13(<1e-10)	0.33(<1e-10)	0.54(<1e-10)
50144000	17.44(<1e-10)	0.25(<1e-10)	0.23(<1e-10)	0.26(<1e-10)	0.36(<1e-10)	0.38(<1e-10)
50147800	13.14(<1e-10)	0.18(<1e-10)	0.43(<1e-10)	0.17(<1e-10)	0.61(<1e-10)	0.23(<1e-10)

50148890	14.55(<1e-10)	0.18(<1e-10)	0.37(<1e-10)	0.12(<1e-10)	0.61(<1e-10)	0.27(<1e-10)

Table S10. Streamflow quantile estimates of LP3 used in HEC-RAS models in this study.

USGS Site ID	10-y Streamflow Quantile Estimate (including Maria) (m³/s)	100-y Streamflow Quantile Estimate (including Maria) (m³/s)	10-y Streamflow Quantile Estimate (excluding Maria) (m³/s)	100-y Streamflow Quantile Estimate (excluding Maria) (m³/s)
50024950	1069	3965	882	2643
50035000	1787	5685	1590	4290
50039500	612	2926	558	2407
50045010	2984	8180	2596	6316
50046000	2476	6092	2324	5479
50047560	169	1466	144	1385
50047850	558	1245	564	1306
50051800	865	2425	858	2578
50055000	1304	1850	1285	1829
50055750	385	775	333	579
50057000	1537	3833	1452	3494
50063800	437	687	414	621
50064200	398	852	379	795